

Washington University in St. Louis

Washington University Open Scholarship

McKelvey School of Engineering Theses & Dissertations

McKelvey School of Engineering

Winter 1-3-2023

Comparison of In-vitro 3D human Embryoids with Current Models for Gastrulation

Jin Park

Washington University in St. Louis

Follow this and additional works at: https://openscholarship.wustl.edu/eng_etds



Part of the [Biological Engineering Commons](#), [Cell Biology Commons](#), and the [Developmental Biology Commons](#)

Recommended Citation

Park, Jin, "Comparison of In-vitro 3D human Embryoids with Current Models for Gastrulation" (2023). *McKelvey School of Engineering Theses & Dissertations*. 768. https://openscholarship.wustl.edu/eng_etds/768

This Thesis is brought to you for free and open access by the McKelvey School of Engineering at Washington University Open Scholarship. It has been accepted for inclusion in McKelvey School of Engineering Theses & Dissertations by an authorized administrator of Washington University Open Scholarship. For more information, please contact digital@wumail.wustl.edu.

WASHINGTON UNIVERSITY IN ST. LOUIS

McKelvey School of Engineering
Department of Biomedical Engineering

Thesis Examination Committee:
Lilianna Solnica-Krezel, Chair
Guy Genin
Michael Vahey

Comparison of In-vitro 3D Human Embryoids with Current Models for Gastrulation
by
Ajin Park

A thesis presented to
the McKelvey School of Engineering
of Washington University in
partial fulfillment of the
requirements for the degree
of Master of Science

December 2022
St. Louis, Missouri

© 2022, Ajin Park

Table of Contents

List of Figures	iv
List of Tables	vi
Acknowledgments.....	vii
Abstract	ix
Chapter 1: Introduction	1
1.1 introduction to gastrulation.....	1
1.1.1 Evolutionarily conserved aspects of gastrulation	1
1.1.2 What do we know about human gastrulation.....	4
1.1.3 Clinical relevance in gastrulation.....	6
1.2 Gastrulation across different species	8
1.2.1 Zebrafish gastrulation	8
1.2.2 Chick gastrulation	11
1.2.3 Mouse gastrulation.....	13
1.3 2D micropatterned embryonic stem cell gastruloids.....	20
1.3.1 Micropattern technique	20
1.3.2 2D gastruloids compared to in vivo embryos	25
1.3.3 Limitations of 2D human gastruloids	28
1.4 Evolution of mouse models to study gastrulation.....	30
1.4.1 Mouse embryoid bodies.....	30
1.4.2 Development of mouse gastruloids.....	34
1.4.3 3D gastruloid models in Humans.....	35

1.4.4 Comparison of 3D human gastruloid models with other models	38
1.4.5 Limitaitons of 3D human gastruloids	39
1.5 Conclusion	40
Chapter 2: Methods	42
2.1 Experimental setup.....	42
2.1.1 Materials	42
2.1.2 Cell culture conditions	43
2.2 Human 3D gastruloid protocol.....	47
2.3 3D gastruloid to micropattern protocol.....	48
2.4 Immunofluorescent imaging and analysis	49
Chapter 3: Results.....	52
3.1 Optimization of H1 cell line and RUES2-GLR comparison	52
3.2 Monitoring mesoderm, endoderm and ectoderm formation in H1 and RUES2-GLR 3D gastruloid model.....	64
3.3 3D human gastruloid germ layer cells exhibit sorting behaviors as reported for 2D gastruloids	70
Chapter 4: Discussion	79
4.1 H1 and RUES2-GLR protocl optimization.....	79
4.2 3D Confirming formation of the three germ layers in H1 and RUES2-GLR gastruloids .	83
4.3 Reseeded 3D gastruloids onto micropatterns exhibit self-organization	85
4.4 Limitations of my 3D gastruloid models	88
References	90
Appendix.....	105

List of Figures

Figure 1.1	Diagram of human embryo at 14 dpf..	5
Figure 1.2	Illustration of Zebrafish gastrulation, starting at around epiboly..	10
Figure 1.3	Cross section of Chick embryo, showing emboly movements during gastrulation..	12
Figure 1.4	Early stages of mouse development, from fertilization to implantation	14
Figure 1.5	Schematic of crucial signaling components during streak formation in gastrulating mice.....	18
Figure 1.6	Expression pattern of Warmflash et al's 2D gastruloids summarized...	22
Figure 1.7	Expression pattern of Minn et al's 2D gastruloids summarized.....	24
Figure 1.8	ETiX embryoids created by Amadai et al.	34
Figure 1.9	The first 3D human gastruloids	36
Figure 1.10	EMLO gastruloids by Olmsted and Paluh.....	37
Figure 3.1	H1 cell colony confluency comparison	52
Figure 3.2	Comparison of H1 colonies before and after different Chiron pre-treatment	53
Figure 3.3	H1 gastruloids with different cell number and Chiron pre-treatment	54
Figure 3.4	H1 gastruloids with different pre and post Chiron treatemnt.	56
Figure 3.5	Graph of average length-to-width ratio of gastruloids from figure 3.4.....	59
Figure 3.6	H1 gastruloids with different Chiron post-treatment	60
Figure 3.7	Bar graph of average length-to-width ratio of gastruloids from figure 3.6.....	61
Figure 3.8	H1 vs RUES2-GLR gastruloids.....	62
Figure 3.9	RUES2-GLR gastruloids grown to 144 h	63
Figure 3.10	IF image of H1 gastruloids (SOX17/TBRA, SOX2, and CDX2)	65
Figure 3.11	IF image of RUES2-GLR gastruloids (SOX17/TBRA, SOX2, and CDX2).....	68

Figure 3.12 BF of 3D H1 gastruloids reseeded onto micropattern	71
Figure 3.13 IF of 3D H1 gastruloids reseeded onto micropattern	72
Figure 3.14 BF of 3D RUES2-GLR gastruloids reseeded onto micropattern	75
Figure 3.15 IF of 3D RUES2-GLR gastruloids reseeded onto micropattern.....	76

List of Tables

Table 1 Summary of Minn et al's scRNA seq analysis on 2D gastruloids against Cyno monkey and mouse embryos.....	28
Table 2 Inventory of materials.....	42

Acknowledgements

I'd first like to acknowledge my PI: professor Lilianna Solnica-Krezel, for entrusting me to take on a Masters thesis in her lab. Her support in directing the trajectory of my project, as well as providing advice during the thesis writing process, had helped me tremendously in finishing my thesis and grow as a scientist.

I'd next like to acknowledge the LSK lab for their continuous support throughout the duration of my time in lab, as well as advice given that helped me with my experiments, personal life, and thesis presentation.

I'd also like to acknowledge my committee members, Professor Guy Genin and Michael Vahey for not only agreeing to graciously attending my thesis defense after Christmas, but for also being great professors in my past courses.

And last but most importantly, I'd like to acknowledge Dr. Blerta Stringa for being my personal mentor throughout my Masters thesis. Not only did she teach me everything I know about working in lab, but she as also helped me in understanding the expectations and attitude of being a researcher. Without her, It's no overstatement that I would not have been able to complete my thesis. Even beyond lab, Blerta has assisted me to make sure that I can focus on my thesis. And for all that, I am forever grateful.

Ajin Park

Washington University in St. Louis

December 2022

Dedicated to my parents, advisor, and mentor

ABSTRACT OF THE THESIS

Comparison of *In-vitro* 3D Human Embryoids with Current Models of Gastrulation

by

Ajin Park

Master of Science in Biomedical Engineering

Washington University in St. Louis, 2022

Professor Liliana Solnica-Krezel, Chair

Gastrulation is an early morphogenetic process that is conserved across most metazoans and lays out the future body plan through the formation and shaping of the three germ layers: endoderm, mesoderm, and ectoderm. Despite its importance, not much is known about the events surrounding human gastrulation that occurs *in utero* due to ethical and technical limitations on studying human embryos. Therefore, many researchers have devised protocols for creating *in vitro* models of gastrulation using embryonic stem cells. Initially starting with mouse embryonic stem cells, the field of *in vitro* embryo models has advanced rapidly, with protocols using human embryonic stem cells being only recently published in 2020. However, validation of these models through comparison with other *in vitro* models or with animal gastrulae has only started. As such, this study investigates one of the first 3D gastruloid protocol using human embryonic stem cells to create an optimized protocol using the H1 embryonic stem cell line, which is then validated with immunofluorescent staining for germ layer markers. And lastly, cells from 3D gastruloids generated from H1 and RUES2-GRL cell lines were tested for the ability to self-aggregate through a dissociation and reseeded experiment onto 2D micropatterns. Whereas cells from dissociated RUES2-GRL 3D gastruloids showed clear evidence of self-aggregation

comparable to what was reported in a similar experiment with 2D gastruloids, cells from H1 3D gastruloids did not. However, further optimization of the protocol is needed. Overall, the results reported in this thesis have identified conditions to generate *in vitro* H1 3D elongating gastruloids with three germ layers, as well as showing the evolutionarily conserved sorting ability of 3D RUES2-GRL gastruloid cells.

Chapter 1

Introduction

1.1 Introduction to gastrulation

Gastrulation is an early morphogenetic process for triploblastic organisms that takes place after the events of fertilization and implantation. The main role of gastrulation is to establish three germ layers; the ectoderm, which gives rise to the superficial layers of the skin, neurons, the endoderm, giving rise to the intestines, liver, pancreas, thyroid, and lungs; and the mesoderm, giving rise to muscles, bones, and connective tissues. And through internalization, followed by convergence and extension, these three germ layers are shaped into the future body plan (Durstun, 2019; Ferretti & Hadjantonakis, 2019; Loh et al., 2014).

1.1.1 Evolutionarily conserved aspects of gastrulation

Early embryonic development begins with fertilization: the creation of a zygote through union of an egg with a cognate sperm. The resulting single-celled zygote undergoes a series of mitotic cleavages to produce multiple blastomeres exponentially by the power of two (Condic, 2014). Blastomeres aggregate to form the morula and continue to divide and undergo compaction to form a blastocyst, in which the outer cells differentiate as the trophoblast. Meanwhile, the inner cells remain pluripotent and become the inner cell mass (ICM). In conjunction with the trophoblast, a cavity is formed in the center called the blastocoel where a portion of the ICM cells lining the blastocoel form the primitive endoderm. The ICM will give rise to all the tissues

and organs of the embryos, whereas trophoctoderm and primitive endoderm differentiate into extraembryonic structures that protect and connect the embryo to the maternal tissues. Once these three components are formed, the morula has successfully transformed into a blastocyst and is ready for implantation (Zhang & Hiiragi, 2018).

The process of implantation involves the attachment of the blastocyst to the lining of the uterus (endometrium) through contact with the trophoctoderm, crossing the epithelial barrier to invade the endometrial stroma (Enders et al., 1986) . After implantation, the embryo is soon ready for gastrulation. It's worth mentioning that in nonmammalian vertebrates that develop externally, such as frogs or fish, most of the blastula cells will form embryonic tissues with few or absent extraembryonic cell types (McGowen et al., 2014).

To start gastrulation, the ICM cells of mammalian embryos continue to proliferate and undergo morphogenesis to form the epiblast, which is shaped as a cup in the mouse or as a flat disc in humans. Underlying the epiblast is primitive endoderm. In mice, primitive or visceral endoderm, including so-called the anterior visceral endoderm (AVE) plays a role in signaling during primitive streak formation, while in chick, the equivalent of primitive endoderm, called hypoblast does not contribute to any cells of the embryo, though both still play a role in determining embryonic polarity (Bertocchini & Stern, 2002).

The first stage of gastrulation is internalization, which begins when an opening forms in the epiblast and is referred to as the blastopore in frog and primitive streak in avian and mammalian embryos (Solnica-Krezel & Sepich, 2012). From here, cells of the epithelial epiblast migrate

into the blastopore after undergoing an epithelial-to-mesenchymal transition (EMT), which entails downregulation of cell adhesion molecules and disassembly of epithelial junctions while attaining motility (Thiery et al., 2009; Wu et al., 2007). Cells remaining in the epiblast will become the ectoderm, whereas those that internalize through the blastopore will form the deepest endoderm layer, and those between the epiblast and endoderm will become the mesoderm. In some species, gastrulation also involves epiboly, during which all the germ layers begin to thin and spread through the process of radial intercalation and cell shape changes in an organized fashion (R. E. Keller, 1980; Warga & Kimmel, 1990). Concurrently, the embryo undergoes convergence and extension movements where nascent germ layers elongate down the head to tail embryonic axis while narrowing from back to belly. This process starts with convergence where the tissue is narrowed down through cell migration, and planar intercalations towards the midline (Solnica-Krezel & Sepich, 2012). Meanwhile, elongation also occurs via polarized cell division, cell shape changes, and polarized radial or planar intercalation of cells between their anterior and posterior neighbors to extend the anterior-to-posterior (AP) axis (Sepich et al., 2005). With that, the end result of gastrulation is the emergence of the three germ layers, ectoderm, endoderm, and mesoderm through internalization, that are shaped through epiboly, convergence and extension to form a body rudiment with a head, trunk, tail, and organ rudiments (Zhang & Hiiragi, 2018).

Although the major morphogenetic processes of gastrulation are conserved (internalization, epiboly, convergence, and extension), the timing of these events, and the cellular behaviors driving these morphogenetic events themselves, vary between species. Additionally, our understanding of human gastrulation is extremely limited due to both experimental and technical constraints. Experimental constraints have been recently eased with the Warnock report of 1985

being waived in 2022 by the International Society for Stem Cell Research (ISSCR), allowing the culture of human embryos to surpass 14 days with specialized oversight (Lovell-Badge et al., 2021; Wt, 1984). On the other hand, alleviating the technical limitations has seen little progress, with difficulty stemming from the fact that gastrulation in humans takes place in utero. To compensate, stem cell models have been in development, such as the work of Casterjeon et al in 2021 where mouse embryos were successfully cultured ex-utero with post-implantation mouse embryos all the way through gastrulation and up to early organogenesis (Aguilera-Castrejon et al., 2021). As well, experimental and technical limitations in studying human gastrulation are not seen in other species. Zebrafish, for example, is transparent during the early stages of development, allowing easy observation as demonstrated by Kimmel et al in 1995. (Kimmel et al., 1995) . As each species has its own advantages over humans for studying gastrulation, most of our knowledge of gastrulation comes from model organisms such as zebrafish, chick, and mouse.

1.1.2 What do we know about human gastrulation

Due to the technical and ethical limitations, most of our current knowledge of human gastrulation comes from anatomical and histological embryology studies such as the Carnegie and Kyoto embryo collection, and rare medical studies such as Langman’s medical embryology and Larsen’s Human embryology (Hill, 2018; O’Rahilly & Müller, 2010; Wt, 1984) (Sadler & Langman, 2015). From these studies, as well as recent transcriptomic analysis of human *in vitro* post-implantation embryos and a single human gastrula, our knowledge of human gastrulation is slowly expanding (Molè et al., 2021; Tyser et al., 2021).

Human gastrulation begins 14 days post fertilization (dpf), corresponding to Carnegie stage (CS) 6 embryos. At this stage, the human embryo, encapsulated by the trophoblast, is an epithelial cyst with the central epiblast disc facing the amniotic cavity and amnion on one side, with primitive endoderm (PE) on the other, all surrounded by tissues arising from the trophectoderm (TE) (Hafez, 2017). The luminal conceptus (structures of the lumen that developed from the zygote) is made up of two tissues; the amnion, in the form of a squamous epithelium surrounding the amniotic cavity; and the epiblast, where the amnion originates from and is seen in the form of a disc. Underneath the epiblast lies the visceral or primitive endoderm (VE), which extends laterally from the epiblast to form the definitive yolk. (**Figure 1.1**)

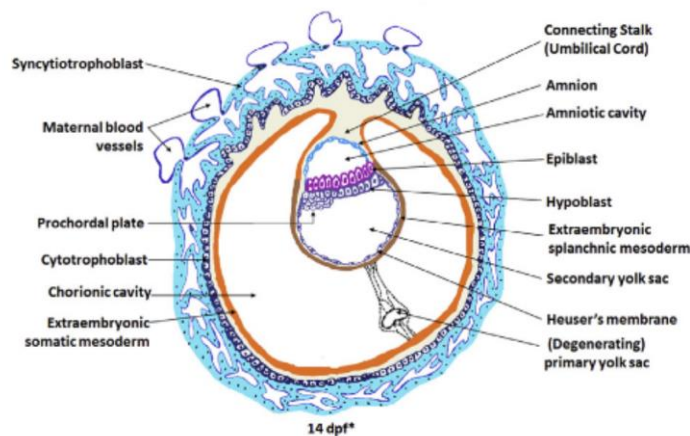


Figure 1.1: Diagram of human embryo at 14 dpf. (Ghimire et al., 2021)

The processes that establish the anteroposterior (AP) axis within the human epiblast remains to be determined. However, as gastrulation progresses, the primitive streak forms in the posterior pole and extends anteriorly to the center of the epiblast (Müller & O’Rahilly, 2004; Sadler & Langman, 2015). During CS6b (14 dpf), cells are thought to move out from the epithelial epiblast through the primitive streak, likely through EMT, and burrow at the caudal end of the epiblast at the base of the connecting stalk, becoming the extraembryonic mesoderm which will

give rise to the allantois, as well as becoming mesoderm, and definitive endoderm (O’Rahilly & Müller, 2010)

At CS7 (15 to 17 dpf), the primitive streak is clearly visible with the primitive node at the anterior tip. Additionally, anterior to the primitive node is the notochordal process, mesodermal tissue which will fuse with the endoderm at CS8 (17 to 18 dpf). Finally, epiblast cells that underwent EMT and internalized, occupy the space laterally under the epiblast to form the mesoderm (Sadler & Langman, 2015). Additionally, all structures that appeared in CS7 are more pronounced and the primitive streak has reached its maximal length, occupying 50% of the epiblast. Lastly, the notochordal process fuses with the endoderm and forms the notochordal plate, presumably instructing neural induction of the anterior epiblast similar to mouse gastrulation in Embryonic day (E) 7.5 (de Bree et al., 2018). At late gastrulation at CS9 (19 to 21 dpf), the embryonic disc has become an oval, with recognizable outlines of the body plan and a regressed primitive streak (Sadler & Langman, 2015).

1.1.3 Clinical relevance in gastrulation

Aside from providing fundamental knowledge, studying human gastrulation has a significant clinical impact as well. It is estimated that a miscarriage occurs in the case of 10% to 25% of all clinically recognized pregnancies, with any defects occurring during gastrulation to result in death, but in rare circumstances, severe birth deformities (X. Wang et al., 2003; Zinaman et al., 1996). Some examples of defects in gastrulation include; Teratomas, a solid mass or germ cell tumor made of a combination of three germ layers; Sirenomelia, a congenital deformity presented as fusion of the legs; and Tethered cord syndrome, a congenital defect of the spine,

causing restricted movement and paralysis in later life (Kanda et al., 2015; Kremer et al., 2018; Valenzano et al., 1999). All three examples have been suspected to be defects that occur during gastrulation, whether it is a defect in germ layer formation, or errors in primitive streak regression (Acharya et al., 2017; Samal & Rathod, 2015). The lack of knowledge about human gastrulation puts us at a disadvantage because we do not understand what exactly causes miscarriages and birth deformities, not being able to take steps to prevent or treat them. Therefore, understanding gastrulation can help aid in reducing the number of miscarriages and birth deformities, as well as expand our knowledge of early human development.

1.2 Gastrulation across different species.

1.2.1 Zebrafish gastrulation

The zebrafish model stands out amongst the other models when it comes to gastrulation. The major advantages of using zebrafish are; embryos are transparent and gastrulation takes place externally, allowing researchers to observe the early zebrafish development under a microscope; gastrulation is relatively quick, taking only 12 hours from the blastula to early segmentation stages (corresponding to CS9 human embryos), and a total 3 dpf to free-swimming larvae; and zebrafish are economical because they're easy to breed and relatively inexpensive to maintain, allowing multiple experiments with lesser funding. For these reasons, zebrafish is one of the best models for gastrulation, especially for large-scale mutagenesis and forward genetic screening (Kimmel et al., 1995; Solnica-Krezel et al., 1996; Varshney & Burgess, 2014).

Like with most organisms, life begins at the single-cell stage, undergoing successive cell division to form an aggregate of blastomeres. However, compared to mammalian embryos, cleaving zebrafish embryos contain much more yolk. Additionally, the entire zygote does not undergo cleavage, but rather, the non-yolk cytoplasmic section of the zygote towards the animal pole initially undergoes synchronous meroblastic cleavages to separate itself from the yolk around 500 cell stages and eventually gives rise to all embryonic tissues. The embryo undergoes the mid-blastula transition at the 10th cleavage (512 cells), which is associated with the initiation of zygotic transcription (Kimmel et al., 1995). In the embryonic portion (blastoderm), the superficial cells become the enveloping layer (EVL), whereas cells between the EVL and the yolk become motile and divide asynchronously.

At this stage, the yolk syncytial layer (YSL), found between the blastoderm and the yolk, begins to spread to the vegetal pole, compacting the embryo and causing a new layer of YSL, external and internal (**Figure 1.2**). The start of epiboly is marked by the slight rise of the internal YSL as the deep and EVL cells begin to move towards the vegetal pole, covering the yolk like a melting ice cream through intercalation of the deep cells and thinning of EVL cells. Once the yolk is covered halfway, the distribution of germ layer precursors can be seen where prospective endodermal cells are closest to the blastoderm margin, analogous to the blastopore. Through intercalation of the epiblast and hypoblast, the thickening of the germ layer (germ ring) creates the dorsal embryonic shield, which acts analogously to the node of the primitive streak by introducing dorsal to ventral polarity (Shih & Fraser, 1996). In the animal pole region, ectodermal precursors are located while mesodermal precursors reside between the prospective endoderm and ectoderm. During internalization, individual blastomeres near the blastoderm margin undergo ingression between the superficial blastoderm and YSL. These mesodermal and endodermal precursor cells initially move toward the animal pole. When epiboly movements cover 75% of the yolk cell, the germ layers start convergence and extension movements which elongate the germ layers down the anteroposterior axis, narrowing them mediolaterally (Sepich et al., 2005). Cells in the lateral part of the blastopore region undergo convergence and extension by directed migration, while those in the dorsal do so via polarized intercalations (Jessen et al., NCB, 2002; Kane & Adams, 2002; Montero et al., 2005; Shih & Fraser, 1995).

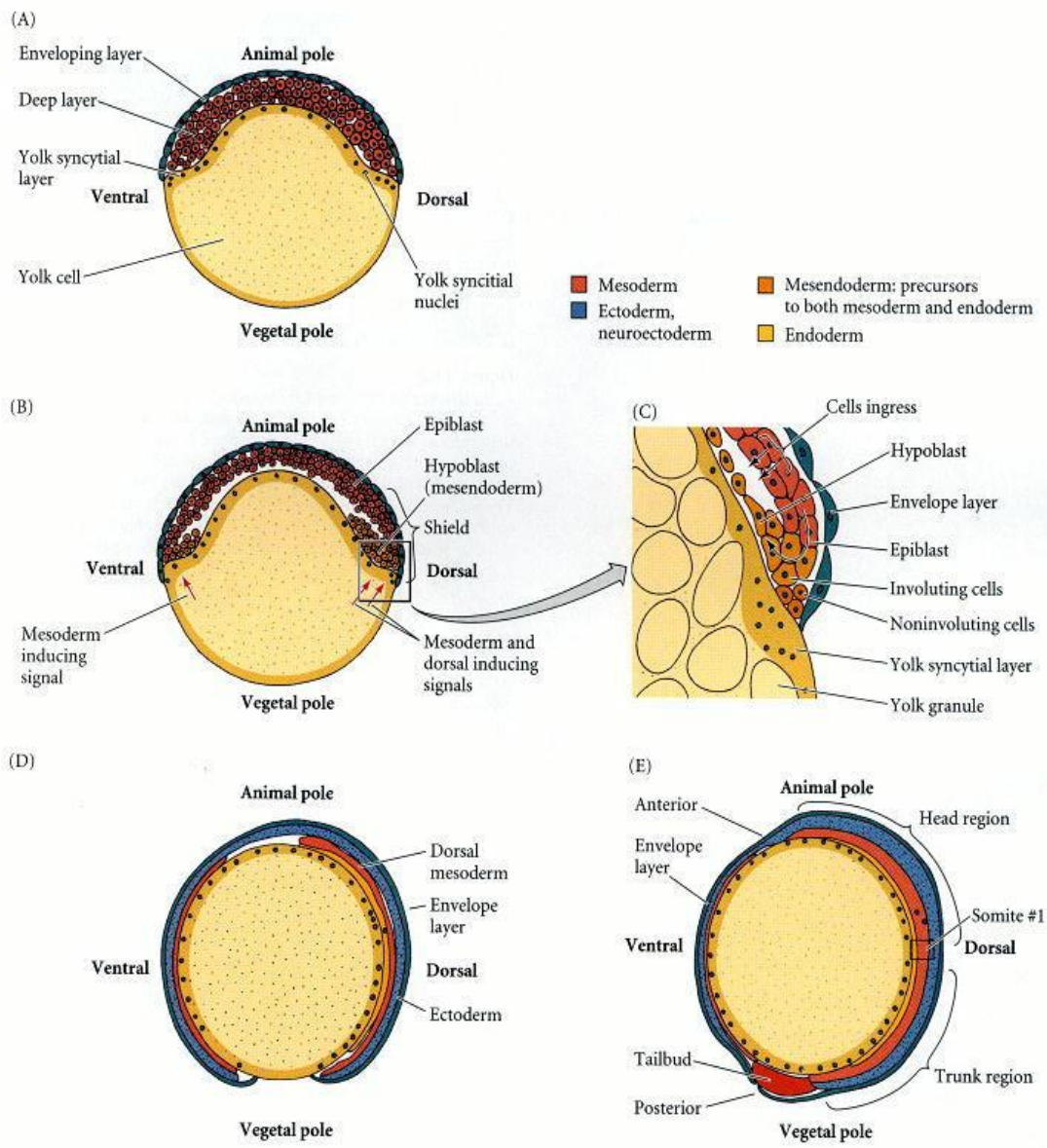


Figure 1.2: Illustration of Zebrafish gastrulation, starting at around epiboly (Gilbert & Barresi, 2016)

1.2.2 Chick gastrulation

Fertilization of the egg occurs in the oviduct, which it leaves once becoming a blastocyst. Similar to zebrafish, the zygote will undergo meroblastic cleavage above the yolk mass, but the blastoderm is not as pronounced as in the zebrafish embryo (Bellairs et al., 1975; Lee et al., 2013). The submarginal cavity lies between the dividing blastoderm cells and the yolk, absorbing fluid to become the egg white. As more blastoderm cells emerge from cleavage, the epiblast is established with deep cells underneath at the posterior end (Koller's sickle region). Through delamination, the hypoblast cells originate from the epiblast and deep cells migrate and aggregate in the subgerminal space. Once the embryo has reached approximately 20,000 cells, the egg is laid. Interestingly, the hypoblast does not contribute to any of the three germ layers but, rather, the germ layers are formed mostly from epiblast cells (New, 1956).

Soon after the egg is laid, gastrulation begins with the formation of the primitive streak near the posterior end of the epithelial epiblast and extends towards the anterior. Internalization occurs through EMT and subsequent ingression of endodermal precursors from the epiblast into the blastocoel (Bellairs, 1986; Eyal-Giladi et al., 1992; VAKAET, 1984). The primitive streak will continue to grow in length towards the anterior end, which will become the future head region with the development of the Hensen's node at the anterior end (Schoenwolf et al., 1992)(**Figure 1.3**)

The initial epiblast cells that internalize via the Hensen's node are destined to become endodermal cells of the foregut, while cells internalizing later will reside in between the

endoderm and epiblast to become the head mesenchyme and prechordal plate mesoderm. Additional cells that enter through the Hensen's node become notochord and endodermal cells. Meanwhile, the mesodermal precursors that internalize via the primitive streak spread between the endoderm and epiblast to form a loose layer of cells that will generate the mesodermal portion of the embryo. During mesodermal ingression, the primitive streak begins to regress, moving the Hensen's node from the center to the posterior end of the embryo. The regressing Hensen's node marks the midline of the embryo where the future notochord and parts of the floor plate of the prospective neural tube are formed (Gray & Dale, 2010; S. Ma & Cd, 1991). Along this midline, mesodermal cells begin to converge (similar to the convergence and extension movement described for zebrafish) and the epiblast will comprise of mostly ectodermal cells (Darnell et al., 1999; Le Douarin, 1996). After this, convergence and extension, driven by cell migration and intercalation, takes place to shape the embryonic body (Solnica-Krezel, 2005).

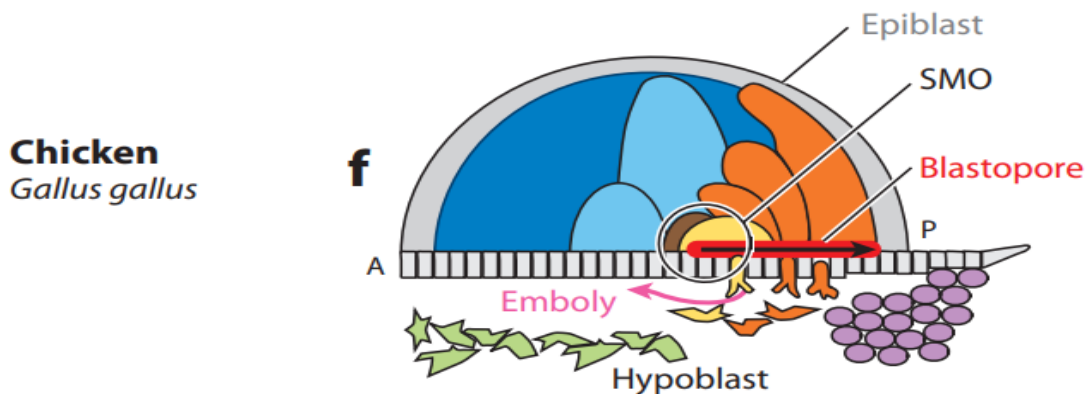


Figure 1.3: Cross section of Chick embryo, showing emboly movements during gastrulation (Solnica-Krezel & Sepich, 2012)

1.2.3 Mouse gastrulation

From fertilization, the zygote undergoes cleavage to form multiple blastomeres. Compaction follows at the 16-cell stage to 3 dpf, which leads to segregation of the inner cell mass (ICM; future epiblast) and trophectoderm, reminiscent of deep cells and the EVL (or potentially amnion) of the zebrafish respectively (Pratt et al., 1982). At 3.5 dpf, blastocoel formation begins, initially occupying half of the embryo with the other half housing the ICM at the proximal end. At 4.5 dpf, the embryo enters the late blastocyst stage where the visceral endoderm (VE) emerges from the ICM/Epiblast while trophectoderm cells surrounding the embryo begin to enlarge, causing the embryo to take on an oval shape. Enlarged trophoblast cells are also referred to as the mural trophectoderm while those located near the tip of the ICM are referred to as the polar trophectoderm (Bonnievie, 1950; Pratt et al., 1981).

Right before 5 dpf, the embryo undergoes implantation, following the ICM's growth into the blastocyst cavity to form the epiblast (Bedzhov & Zernicka-Goetz, 2014; Das et al., 1994) (**Figure 1.4**). At 5.5 dpf (pre-gastrula stage), precursor cells from the ICM (distal or parietal endoderm), comprised of pluripotent epiblast cells, extraembryonic ectoderm (EXE), and an enveloping layer of VE, continue to grow along the inner surface of the trophectoderm until they cover the entire inner surface in an evenly spaced matter. Concurrently at 5.5 to 6 dpf, the rest of the ICM, consisting of mostly epiblast precursors, will grow down into the blastocoel surrounded by the VE. This ICM takes shape of the egg cylinder with two sides; the proximal side, consisting mostly of extraembryonic ectoderm; and the distal portion, consisting of mostly epiblast cells with the visceral endoderm at the most distal end (Mishina et al., 1995).

From 6 to 6.5 dpf, the embryo enters the early gastrulation stage. The mesoderm begins to emerge at the posterior end of the epiblast which would become the primitive streak and serve as the blastopore for ingress of mesodermal and endodermal cells (Bonnievie, 1950; Bridgman, 1948; Williams et al., 2012a). Both extraembryonic and embryonic mesoderm cells undergo EMT and ingress through the posterior proximal side of the primitive streak while the streak itself elongates distally along the posterior side to the distal tip of the embryonic epiblast. Meanwhile, the endoderm utilizes both ingress through the primitive streak, and subsequently radial intercalation into the visceral endoderm, thus expanding it like in epiboly (Kwon et al., 2008; Williams et al., 2012). Finally, at E7.5 to 8.5, convergence and extension is driven by intercalation and cell migration along the mediolateral embryonic axis (perpendicular to the primitive streak and AP embryonic axis) (Wymeersch et al., 2021; Yen et al., 2009, p. 7).

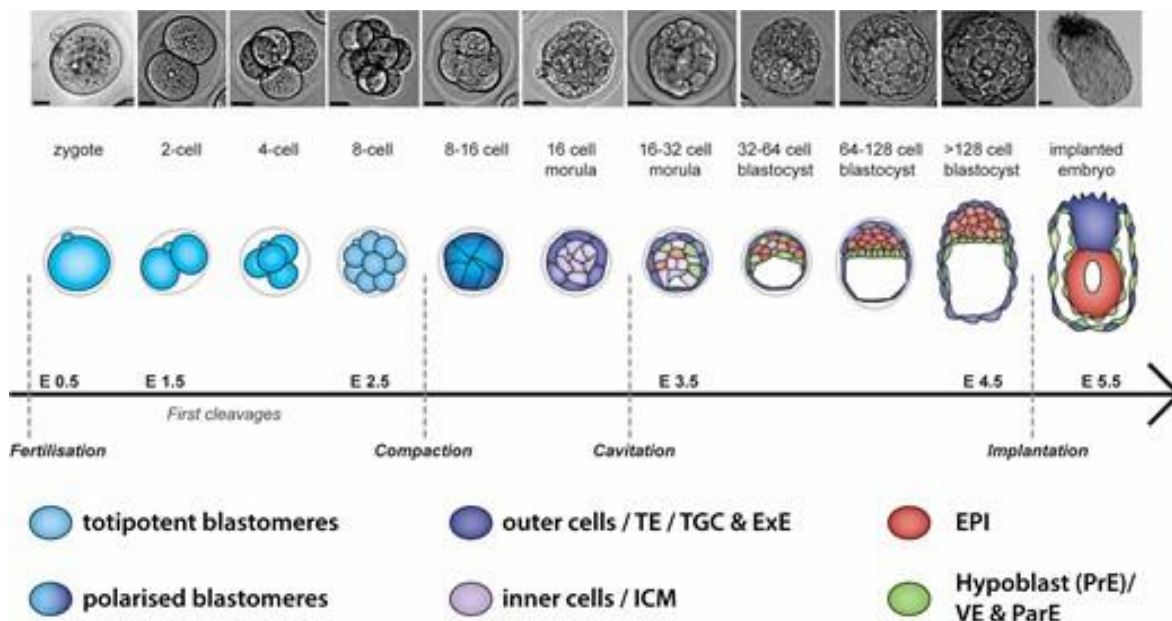


Figure 1.4: Early stages of mouse development, from fertilization (zygote) to implantation (implanted embryo). (Piliszek et al., 2016)

Mouse gastrulation signaling events.

One of the main benefits of using mouse to study gastrulation is the significantly conserved gene expression pattern and sequence with humans, even though the timing of expression and gastrula morphologies are slightly different (Molè et al., 2020). Additionally, many of the stem cell models discussed in the later chapters focus on either mouse embryonic stem cells (mESC) or human embryonic stem cells (hESC). However, mESC based models have seen the most progress as of 2022, leveraging the understanding of the signaling events surrounding mouse gastrulation and the existing mutant lines. Knowledge of mouse gastrulation informs the comparison between hESC and mESC gastruloids.

As mentioned, gastrulation in mice takes place between E6.5 and E9.5. In the course of these 3 days, major cell fate specification and morphogenic events occur through the coordination of signals via several evolutionarily conserved signaling pathways.

From E6 to E6.5 (start of gastrulation) the enveloping layer of VE begins to break symmetry by signaling to the epiblast. On one side, Anterior VE (AVE) secrete antagonists of Bone morphogenic proteins (BMP), Nodal, and WNT into the epiblast, turning the majority into ectodermal cells. The EXE secretes BMP to initiate the expression of Wnt3 and Nodal at the opposite side of the epiblast, marking it as the posterior end of the embryo (Rivera-Pérez & Hadjantonakis, 2014). Nodal and Wnt3 activation on the posterior end of the VE (and later epiblast) induce expression of T/BRA transcription factors (TF) in the proximal region, initiating the formation of the primitive streak by promoting EMT (Turner et al., 2014). This entails the downregulation of E-Cadherin with TF inhibitors such as Snail and TCF/LEF, increasing WNT

signaling through the release of **β -Catenin**. (Morgani & Hadjantonakis, 2020a). And finally, propagation of EMT along the midline of the epiblast, from proximal to distal marks the expansion of the primitive streak and lays down the anteroposterior (AP) axis (Camus et al., 2000). (**Figure 1.5**)

From E6.5 to E7.5, prospective mesodermal and endodermal cells from the epiblast whose fates are determined through the balance of BMP and Nodal in a cross-inhibiting fashion along different positions of the PA axis upon EMT invade the primitive streak through ingression (Vincent et al., 2003; Williams et al., 2012a; Winnier et al., 1995). The formation of the primitive streak relies on high FGF and BMP signaling while its elongation is mediated by Wnt3 (from the posterior VE, also induced by Wnt3), which has the downstream effect of stimulating Nodal within the epiblast. This interaction of BMP, Wnt, and Nodal provides a strong signaling event within the proximal posterior epiblast (Ciruna & Rossant, 2001a; Mishina et al., 1995a; Rivera-Pérez & Magnuson, 2005a). As the primitive streak elongates distally, Wnt3 and Nodal expression follows, and BMP4 is expressed mostly within the EXE, meaning that cells traversing the primitive streak within the distal region of the embryo are furthest from the source of BMP4, showing reduced BMP signaling but high Nodal signaling from the distal region as a result (Morgani et al., 2018). As the development ensues, the AVE of the anterior epiblast secretes CER1, LEFTY1, and DKK1 to inhibit BMP, Nodal and WNT signaling respectively in response to and to inhibit the posterior signals (Belo et al., 1997; Kawano & Kypta, 2003; Zinski et al., 2018).

At E7.5, the primitive streak reaches the distal-most region of the epiblast where the node (equivalent of the Hensen's node in the chick and the embryonic shield in zebrafish) will appear. At the anterior side, the epiblast influenced by the AVE acquires neuroectodermal fates while mesoderm patterning relies on FGF signaling (Camus et al., 2000; Yamaguchi et al., 1994). Finally, at E9.5 the final phase of gastrulation, is marked by the disappearance of the primitive streak and ceasing of ingression through suppression of EMT by upregulation of Noggin within the tail ventral mesoderm, inhibiting BMP signaling and restoring E-cadherin expression (V & Rs, 1996).

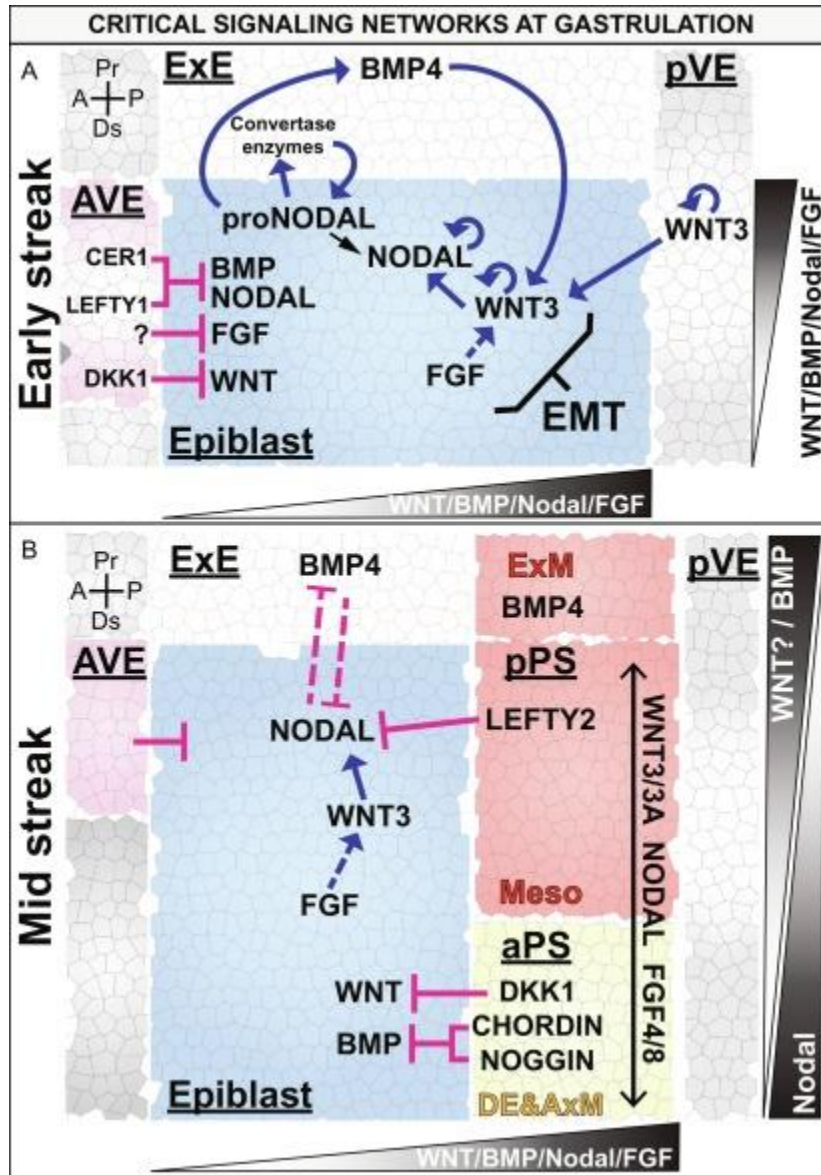


Figure 1.5: Schematic of crucial signaling components during streak formation in gastrulating mice. (Morgani & Hadjantonakis, 2020)

Stem cell-based models for gastrulation

Efforts into studying early development in humans have centered around the technical limitations caused by the in utero environment. Ethical limitations and international agreements in the research community such as the Warnock report have also halted progress, and despite the lifting of this 14 day limit by the ISSCR in 2021, replication of this process in culture is nearly impossible without a way to simulate implantation. As a result, many researchers have invested in creating *in vitro* embryo models with mESC and hESC. So far, two types of gastruloids have been developed: 2D and 3D.

2D gastruloids require the use of a micropattern to plate extracellular matrix (usually matrigel) in a disc with a diameter of 250 μm to 1000 μm . This method was pioneered by Sakai et al where the micropattern was created in 2007 and tested with cells in 2010 and 2011 using mESCs. Warmflash et al in 2014 would later use hESCs to study cell fate specification during gastrulation, and the ability of the germ layers to self-organize when stimulated with BMP. In the same year, the first 3D gastruloid protocol was developed in Alfonso Martinez Arias's lab by Susanne C van den Brink in 2014, and Peter Baillie Johnson in 2015. Likewise, the first 3D gastruloid protocol using hESCs would be established in 2020 by Moris et al., (Brink & Oudenaarden, 2021).

1.3 2D embryonic stem cell gastruloids

1.3.1 Micropattern technique

2D gastruloids are made with hESCs, and most protocols utilize the 2D micropattern Matrigel stamps. One of the first publications using micropatterned chips to control cell growth is credited to Sakai and Nakazawa in 2007. Saki and Nakazawa created microfabricated chips with a silicone elastomer and polymethylmethacrylate coated with polyethylene glycol (to prevent cell adhesion) to control the spheroid shape and diameter of the growth of HepG2, liver-derived colonies (Sakai & Nakazawa, 2007). The micropatterned chips were created through microfabrication on a micro-milling system, though micropatterning is also achievable with photolithography (Alom Ruiz & Chen, 2007). In 2010, Sakai and Nakazawa tested cell growth with HepG2 cells, mESCs, and mouse neural progenitor stem cells, demonstrating the flexibility of this system. In the next year, Sakai would focus on generating mouse embryoid bodies without using hanging drop cultures. The issue with hanging drop culture was the lack of control in both the size of the drop and sometimes, the shape in which the micropatterns resolved (Sakai et al., 2011).

In 2014, Warmflash would take inspiration from Sakai and Nakazawa to investigate the ability of hESC to self-organize and form the three germ layers *in vitro*. Previous attempts involved applying growth factors to cells growing on plates without micropattern to produce irregular colonies and multiple fates but failed to yield consistent spatial ordering. Therefore, the use of micropatterns was essential in providing a geometric cue for the growth and expansion of hESC gastruloids in a circular area (Blauwkamp et al., 2012). The motivation behind BMP4 application

came from previous studies indicating that in fish, frog, and mouse embryos, spatial patterning during gastrulation is under the control of Nodal, BMP, and WNT pathways, which can be manipulated in hESC culture to create any of the three germ layers (Chambers et al., 2009; D'Amour et al., 2005; Kattman et al., 2011; Ozair et al., 2013).

Through immunofluorescent imaging, markers for specific germ and extraembryonic cell types were identified. In the first 24 hours of BMP4 treatment, morphological differentiation could already be detected. Initially, SOX2 expression is dominant throughout the gastruloid, with SMAD1/5/8 signaling elevated but confined to the colony edge. Measures of SMAD1/5/8 can be positively correlated with BMP signaling which Warmflash showed. Additionally, organization of SMAD1/5/8 shows potential evidence for self-organized differentiation. At 42 hours, 2D gastruloids form largely single-cell epithelial colonies in which germ layer formation is prominent, starting at the center of the gastruloids where only SOX2 was expressed (no NANOG, T/BRA, Eomesodermin (EOMES), SOX17 and NODAL signals), representing prospective ectodermal differentiation (M. Thomson et al., 2011; Warmflash et al., 2014). The first cellular ring distal from the center expressed NANOG and OCT4 with the presence of EOMES, GATA6, and CDX2, but not SOX2, indicating mesodermal fates (Z. Wang et al., 2012). In the next distal ring, expression of SOX17 (definitive endoderm) was detected and overlapped the second outermost ring of cells positive for EOMES or GATA6 with high levels of NANOG (endodermal differentiation) (Teo et al., 2011). Finally, cells in the outermost ring of cells expressed CDX2 without the mesendodermal markers (T/BRA, SOX17, GATA6) and pluripotency markers (OCT4, NANOG, and SOX2) (Chawengsaksophak et al., 2004). (**Figure 1.6**) Geometrically, the outer cells are similar to the extraembryonic trophoblast cells with gene

expression patterns resembling the trophoblast and amnion as revealed by Minn et al in 2021. However, the exact identity of these trophoblast-like cells has not yet been verified.

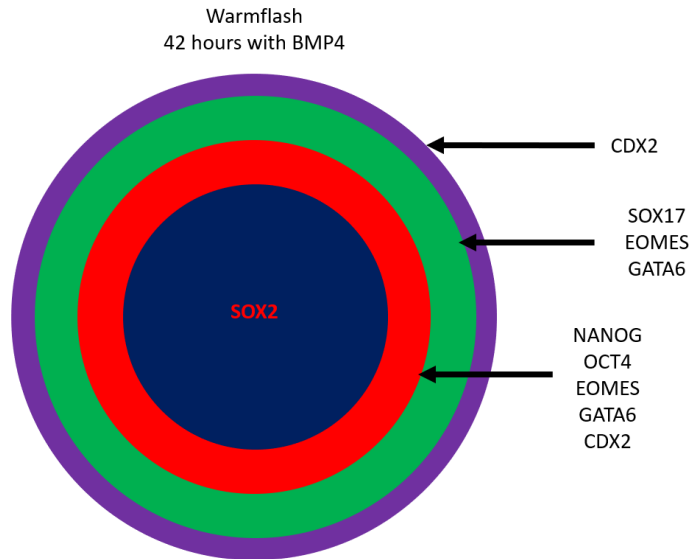


Figure 1.6: Expression pattern of Warmflash et al’s 2D gastruloids summarized.

Additional markers tested include: Phospho-ERK (pERK, marker of EMT), Fibroblastic Growth Factor (FGF, promotes EMT during primitive streak formation), and TF SNAIL with E-cadherin (E-CAD, promotes cell adhesion), where pERK was primarily localized to regions of T/BRA expression and upregulation of SNAIL (Nie & Chang, 2007). Cells in the primitive streak-like region piled and formed 2 to 3-cell layers, with higher activity of the cytoskeleton at the bottom layers, resembling migratory cells that have undergone EMT. And finally, cells in the top layer expressed epithelial cell adhesion molecule, EPCAM, and SOX2 whereas cells in the bottom layer expressed SNAIL. This would all indicate that the T/BRA expressing cells underwent EMT and ingressed towards the surface, then migrated underneath the upper epithelial layer (Warmflash et al., 2014). In summary, hESCs cultured in micropatterns and treated with BMP4

will generate 2D gastruloids with all three germ layers (Ectoderm, Endoderm, and mesoderm from center to edge), and an outer ring of trophoblast-like cells.

In 2020, Minn et al., would expand on the Warmflash experiments, by conducting extensive scRNA-seq analysis at 0, 12, 24 and 44 h of 2D gastruloid differentiation, showing its full cellular composition, the reproducibility of this self-patterning with a separate cell-line, self-organization through motility of disaggregated, and improving the micropattern protocol (Minn et al., 2020).

Until Minn et al in 2020, most microprint molds for cell culture were one-time use. Though the PDMS stamps could sometimes be used several times, molds would have to be re-created to make new stamps. In 2020, Minn would innovate a new method of microprinting that yields the same efficiency as Warmflash's micropatterns with a sturdy reusable mold that's easy to de-mold stamps. With the collaboration of McKelvey School of Engineering at Washington University in St. Louis, molds for the micro-patterns were fabricated with photolithography on a silicon wafer. This silicon mold would allow the user to reuse the mold, unlike in Warmflash's mold which was 3D printed with plastic. PDMS stamps created from these molds were also reusable. As for the cell lines, Warmflash utilized the H1, H9 and RUES1 lines, but focused mainly on RUES1. In Minn et al, H1 cells were mainly used as opposed to RUES1. Like Warmflash's protocol, these cells were treated with BMP4 upon seeding on 2D micropatterns and yielded consistent results of radial expression of SOX2 (ectoderm), T/BRA (mesoderm), SOX17 (endoderm), and CDX2 (EXE) from center to edge (**Figure 1.7**).

Extensive single-cell analysis, including IF-based quantification of immunofluorescent stainings to determine cell proportion and scRNA-seq was also conducted to reveal additional cell types not seen in Warmflash et al., (2014) using only antibody stainings. In brief, scRNA-seq revealed and antibody stainings validated seven clusters: Ectoderm (high SOX2, low POU5F1), Mesoderm 1 and 2 (T/BRA, MIXL1), Endoderm (SOX17, PRDM1, FOXA2), EXE like clusters (CDX2, GATA3), PGC-like cells (NANOS3, TFAP2C), EXE enriched in TE markers (CDX2, GATA3), amnion marker (TFAP2A, WNT6, HAND1), and NODAL pathway components (NODAL, GDF3, and TDGF1) (Chen et al., 2019; H. Ma et al., 2019; Niu et al., 2019; Zheng et al., 2019).



Figure 1.7: Expression pattern of Warmflash et al's 2D gastruloids summarized (Minn et al., 2020)

Minn's work also demonstrated that cells from 2D gastruloids exhibit cell sorting ability through cell migration/motility. Cell sorting of gastrula cells was demonstrated in classic experiments with amphibian gastrulae by Holtfretter et al and is thought to explain separation of germ layers, but has never been tested for mammalian gastrulae (R. Keller, 1996). To test whether 2D gastruloid cells have sorting capabilities, fully differentiated 2D gastruloids at 44 hours after BMP4 treatment, were dissociated into single-cell suspension, then reseeded onto new micropatterned wells and cultured without BMP4. IF analyses showed that initially (2 hours), markers of the three germ layers and the EXE exhibited a salt and pepper-like distribution, but in

just 24 hours cells tended to organize themselves, whether in respect to their own markers such as SOX2, T-BRA, SOX17 and CDX2. At 48 hours after disaggregation and reseeded, overlapping was seen with T/BRA and SOX2 cells, but not with SOX17. And lastly, live imaging would show that these cells actively migrate upon reseeded on the matrigel substratum likely providing the basis of the observed sorting.

1.3.2 2D embryoids compared to *in vivo* embryos.

scRNA-seq analysis of hESC 2D micropatterned gastruloids of Minn et al., was compared to Pijuan-Sala et al.'s mouse embryos at E6.5, 6.75, 7.0, 7.25, 7.5, Ma et al.'s *Cynomolgus* monkey embryos at 11, 12, 13, 14, 16, and 17 dpf, and Tyser et al.'s human CS7 gastrula (H. Ma et al., 2019; Minn et al., 2020; Pijuan-Sala et al., 2019; Tyser et al., 2021). Cross-species comparison of the scRNA-seq data revealed that Minn's 2D gastruloids showed high similarity to E7 mouse and 16 dpf monkey embryos, representing early-mid gastrula stage. Comparing E7 mouse and 16 dpf monkey embryos to the 2D gastruloids would reveal similar gene expression patterns, while also revealing an unknown cell population (**Table 1**).

First, two mesoderm clusters, mesoderm-1 and 2, were found to be consistent with mouse primitive streak and the nascent mesoderm respectively. In monkeys, mesoderm 1 and 2 indicates early gastrulation with a fraction of mesoderm 2 predicting monkey EXE mesenchyme. Additionally, nascent mesendodermal cells undergo EMT (up regulation of CDH2), corresponding to Warmflash's CDH2 (T-BRA) and mesendodermal (SOX17) cells, as well as the sc-RNA data by Minn et al (FGFR1 enrichment on SNAI1 for mesoderm 1 and 2). SNAI1 is

also a CDH1 transcriptional repressor and is evolutionarily conserved in EMT induction (Baum et al., 2008; Siemens et al., 2011). Not surprisingly, Minn's comparison demonstrated that cynomolgus monkey embryos showed more transcriptional similarities than in mouse. One example is the low level of *FGF8* in human 2D gastruloids (Minn et al) and human gastrulae (Tyser et al.). In mouse, *FGF8* is not important for EMT, but is required for cell migration away from the primitive streak (Sun et al., 1999). By contrast, in 2D human gastruloids mesoderm 1 and 2, Cynomolgus monkeys, and human CS7 gastrula mesodermal cell clusters express low *FGF8* but high *FGF17* transcript levels. This suggests a different gene encoding an FGF ligand of the same signaling group is responsible for promoting cell migration during human/primate gastrulation.

SOX17 and *PRDRM1* presumptive endoderm clusters were also identified; these clusters expressed exclusively both primitive endoderm markers GATA6 and definitive endoderm marker FOXA2. However, Cynomolgus monkey's dataset of these *in vitro* cultured embryos did not contain definitive endoderm, likely reflecting the early stage of gastrulation. Instead, the 2D gastruloid endoderm clusters corresponded to three different tissues: visceral endoderm, EXE mesenchyme, and gastrulating cells.

Next, human primordial germ cells like cells (hPGCLC) were discovered and compared with Cynomolgus monkey PGCs. PGCLC clusters were enriched in PGC markers (*NANOS3*, *TFAP2C*) with an expression profile of high *SOX17*, *TFAP2C*, *PRDM1*, *POUF51*, *NANOG*, *TBRA*, and low *SOX2* expression. In Cynomolgus monkeys, *SOX17*, *TAFP2C*, *NANOG*, and *NANOS3* were also co-expressed. TAFP2C is primarily co-expressed in *SOX17* positive cells

with some amnion markers (*TFAP2X*) but not in *T/BRA* mesodermal or *GATA3* EXE-like cells. And like with the Mesoderm cluster, a comparison of mouse embryos would show the hPGCLC clusters to be similar to the mouse epiblast.

Finally, EXE-like cluster was found to be enriched in TE markers: *CDX2*, *GATA3*, *KRT7*, *GATA2*, and *TBX3*, genes expressed during trophoblast differentiation in mice and humans. Amnion markers (*TFAP2A*, *HAND1*, *WNT6*) were also expressed in this cluster, with EXE-like cells co-expressing TE (*GATA3* or *CDX2*) but also amnion markers (*TFAP2A*). And in mice, EXE-like clusters of the gastruloids resembled the EXE ectoderm, despite murine gastrulae not having amnion cells. Monkey embryos were shown to contain the TE and amnion cell clusters and the EXE-like clusters resembled both TE and amnion equally with close gene expression correlation.

As a final comparison, Tyser et al in 2021 published the single-cell transcriptional profile of a single CS7 human gastrula, without extraembryonic cell types. This allows an accurate way to validate 2D gastruloids since Minn's analysis concluded the high likelihood of 2D gastruloids corresponding to human CS6-7 embryos. Some similarities between Tyser et al and Minn et al include EMT induction through upregulation of *SNAI1* and low *FGF8* with high *FGF17* as described above. Despite this, the sequencing data has not been utilized to its full potential, though these initial similarities in transcription do show great promise.

2D Human Gastruloid	Cyno Monkeys	Mouse
Mesoderm 1-2 cluster Low FGF8 and high FGF17	Early gastrulation and EXE mesenchyme Low FGF8 and high FGF17	Primitive streak FGF8 for cell migration away from primitive streak
Presumptive endoderm cluster Sox17 and PRDRM1 in GATA6 or FOXA2	Visceral endoderm, EXE mesenchyme, and gastrulating cells. N/A	N/A N/A
hIPGC PGC markers: NANOS3, TFAP2 With high SOX17, TFAP2C, PRDM1, POUF51, NANOG, T-BRA Low SOX2	PGS SOX17, TAFP2C, NANOG, and NANOS3 TFAP2C coexpressed with SOX17	Epiblast N/A
EXE like clusters TE markers CDX2, GATA3, KRT7, GATA2, TBX3 Amnion markers: TFAP2A, HAND1, WNT6	N/A N/A	Trophoblast differentiation and EXE ectoderm CDX2, GATA3, KRT7, GATA2, TBX3

Table 1: Summary of Minn et al’s scRNA seq analysis on 2D gastruloids against Cyno monkey and mouse embryos (Minn et al., 2020).

1.3.3 Limitations of 2D gastruloids.

2D gastruloids are one of the first models for studying human gastrulation that is made of human cells. Unlike any other species, studying human early development is constrained by both technical and ethical limitations, emphasizing the importance of *in vitro* models. Therefore, 2D gastruloids offer a great experimental platform for studying gastrulation because of their ability to reproducibly form all three germ layers, human PGC-like cells, and EXE in a spatially reproducible arrangement. This model is also excellent for studying the transcriptomics that underlies the events of gastrulation as shown by Minn et al’s cross-species analysis. However, 2D gastruloids come with the obvious limitation of being flat in culture, deviating from the 3D

structures found in most natural embryos. Moreover, having radial symmetry, 2D micropatterned gastruloids lack the axial mesoderm cell types, notochord and prechordal plate.

Lastly, Minn et al have demonstrated new potential cell populations in 2D gastruloids not seen in mouse and monkey embryos (such as the EXE cells expressing both TE and amnion markers), and with no further research on *in vivo* human embryos as the EXE tissues were dissected from the CS7 embryo analyzed by Tyser et al. It difficult to assess the validity of these new cell types. However, Minn et al., cautioned that the co-expression of trophectoderm and amnion markers in cells of the external 2D gastruloid cellular ring might represent artifactual cell type that does not exist *in vivo*. Finally, Tyser's analysis could prove useful for validating these 2D gastruloids, though further cross analysis is warranted. Nonetheless, 2D gastruloid models have served as the first big leap in the creation of human models of aspects of gastrulation.

1.4 Evolution of mouse models to study gastrulation

With advancements in cell culture techniques, the growth of embryonic and pluripotent stem cells has never been easier, allowing researchers to take advantage of growing, expanding, differentiating, and utilizing these cells in organoid cultures. One example of their utilization includes the creation of 3D embryo-like structures as potential model systems to study early human development.

1.4.1 Development of mouse embryoid bodies

Since Warmflash et al's publication, we have witnessed a boom in new publications for embryoid model development. For example, the Martinez Arias laboratory would publish the first protocol for generating 3D gastruloids with Sussanne C. van den Brink in 2014 and Peter Baillie Johnson in 2015. Both utilize mESC and similar culture conditions that allow mESCs to self-aggregate and form embryoid-like structures termed 3D gastruloids.

However, the first instance of 3D embryonic stem cell cultures, termed embryoid bodies (EBs) dates to 1985 with Doetschman et al. In this work, mouse blastocyst-derived embryonic stem cells were cultured in a suspension culture with Dulbecco's Modified Eagle Medium (DMEM) for 3 to 8 days. The results of their experiments would show irregularly shaped and sized EBs expressing markers of endoderm, mesoderm, ectoderm, and basal lamina, with the caveat of inconsistent the morphology (Doetschman et al., 1985). The next leap in EB progression was led by Desbaillets et al., in 2000, where mESC isolated from the ICM of mouse blastocysts were cultured in a hanging drop culture until the EBs could be observed (Desbaillets et al., 2000). As

EBs began to form reproducible shapes, EBs would later be called embryo models (EM). In 2004, Hopfl, Gassmann, and Desbaillets would refine their original protocol for EM formation (Höpfl et al., 2004). However, these early EM's mostly comprised of rudimentary tissues and organs that do not resemble the embryo in any significant way, steering the research on EM's to differentiate into more regularly arranged tissues that resemble native embryos.

One of the first structures created with EM's was the eye cup and anterior neural cortical structures, led by Eiraku, Lancaster, Nakano and Sasai. Amongst this group, Eiraku was the first to publish their results in 2011 where EB's autonomously formed optic cups, showing invagination of the neural retina (Eiraku et al., 2008). From 2012 to 2013, similar experiments were published, showing additional evidence that EM's were capable of generating various neuroectodermal and endodermal tissues, with the overall morphology of the EMs resembling aspects of E5.5 to E7.5 mouse embryos. Generation of optic cup EMs makes use of the three-dimensional aggregation culture (SFEBq) protocol created by Eiraku in 2008. The SFEBq protocol uses a differentiation medium consisting of recombinant proteins, serums, and compounds that act as WNT inhibitors, provide ECM, promote Hedgehog signaling, and provide Fetal Bovine serum (FBS) treatment (Eiraku et al., 2008, 2011; Lancaster et al., 2013; Nakano et al., 2012; Sasai et al., 2012).

More recent and advanced examples of EMs include murine ETS/X embryos (Embryonic stem cell, Trophoblastic stem cell (TSC), and/or Extra embryonic endoderm) pioneered by Žernicka-Goetz's laboratory. ETS/X mostly model the pre and post-implantation blastocyst and only reach the early stages of gastrulation. Thus, ETX/X EBs lack the ability to replicate the morphogenetic

events during gastrulation, though some of these concerns are addressed in ETS/X embryos in 2022, which are discussed in a later section. Generation of ETS/X embryos involves combining single ESCs with small clumps of TSC in a concave style well such as the AggreWell by StemCell Tech or a U well plate. A concave well helps to combine the ESC with TSC and EXE cells. The culture environment can be further modified like in Harrison et al where a 3D scaffold of ECM is used to act as a substitute for the primitive endoderm essential for epiblast polarization and lumenogenesis (Amadei et al., 2021; Harrison et al., 2017; Sozen et al., 2018).

Another recent EM is the post-implantation amniotic sac embryos (PASE). The intention of this model is to recapitulate many of the post-implantation embryogenic events of amniotic sac development by self-organizing into an epithelial cyst in an asymmetric amniotic ectoderm-epiblast pattern with just human pluripotent stem cells (hPSC) alone upon BMP4 treatment. This model also initiates a process similar to the posterior primitive streak development. Certain variations of developing PASE have been published, but all use Geltrex as a method to provide a 3D ECM to mimic the soft tissue bed of the uterine wall during implantation (Shao, Taniguchi, Gurdziel, et al., 2017; Shao, Taniguchi, Townshend, et al., 2017; Zheng et al., 2019). Similar to ETS/X embryos, the surrounding environment can be modified like with Zheng's method in 2019 where a combination of Geltrex and microfluidics can help achieve a more controllable model system that further recapitulates the post-implantation environment.

In summary, the evolution of the EMs is nothing short of impressive. However, for studying gastrulation, these EMs must show symmetry breaking and markers for the three germ layers. Therefore, many recent publications have created protocols for EMs that can exhibit these processes, termed 3D gastruloids.

1.4.2 Development of mouse 3D gastruloids

From 2014 to 2015, members of the Martinez Arias laboratory, Van den Brink and Johnson, would create the first EMs that could elongate, form derivatives of all three germ layers, and show clearly defined anterior-posterior, left-right, and dorsal-ventral body axes. These EMs would be termed 3D gastruloids with the purpose of modeling the early stages of development, most notably gastrulation (Baillie-Johnson et al., 2015; van den Brink et al., 2014). Like the eye cup organoid protocol, Van den Brink and Johnsons' protocol uses a 96 U well plate (or any plate capable of growing aggregates in suspension), but a major difference is the use of CHIR99021 (CHIR), a WNT/ β -catenin pathway agonist. The motivation behind activating WNT signaling comes from previous experiments demonstrating primitive streak induction in mESCs through activation of WNT/ β -catenin (Baillie-Johnson et al., 2015; Gadue et al., 2006; Turner et al., 2014; van den Brink et al., 2014).

5 years later, Veenvliet would make a new protocol for mouse gastruloids that could self-organize into trunk-like structures with somite and neural tube. For Veenvliet's protocol, CHIR and BMP inhibitor were also used, along with a plate coated with ECM (Veenliet et al., 2020). The year after in 2021, Girgin would make EpiTS gastruloids which takes inspiration from the ETS/X EMs by Amadei et al. mESCs are aggregated in a similar manner as Brink and Johnson, but co-cultured with TSCs, resulting in a hybrid structure capable of initiating gastrulation like events with axial morphogenesis to produce pronounced anterior and brain like regions. Interestingly, Activin is used in place of CHIR, reflecting the protocol shared by eye cup- like

organoids in Eiraku (2008). BMP4 is also shown to increase WNT activity compared to solely adding WNTA3A (Girgin et al., 2021).

Finally, in August of 2022, Amadei et al would make the biggest leap with the creation of mouse 3D gastruloids undergoing gastrulation events, and capable of generating a defined forebrain and midbrain region, a trunk comprising of neural tube and somites, a tail bud of neuroectodermal progenitors, gut tube, and most impressively, primordial germ cells and a beating heart-like structure (Amadei et al., 2022). The protocol is based on their previous work from 2021 where they created ETX EMs/gastruloids using a combination of EXE, TSC, and mESCs that transiently express GATA4. ETX EMs/gastruloids induced an embryo-like structure that was transcriptionally similar to the mouse gastrula but lacked the ability to recapitulate any of the morphogenic events such as gastrulation. Therefore in 2022, the ETiX EMs/gastruloids were created and were able to complete the morphological events of gastrulation and can develop up to the natural equivalent of E8.5 mouse embryos (Amadei et al., 2021). The major breakthrough in the ETiX EM protocol is the replacement of XEN derived from the visceral endoderm precursors with induced XEN (iXEN), XEN cells that transiently express GATA4 (**Figure 1.8**).

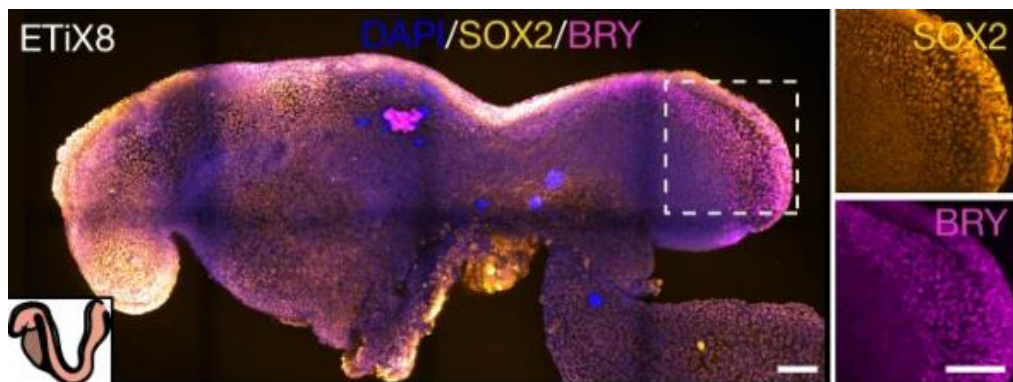


Figure 1.8: ETiX embyoids made with mESC. (Amadai et al., 2022)

As a model, ETiX EMs/gastruloids can generate a brain, neural tube, heart, foregut, somite, allantois, yolk sac structures, and even PGCs without the need to provide additional external signaling cues (such as Chiron). This captures the natural development of embryos such as the emergence and shaping of the three germ layers. However, issues with reproducibility were shown likely due to deviations in the EXE lineages from the lack of contact with a maternal environment. Regardless, it's still an improvement from using induced TS which showed lower levels of efficiency in embryonic tissue formation . Additionally, EtiX gastruloids were shown to display similar developmental events to natural embryos. This was demonstrated in a *PAX6* knockout experiment (knock out in only embryonic stem cells) to successfully recapitulate the defects that occur during neurulation in natural embryos, further validating these gastruloid as a potential model (Amadei et al., 2022; Y et al., 2020).

1.4.3 3D gastruloid models in Humans

Work on mESC 3D gastruloids/EBs has come a long way since the first heterogenous EBs during the mid-80's. Protocols with hESCs however, were only recently developed, but are quickly catching up to mESC-based models in such a short time span. First accounts of hESC 3D EBs/gastruloids are fairly recent, with Marikawa et al and Moris et al publishing their paper on the first human EBs/gastruloids in 2020.

Marikawa et al., (2020) focused on using hESC aggregates as a method for teratogenicity assessments, with an emphasis on studying teratogenic compounds and its effects on EB morphology. Marikawa et al.,'s protocol uses the H9 cell line with aggregation culture medium, Chiron, Nodal inhibitors, and retinoic acid. Marikawa et al.'s results focus on the morphology of

the aggregates and RNA-seq analysis in response to teratogenic compounds. The morphology of their aggregates before treatment resembles 48h embryoids from Moris et al (2020) after 5 days in culture, while embryogenesis regulators involved in axial patterning and morphogenesis (ALDH1A2, FGF8, HOXB9, MEOX1, and WNT5A) were shown to be upregulated (Y et al., 2020). However, the lack of germ layer verification makes it difficult to assess whether these EBs could be considered as gastruloids.

In comparison, Moris et al.,’s intentions were to observe the morphology, emergence of germ layers, and spatial transcriptomics, as well as test the reproducibility of the formation of different cell types. And unlike Marikawa et al, Moris et al used E6 and Nutristem media with specific Chiron treatment across multiple cell lines (Rues-2-GLR variants and Masterchef) without retinoic acid. Results from Moris et al emphasize the creation of gastruloids by showing expression of Ectoderm (SOX2), Endoderm (SOX17), and Mesoderm (BRA) at different time points during embryoid development (Moris et al., 2020) **(Figure 1.9)**

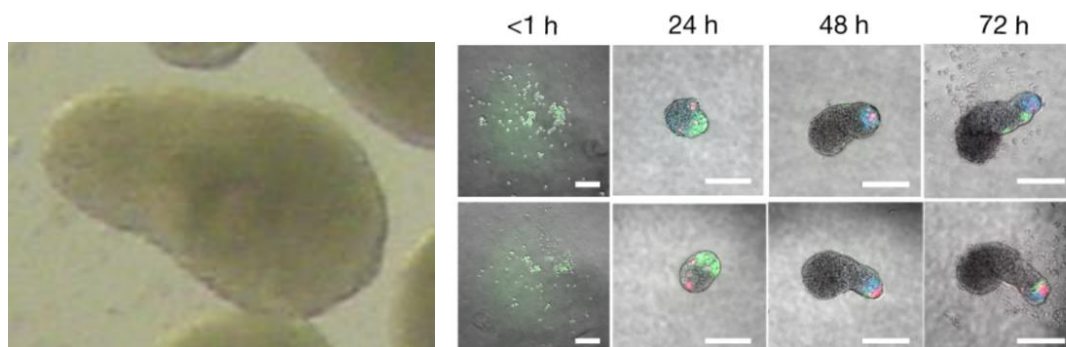


Fig 1.9: The first 3D gastruloids made with hESC , Marikawa et al on left, and Moris et al on right. (Marikawa et al., 2020, Moris et al., 2020)

Interestingly, Moris et al. demonstrate that retinoic acid reduced the elongation process of their gastruloid, increasing SOX2 expression and reducing T/BRA expression. Moris et al’s extensive tomography sequencing was compared to mouse embryos, demonstrating similarities such as

HOX gene expression, as well as differences like the lack of expression associated with developing anterior neural structures.

Progress in developing the protocol for human gastruloids continue to 2021, with Olmsted and Paluh, and Libby et al. Olmsted and Paluh's protocol use 9 ethnically diverse human induced pluripotent stem cell (iPSC) lines from fibroblast donors grown in N2B27 basal medium supplemented with Chiron and basic FGF. Olmsted and Paluh's model, referred to as the elongating multi-lineage organized (EMLO) gastruloid, was created with the intention of studying the neuronal trunk interactions with other primordial endoderm organ structures (primitive gut tube and enteric nervous system), making EMLO gastruloids a potential model for studying neurodevelopment of early CNS-PNS, endoderm, and neuromuscular processes. Some of the main discoveries of their work include the EMLO gastruloids ability to allow the primitive gut to be to act as a morphological organizer of neuronal fibers, inducing cell fates and pattern formation of other lineages (Olmsted & Paluh, 2021) (**Figure 1.10**).

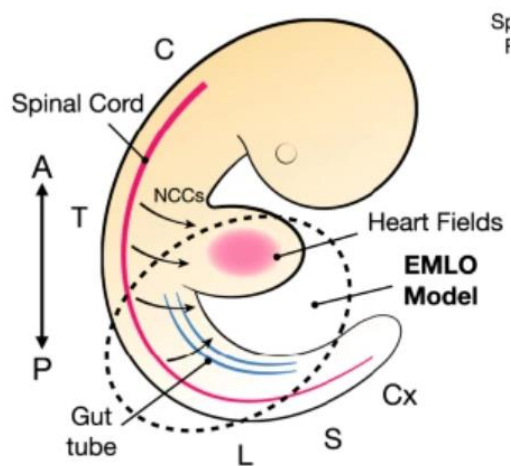


Figure 1.10: EMLO human 3D gastruloid model (Olmsted and Paluh., 2022)

Libby et al.'s protocol uses WTC11, WTC11-LaminB, H7, and H1 cell lines, with WTC11-LaminB being modified with CRISPR and TALEN to make an inducible knockdown of TBXT. During cell aggregation, cells were treated with Chiron, neural induction media, retinoic acid, and BMP inhibitors. Similar to Olmsted and Paluh's results, Libby et al.'s model demonstrated neural tube extension and axial elongation supported by temporal gene expression of TBXT, SOX2 neuromesodermal progenitors, and PAX6 neural progenitors. Additionally, Libby et al. show anterior to posterior HOX gene expression with distinct hindbrain regions from the brachial and thoracic regions, reflecting Moris et al.'s tomography analysis. Lastly, Libby et al.'s intentions are similar to Olmsted and Paluh, focusing on early human nervous system development as opposed to gastrulation (Libby et al., 2021).

1.4.4 Comparison of 3D human gastruloid models with other models.

An advantage of 3D gastruloids over 2D is the process of symmetry breaking and axis elongation allowed by the suspension of the cell aggregates. And similar to Minn's scRNA-analysis, Moris et al would take advantage of this 3D system through tomography sequencing and cross-species analysis (mouse gastruloid models and mouse embryos). As a result, through morphological and tomography sequence analysis, Moris et al concluded that their 3D models resemble CS8 to CS9 embryos with gene expression patterns associated with the onset of somitogenesis, a more advanced stage to CS6-7 thought to be modeled by 2D micropatterned gastruloids (Minn et al., 2020).

Comparing mouse gastruloids to 72-hour 3D human gastruloids, genes expressed in the tailbud of mouse embryos (*T/BRA*, *CDX2*, *CYP26A1*), cardiac and anterior endoderm development

(*KDR, MEIS1, MEIS2, PBX1, TWIST1, ISL1, IRX1, IRX2, IRX3, PRDM1*) were expressed in human 3D gastruloids as well, though transcripts of the genes associated with anterior neural development were not found. In general, there was high conservation of axial patterning (conserved pattern of mesodermal differentiation) between human and mouse gastruloids with posterior to anterior expression of tailbud genes (*T/BRA, CDX2, LFNG*). This mirrors the organization of paraxial mesoderm specification and differentiation in mammalian embryos (Koch et al., 2017), and somitogenesis in hESCs (Diaz-Cuadros et al., 2020; Loh et al., 2014). Other findings include *WNT3A* and *LEFTY1* expression (WNT and Nodal signaling, respectively), at the posterior end of human gastruloids suggesting high Nodal signaling (*NODAL, LEFTY1, LEFTY2, CER1*) (Moris et al., 2020).

1.4.5 Limitations of 3D human gastruloids

3D gastruloids address some of the limitations in 2D gastruloids such as the lack of spatial-temporal organization that resemble more of their natural in-vivo counterpart. At the same time, primitive streak formation and axial mesoderm formation are still lacking. Moreover, as 3D gastruloid cultures are seeded with mesenchymal-like cells, the role of EMT in their differentiation and morphogenesis remains to be determined. Additionally, 3D gastruloids come with the unique limitation in the lack of primate embryos past the equivalence of CS7 to compare to, especially regarding the transcriptomic characterizations. Therefore, most validation comes from mouse embryos and gastruloids, as well as morphological comparisons with preserved human embryos.

In conclusion, while advancing, 3D human gastruloids as models of gastrulation are still in their infancy, with the first publication released in 2020. Nonetheless, exponential progress has been seen and the current progress shows great promise for 3D human gastruloids as potential models.

Conclusion

Although 3D human gastruloids are still in their infancy stage, the amount of progress made in such little time is astonishing. The field of 3D gastruloids first started with mESC, taking nearly decades to establish a protocol capable of generating complex structures like a structure resembling a beating heart, or complex cells such as a primordial germ cell. With 3D gastruloids made with hESC, the first protocol was established in 2020, yet, protocols capable of forming distinct hindbrain regions, neural tube extension, and axial elongation have already been established in the span of just 2 years.

With this, the future of 3D hESC gastruloid models is promising. As demonstrated by many, the limitations of 3D gastruloids, both human and mouse, are being surpassed with every new publication. However, this brings up ethical concerns already in the field of human embryology, that is, once human 3D gastruloids models have advanced far enough, should there be limits on experiments regarding 3D human gastruloids? For example, Amadai et al have created 3D gastruloids made with mESC that are capable of creating primordial germ cells, though without sperm and eggs. However, once this barrier has been broken, would these gastruloids be considered living human beings? As the protocol for 3D gastruloids advance, the barrier that separates life and models become thinner. This would pause ethical concerns once human 3D gastruloids have reached this stage as well.

Despite this, we cannot completely abandon decades of research done to reach this point as the benefits of 3D gastruloids should not be ignored. Compared to natural embryos, in-vitro 3D gastruloids can be created using embryonic or pluripotent stem cells, and do not require the need to culture and use totipotent stem cells, a feat that has only recently been established in mice (Shen et al., 2021).

Additionally, the cells used to create 3D gastruloids can be genetically modified, such as the PAX6 knockout by Amadai et al, to study the morphological consequences of known genetic mutations. In fact, 3D gastruloids were recently found to be used to find new phenotypes by Brink and Oudenaarde in 2021, where it was discovered in mouse gastruloids, WNT activation can result in the excess of a somite like structure in the anterior region, potentially providing insight into certain human congenital malformations that can occur during gastrulation (Brink & Oudenaarden, 2021; Moris et al., 2021). And as long as the technical and experimental limitations remain, 3D gastruloids will always have their place in the field of human early development.

Chapter 2: Methods

2.1 Experimental setup

2.1.1 Materials

Resource type	Designation	Source or reference
Plates	96 well, U-Bottom plate with cell-repellent surface	Greiner, Bio-one
	6 well, Nun TM Cell-Culture Treated Multidishes	ThermoFisher Scientific
Media	mTeSR TM 1	StemCell Technologies TM
	TeSR TM -E6	StemCell Technologies TM
	NutriStem® hPSC XF Media	SARTORIUS
	Dulbecco's Modified Eagle's Medium-F12 (DMEM)	Sigma-Aldrich#D0697
	Dulbecco's Phosphate-buffered saline solution, No calcium, no Magnesium (DPBS -/-)	ThermoFisher Scientific
Cell-culture supplies	Ethylenediaminetetraacetic acid (EDTA) solution	Sigma-Aldrich
	Gentle Cell Dissociation Reagent (GDR)	StemCell Technologies TM
	BIOLIFE SOLUTIONS INC CryoStor®	ThermoFisher Scientific
	Corning® Matrigel® Growth Factor Reduced (GFR) Basement Membrane Matrix, LDEV-free	Corning
	Vitronectin	Gibco #A14700
	Accutase solution	Sigma-Aldrich
	Sylgard 184	Corning
	CHIR99021 (CHIR) #SML1046	Sigma
	ROCK Inhibitor (Y-27632)	Millipore Sigma
	Corning Cryogenic Vials (Cryotube)	StemCell Technologies TM

	Mr. Frosty™ Freezing Container	ThermoFisher Scientific
Antibodies	anti-SOX2 (Mouse monoclonal)	Cell Signaling Technology
	anti-SOX2 (Rabbit monoclonal)	Cell Signaling Technology
	anti-T/BRA (Goat polyclonal)	R&D Systems
	anti-SOX17 (Goat polyclonal)	R&D Systems
	anti-CDX2 (Rabbit monoclonal)	Cell Signaling Technology
	Anti-FOXA2 (Rabbit monoclonal)	Cell Signaling Technology
	anti-GATA3 (Rabbit monoclonal)	Cell Signaling Technology

2.1.2 Cell Culture Conditions

Cell lines

Two human embryonic stem cell (hESC) lines have been used for this thesis; the H1 cell line, obtained directly from WiCell (karyotype 46, XY, WiCell, Madison, WI); and RUES2-GLR, kindly provided by the Brivanlou lab (Rockefeller University).

Cell culture protocol

The following protocol was used, regardless of cell type, for unfreezing, initial plating, maintaining, expanding, freezing or splitting, and controlling contamination.

Maintaining sterile culture conditions

Anything going into the laminar flow hood was sterilized with 75% EtOH. When the laminar flow hood was no longer needed, all media was removed and stored at their respective temperatures before wiping the work surface with 75% EtOH and sterilizing the vacuum tube with 5% bleach. Once the hood has been wiped, the UV light was turned on overnight or until next use.

Cell culture maintenance

Cells were maintained daily in a 6-well plate through the exchange of their respective media. For each well, 2 mL of media was removed and replaced before incubating in a humidified incubator overnight (37°C, 5% CO₂). Normal procedures for maintenance included cleaning colonies from differentiated and/or dead cells and washing with Dulbecco's Modified Eagle's Medium (DMEM/F12) or Dulbecco's phosphate-buffered solution (PBS) without magnesium and calcium (DPBS -/-) twice before media was applied.

Generic protocol for cell maintenance

For maintaining and expanding cell lines, sterile 6 well plates coated with a matrix such as Vitronectin or Matrigel were used. Vitronectin was dissolved at a final concentration of 0.5 µg/cm² with DPBS (-/-) and Matrigel was dissolved in DMEM/F12 at a final concentration of 0.25 µg/cm². After dissolving, plates were incubated at room temperature (RT) for at least 1 h, or maintained at 4°C until use. Passages of cells in culture were similar for each cell type used in the described experiments.

Thawing cells: Cells were taken from a liquid nitrogen chamber (-196°C) and placed in a warm bath at 37°C for not more than 5 min. Then, cells were transferred to a 15 mL tube with mTESR media and centrifuged at 300 RCF (relative centrifugal force, ~1000 RPM) for 5 minutes. Once the supernatant was removed, pellet was disaggregated with 1 mL of mTESR and transferred to a plate containing an additional 1 ml of mTESR.

Freezing cells: When colonies reached 60 to 70% confluency, they were considered ready to be transferred to a new well. In the case of normal maintenance, cells were dissociated with Gentle Dissociation Reagent (GDR). Whereas, if cells were going through a process of differentiation, they were split with either Accutase or EDTA (5 mM in PBS). Once the dissociation reagent was added, cells were incubated from 5 to 10 min at RT, after which GDR was aspirated and 0.5 mL of Cryostore (ThermoFisher Scientific, 210373) and culture medium was added to the well. Cell colonies were detached from the bottom of the well using a cell scraper and collected into a Cryostor tube. Cryotubes were transferred to Mr.Frosty™ or a Cell freezing container and maintained at -20°C overnight. Cell freezing containers were then transferred to -80°C overnight before transferring to liquid nitrogen (-196°C).

Handling contamination

In the event of a contamination, usually detected in a plate with the help of an optical microscope, contaminated plates were sterilized and discarded. The laminar flow hood, along with any equipment present under the hood was cleaned with bleach. Media used for the plate was discarded, and other plates present in the incubator were monitored for additional contamination. Before using the hood again, a cycle of UV exposure was applied for at least 1 h.

Cell-specific requirements

H1: Cells were maintained as specified with mTeSR (StemCell Technologies, 85850) media, grown in Matrigel, and cleaned with DMEM/F12.

RUES2-GLR: Cells were maintained as specified with Mouse embryonic fibroblast conditioned media (MEF-CM), grown in Matrigel, and cleaned with DMEM/F12.

MEF cell line was purchased from Applied StemCell (cat #ASF-1213) and maintained in FM10 medium.

MEF-CM media preparation

FM10 medium was prepared by mixing 439 mL of DMEM, 50 ml of Fetal Bovine Serum (FBS), 10 mL of GlutaMAX, and 1 mL of β -mercaptoethanol in a final volume of 500 mL. After filtering through a 0.22- μ m filter, media was stored in falcon tubes of 50 mL at -20°C.

HUESM medium

HUESM medium was prepared by mixing 379 ml of DMEM media with 100 mL of knockout serum replacement, 5 mL of GlutaMAX, 5 mL of Non-essential amino acids solution (NEAA), 1 ml of β -mercaptoethanol and 10 mL of B27 supplement without vitamin A in a total volume of 500 mL. Mixture was filtered with 0.22- μ m filter unit, aliquotted in 50 mL tubes and stored at -20°C.

MEF-CM

A 5 layered flask (875cm²) was coated with 0.1% gelatin for 20 min at 37°C. Nine vials of irradiated MEFs (60x10⁶ cells) were thawed and resuspended in 125 mL of FM10 medium. The gelatin was aspirated from the flask and mixed with MEF/FM10. The flask was then incubated overnight before the medium was replaced with fresh HUESM. Collection of HUESM was followed daily for up to 9 days. MEF-CM aliquots were stored at -80°C for up to 6 months. Before using, bFGF was added at a concentration of 20 ng/mL

MEF cells served as feeder cells supporting the growth of undifferentiated mouse or human ESCs and iPSCs. MEF cells were isolated from 13.5-day old mouse embryos and should have

minimal number of passages. Before being used as feeder cells, MEF cells were mitotically inactivated by γ -irradiation or mitomycin-C treatment. BMP4 was resuspended in 4 mM HCl solution containing 0.1% BSA to the final concentration of 50 $\mu\text{g}/\text{mL}$. Aliquots of 20 μL each were stored at -20°C .

2.2 Human 3D gastruloids

Protocol:

To create human 3D-gastruloids from hESCs, we adapted a protocol from Morris et al., (2020). This protocol was applied for both H1 and RUES2-GLR cell lines that had previously been grown in their normal media as described in the previous paragraph. After at least 2 passages, cells were transferred onto a $0.5 \mu\text{g}/\text{cm}^2$ vitronectin precoated tissue culture-treated plastic plates with Nutristem medium (Sartorius, #05-200-1A). Cells were grown in these conditions for at least 2 days but for no more than 6 passages. When cells reached 30-40% confluency, Nutristem was supplemented with Chiron in a cell line-dependent concentration for 24h. Next, the media was removed and cells were dissociated with 0.5 mM EDTA in DPBS (-/-) for 5 to 10 minutes at RT. EDTA was diluted with 1 mL of Essential 6 media (E6, StemCell Technologies, #05946) supplemented with 1:2000 Rock inhibitor (ROCKi). Once cells were collected in a 15 mL tube and centrifugated at 1000 RPM for 5 minutes, the supernatant was removed and the pellet was resuspended in 200 μL of E6 with 1:2000 ROCKi to make a single-cell suspension. Cells were then counted and seeded at a density of 200-400 cells/well in an anti-adherence treated 96 U well plate (Greiner Bio-one, #650970). To help cells sediment to the bottom, the 96 well plates were spun at 700 RPM for 2 minutes before incubating at 37°C and 5% CO_2 . After the first 24h, 150

μL of E6 media was added to all wells and every subsequent day, 150 μL of E6 was replaced with fresh media until the experiment's end.

Cell line-specific details:

In my experiments, I optimized the Moris et al., 2020 protocol for 3D gastruloid formation and arrived with the following conditions:

For the RUES2-GLR cell line, I used 3.25 μM of Chiron in Nutristem for the pre-treatment, 0.5 μM of Chiron for the post-treatment, and a total concentration of 200-400 cells in 40 μL of E6/Ri.

For the H1 cell line, I used 3.00 or 3.25 μM of Chiron in Nutristem for the pre-treatment, 0.5 μM of Chiron for the post-treatment, and a total concentration of 400 cells in 40 μL of E6/Ri.

2.3 3D to 2D gastruloids protocol

Microprint preparation

Polydimethylsiloxane (PDMS) stamps were created with a silicon mold adapted from Minn et al., (2020). Briefly, PDMS with Sylgard 184 curing agent was mixed to a 10:1 ratio, poured onto and ??? degassed over the mold with a vacuum, and cured at 60°C overnight. The cured PDMS stamp was peeled off, sterilized in 75% ethanol solution and dried in a laminar flow hood. Matrigel diluted in DMEM/F12 at 1:20 dilution was applied over the entire surface of the stamp and left in the laminar flow hood at RT for 45 minutes. The Matrigel solution was aspirated off with canned air

and transferred to a 12-well plate with tweezers, face down with 50 g weights on top for 20 minutes. Stamps were removed and rinsed in 75% ethanol for future use. Matrigel printed plates were washed with DPBS (-/-) 3 times and stored in DPBS (-/-) at 4°C until use.

2D microprint reseeding

3D-gastruloids were collected from 96 well plates after 72h to 96h differentiation and transferred into a 15 mL tube. The supernatant was removed and substituted with 0.5 mM EDTA in DPBS (-/-) for 5 to 10 minutes incubation at RT. To dissociate the gastruloids, the suspension was pipetted up and down with a 1 mL pipet for up to 10 times and centrifuged at 1000 RPM for 5 minutes. The resulting pellet was then dissociated using warm mTeSR (37°C) supplemented with 10 µM ROCKi. Cells were counted on a Countess II Automated Cell Counter and seeded onto a 12-well plate with 2D micropatterned Matrigel from a range of 100,000 to 200,000 cells/cm² per well. After 4h, media was replaced with mTeSR and replaced daily as needed.

Immunofluorescent imaging and analysis

Immunofluorescence staining

3D gastruloids were collected at different time points of differentiation and transferred into a 15 mL tube using a 1 mL pipette with a cut tip to prevent gastruloids from breaking. Once all gastruloids were collected, media was replaced with fresh 4 % Paraformaldehyde (PFA) in DPBS and stored overnight at 4°C. The day after, PFA was removed and gastruloids were washed 3 times with DPBS at RT. Gastruloids were then treated with blocking solution (DPBS (-/-), 0.1 % Triton X, and 3 % Normal Donkey Serum for 1h and incubated with primary antibodies overnight at 4°C.

Next, three washes with PBS-Tween (0.1 %)(PBST) were followed with an incubation of blocking solution with a secondary Ab (1:1000) and DAPI (1:2000) for at least 1h at 4°C. Finally, gastruloids were washed three times with PBST and maintained in DPBS (-/-) at 4°C until images were taken.

Microscopy and fluorescent imaging

On a glass slide, a drop of 2 % methylcellulose was placed at the center. Gastruloids were gently collected with a 200 µL pipette, and 20 µL of DPBS (-/-) gastruloid suspension was deposited into the methylcellulose drop. A microscope coverslip was gently placed over the methylcellulose drop with gastruloids. Imaging was performed once the coverslip has fully settled onto the slide.

All confocal images were taken with an Olympus IX81 Inverted Spinning Disk Confocal Microscope with 10X lenses. The channels used were DAPI (409nm), GFP (488nm), TxRed (555nm), and Cy5 (647nm). Z stack thickness as well as intensity and exposure time were adjusted accordingly based on the individual gastruloids due different orientation of the 3D gastruloids.

After imaging, gastruloids were preserved with nail polish or tape to seal the edges of the glass cover slip, preventing dehydration of the methylcellulose. Slides were stored in a dark container at 4°C.

Image quantification

For all image quantifications (unless specified), Fiji was used to analyze fluorescent microscopic images, as well as quantify the length-to-width ratio for embryos as previously reported (Schindelin et al., 2012).

Length-to-width 3D gastruloid ratio was obtained by dividing the gastruloid length to its width using the number of pixels. The length was measured by measuring the apex of the elongated tip, to the apex at the bottom. If gastruloids were curved, multiple midpoints were defined along the gastruloid body and length was measured with an arbitrary unit. For gastruloids with multiple axes of elongation, only the longest elongated structure was measured. The width was measured by taking the measurement of the diameter of the gastruloid (non-elongated portion resembling a circle) (**Supplementary 1**)

Chapter 3: Results

3.1 Optimization of H1 cell line protocol and RUES2-GLR comparison.

To optimize the protocol for creating H1 3D gastruloids, we adapted the method developed by Moris et al in 2020. H1 cells were first grown in Matrigel and mTeSR at 50 to 60% confluency before being transferred to a new plate coated with Vitronectin and fed with Nutristem. This step is crucial as it is very important that the cell density and size of colonies need to be homogenous across all experiments. Colonies with 30 to 40% confluency are representative of the stage of pre-treatment (Moris et al., 2020) (**Figure 3.1**).

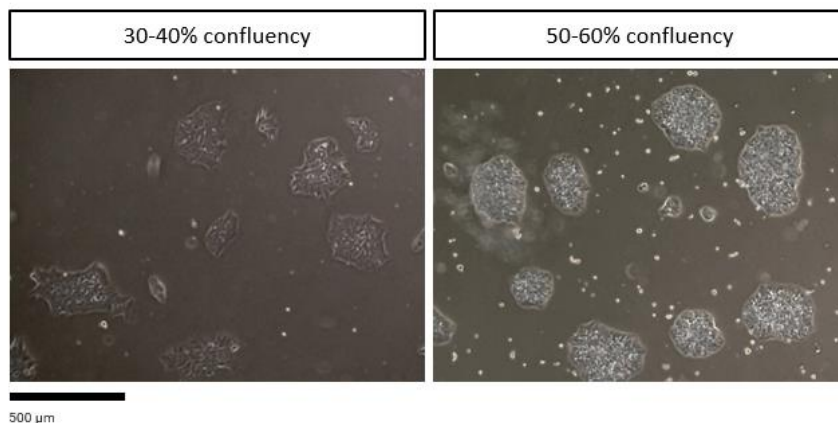


Figure 3.1: H1 cell culture confluency comparison.

In my first experiment, I performed a titration on the Chiron (a Wnt pathway agonist) concentration used for the pre-treatment step. Similar to what is described in the protocol by Moris et al, smoother edges of the colony were evident when Chiron was applied compared to the non-treated cells. However, no significant differences were observed from 3 to 5 μM (**Figure 3.2**)

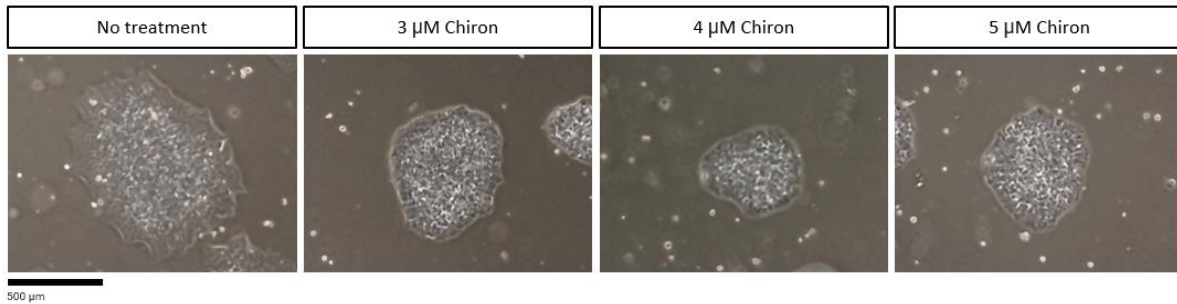


Figure 3.2: Comparison of H1 colonies before and after different Chiron concentration during pre-treatment.

Cell Number

In the Moris protocol, most of the work had been performed on the MasterShef7, S4-GATA6-GFP, and RUES2-GLR cell lines. To optimize the protocol of 3D gastruloid formation with the H1 cell line, I performed titration experiments for the number of cells to seed in each well, and the pre/post-treatment concentration of Chiron. Once the colony size and density conditions were similar to what's shown in figure 3.1, I started by optimizing the Chiron pre-treatment concentration with two conditions, 2.5 and 5 μ M. 24 hours after treatment, cells/colonies were dissociated, centrifuged, and plated onto a 96-well plate with an anti-adherence coating in E6 medium. I added ROCKi to the E6 medium to prevent cell death after splitting. The number of cells tested was 200, 400, 800, and 1000 cells per well. Cells were cultured up to 96 h and E6 media was changed daily in each well. Media was exchanged with a 200 μ L pippete tip and aspired with the tip near the wall of the well, but not touching the bottom to ensure that gastruloids were not destroyed or removed. **(Figure 3.3A and Figure 3.3B).**

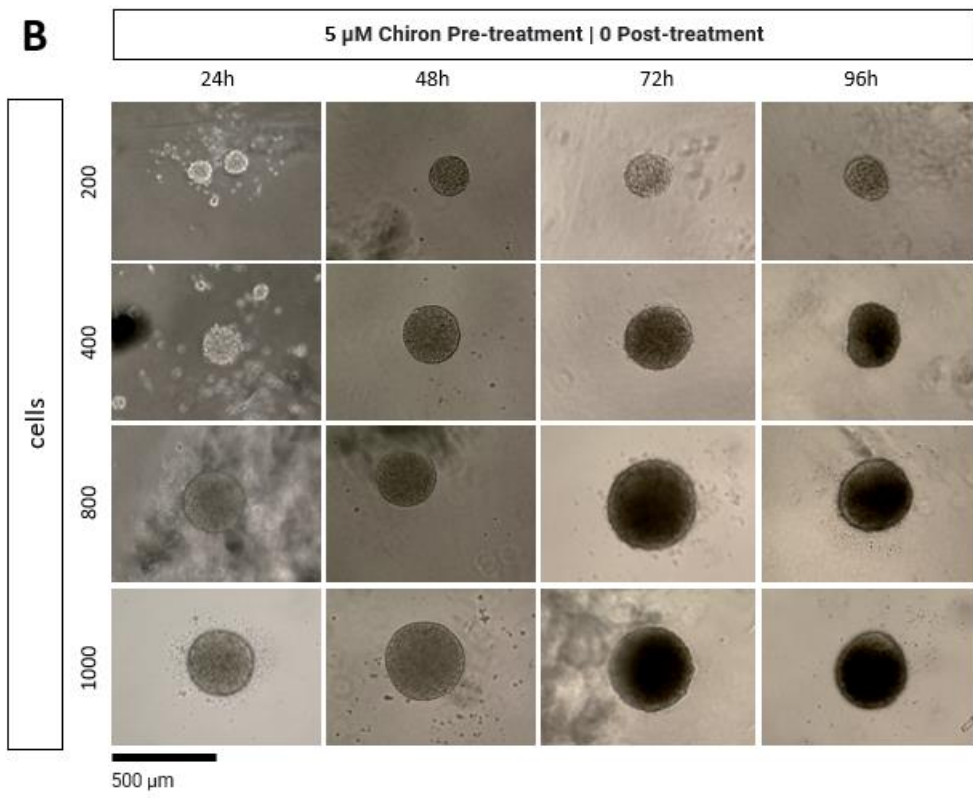
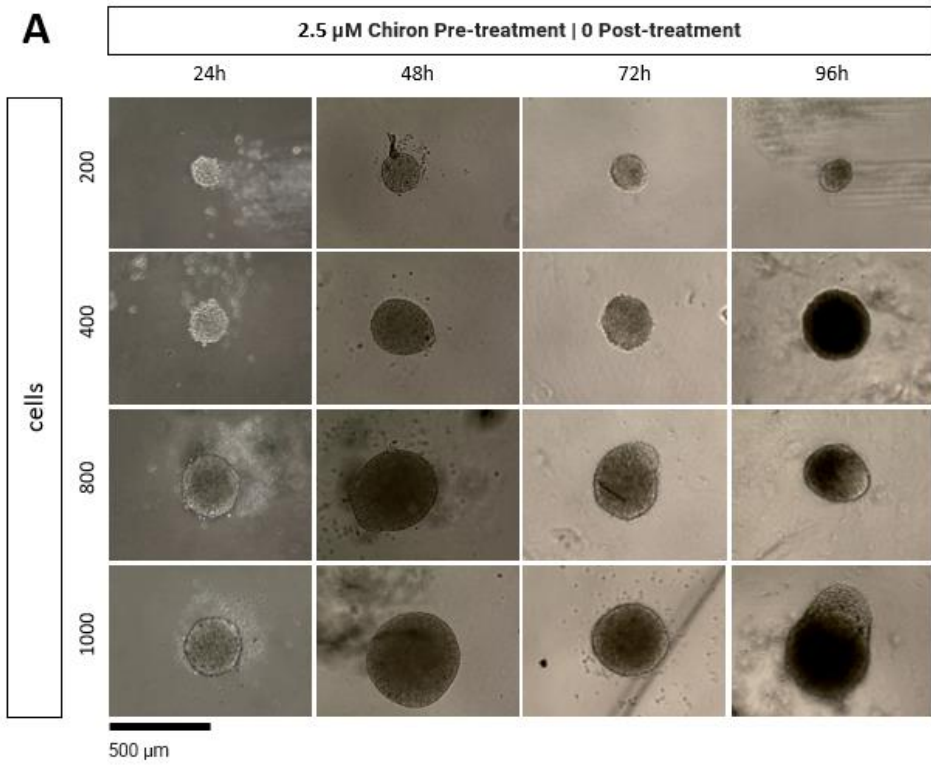


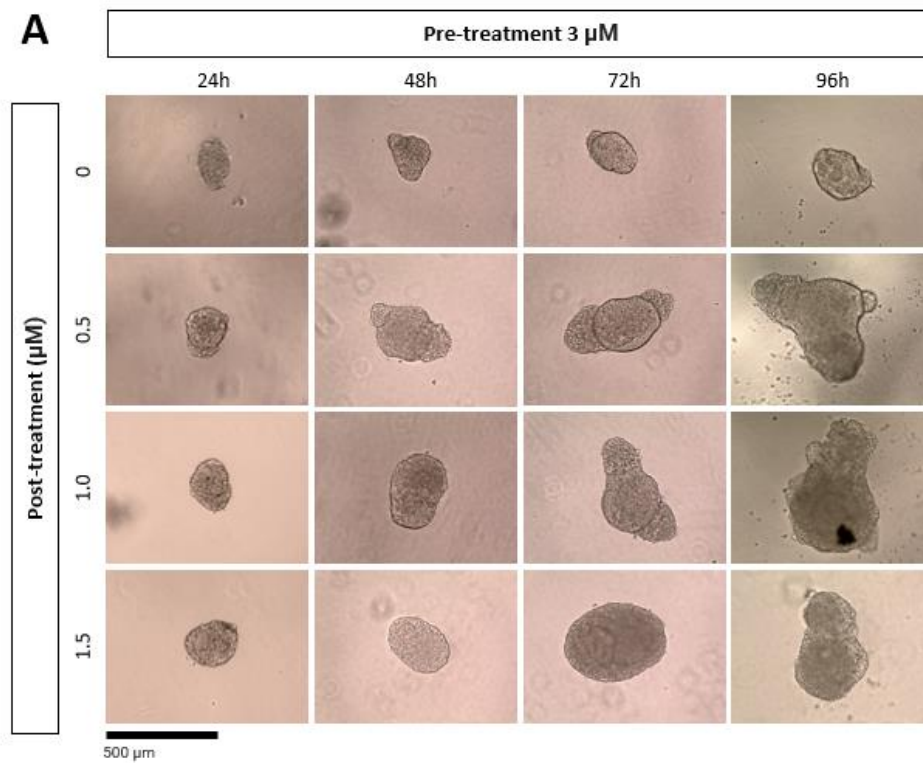
Figure 3.3: H1 3D gastruloid culture: comparison of cell number and Chiron concentration during pre-treatment with no Chiron in post-treatment across 24h to 96h. (A) 2.5 μ M Chiron pre-treatment. (B) 5 μ M Chiron pre-treatment.

Number of cells seeded appeared to influence the size of gastruloid rather than morphology, and aside from elongation, difference in gastruloid size was not noticeably from 24 h to 96 h, suggesting spatial awareness to control growth. Gastruloids pre-treated with 5 μ M show a circular morphology throughout all time points and cell number, whereas gastruloids pre-treated with 2.5 μ M show some elongation from 72 h to 96 h.

In the Moris et al protocol, cell density varied from 200 to 800 cells for MasterShef7, S4-GATA6-GFP, and RUES2-GLR cell lines. Therefore, I used 400 cells in subsequent experiments as it was easier to aggregate into the 96-well plate during the initial step of seeding cells, and it allowed me to focus on optimizing the Chiron concentration at the pre and post-treatment steps. Although the results in Figure 3.3 do not suggest strong differences, I thought that a higher number of cells may inhibit elongation.

Chiron pre-treatment

In my next experiment, I aimed to further optimize the pre-treatment and post-treatment concentration of Chiron. Keeping the cell number constant at 400 cells/well, I tested pre-treatments of Chiron 3, 4, and 5 μM with post-treatments of 0, 0.5, 1, and 1.5 μM to cover a broad range of concentrations (**Figure 3.4A, 3.4B, & 3.4C**).



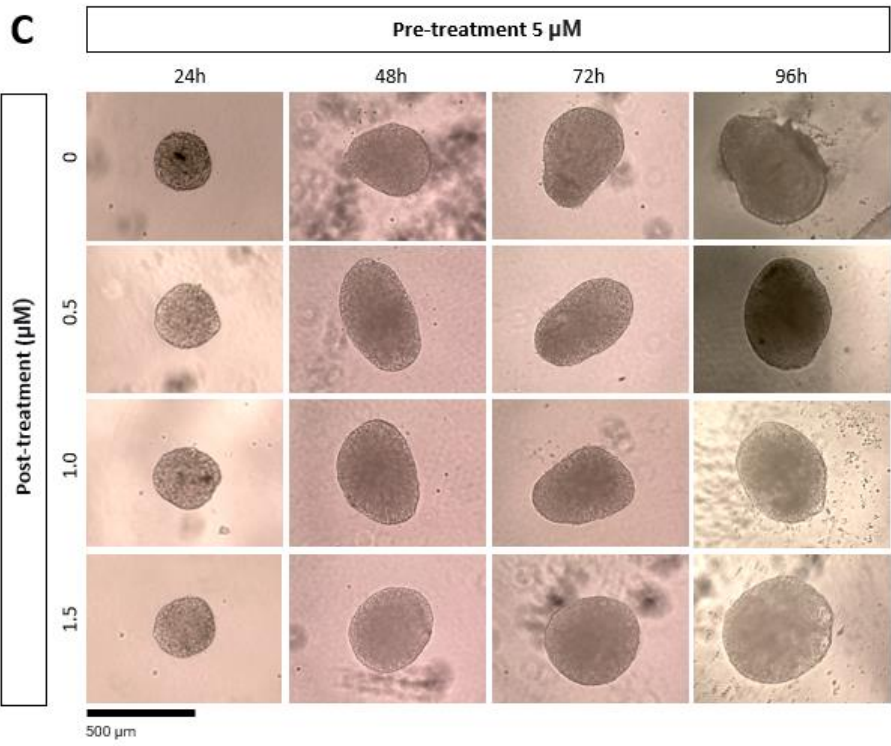
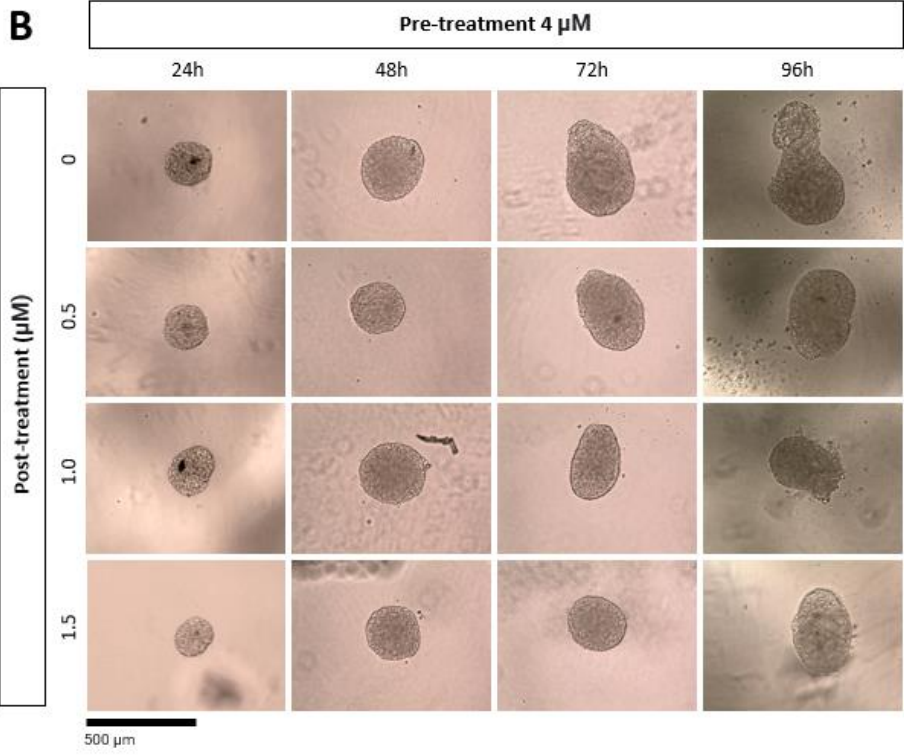


Figure 3.4: H1 3D gastruloids derived from 400 cells and different pre/post-treatment concentrations of Chiron, observed over 24 h to 96 h. 3 μM (A), 4 μM (B), and 5 μM (C) pre-treatment was tested in a range of 0.5-1.5 μM Chiron post-treatment.

In this experiment I confirmed that higher concentrations of Chiron during pre- and post-treatment inhibited gastruloids' elongation, resulting in a more spheroid morphology. The highest Chiron concentration applied during pre and post-treatment (5 μM and 1.5 μM respectively) resulted in a complete spheroid shape. However, with a lower Chiron dosage during post-treatment, the gastruloids presented a modest elongation in the form of an oval shape.

In H1 3D gastruloids treated with 4 μM Chiron, the morphology was consistent but still not comparable to a lower dosage of Chiron. Indeed, in cells pre-treated with 3 μM , elongation started to become strongly evident at 24 h. This feature became more prominent with the increase in post-treatment Chiron dosage. In absence of post-treatment, gastruloids failed to elongate altogether but were not as spheroid as the conditions: 4 μM and 5 μM with 1.5 μM post-treatment. On the other hand, having a post-treatment of 1.5 μM delays the elongation until 96 h. Therefore, these results suggest that the best post-treatment condition is a range of 0.5-1 μM . This notion is also supported by the length-to-width ratio measurements from embryos presented in **Figure 3.5**.

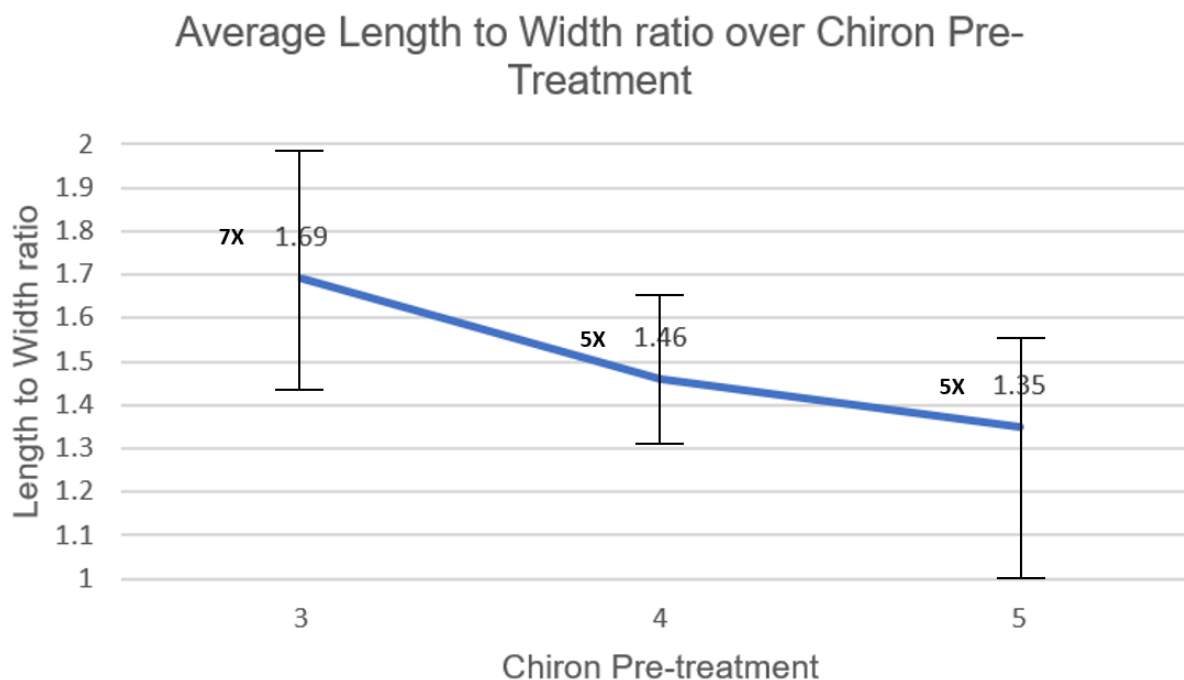


Figure 3.5: Graph of length-to-width ratio of 3D gastruloids from Figure 3.4, as a function of different Chiron concentration during pre-treatment .

The graph (**Figure 3.5**) suggested that a pre-treatment of 3 μM Chiron was optimal, leaving the optimization of Chiron during post-treatment as the next experiment. However, a more detailed titration of Chiron in the post-treatment (0.3, 0.4, 0.5, 0.6, 0.7, and 0.8 μM) with 3 μM pre-treatment and 400 cells, showed no clear difference in the morphology of the gastruloids (**Figure 3.6**). Additionally, the average length-to-width ratio at 72 h was graphed, showing no significant difference or correlation with different post treatment Chiron concentration (**Figure 3.7**).

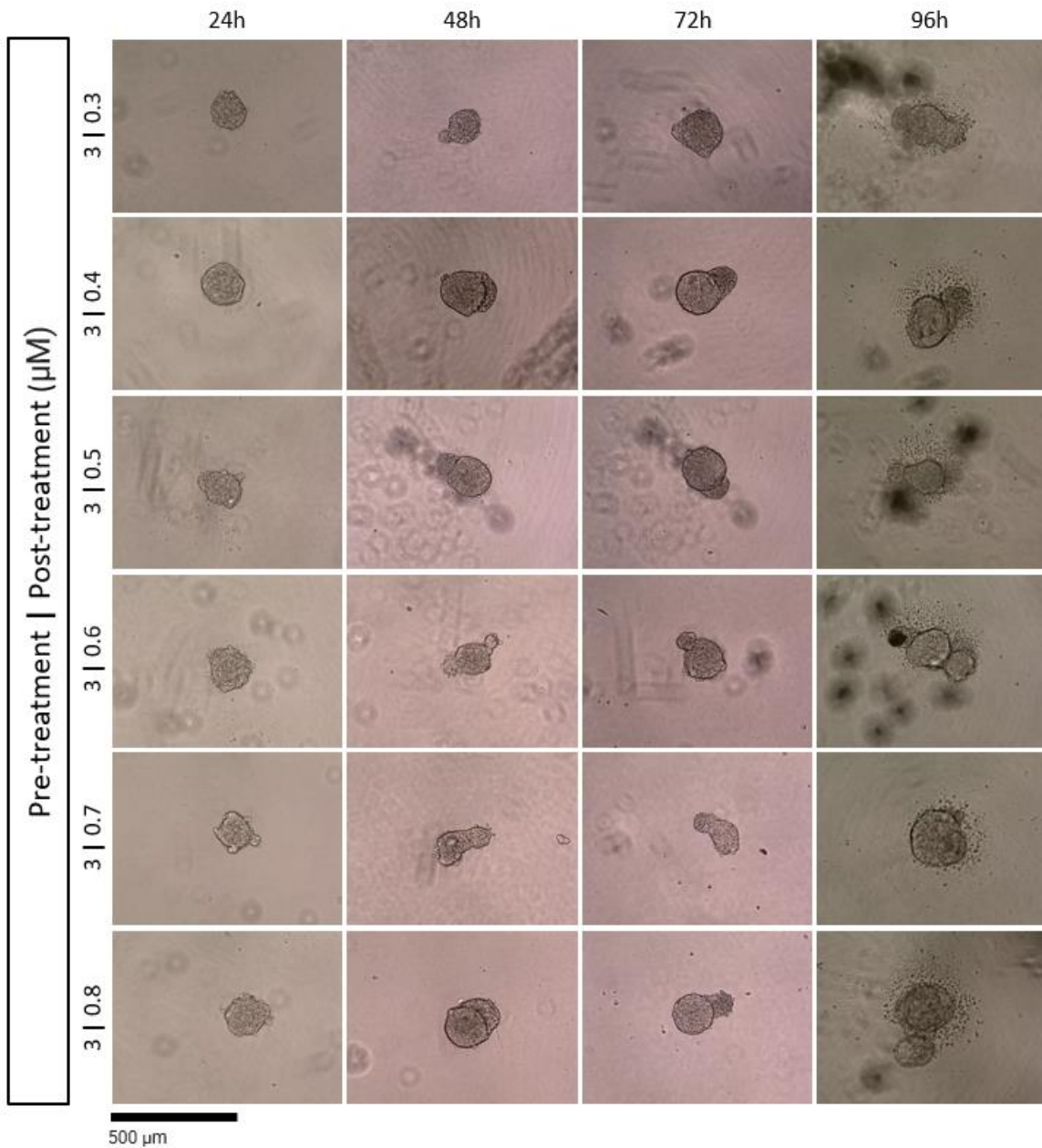


Figure 3.6: H1 3D-gastruloids derived from 400 cells, pre-treated with 3.00 μM and 0.3 to 0.8 μM post-treatment of Chiron from 24 h to 96 h.

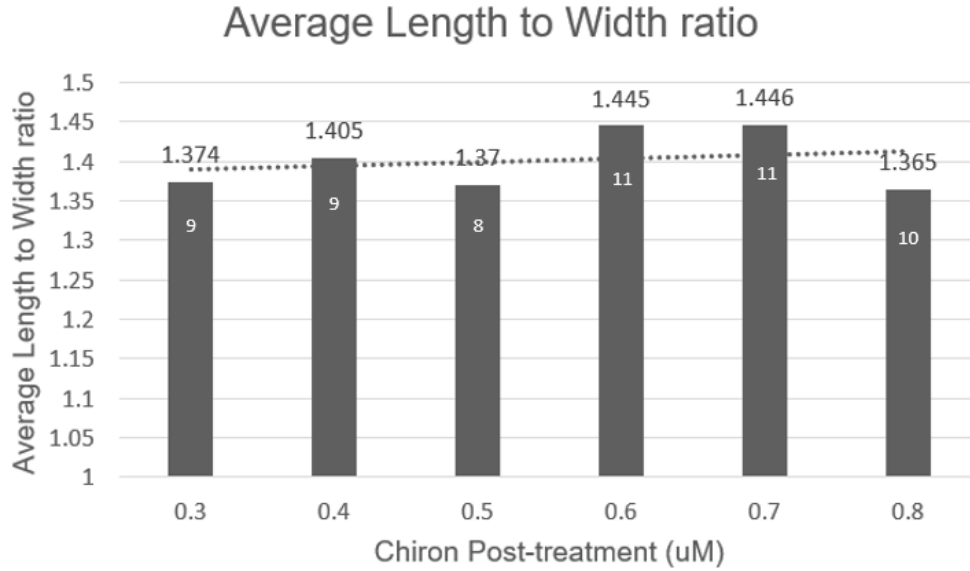


Figure 3.7: Bar graph of the length-to-width ratio of gastruloids from Figure 3.6, plotting against different Chiron concentrations during post-treatment.

From 0.3 to 0.8 μM Chiron, I chose a post-treatment concentration of 0.5 μM for subsequent experiments based on Moris et al's optimized protocol for RUES2-GLR gastruloids (3.25/0.5 μM Chiron pre/post-treatment) due to high similarity with my protocol (3.00/0.5 μM Chiron pre/post-treatment). Because Moris et al's conditions were similar to what I established for H1 cells, I compared our protocols to each other in my next experiment with the following conditions: 3 and 3.25 μM at 0.5 μM Chiron pre and post-treatment in both H1 and RUES2-GLR cells, observing changes in morphology overtime (**Figure 3.8**).

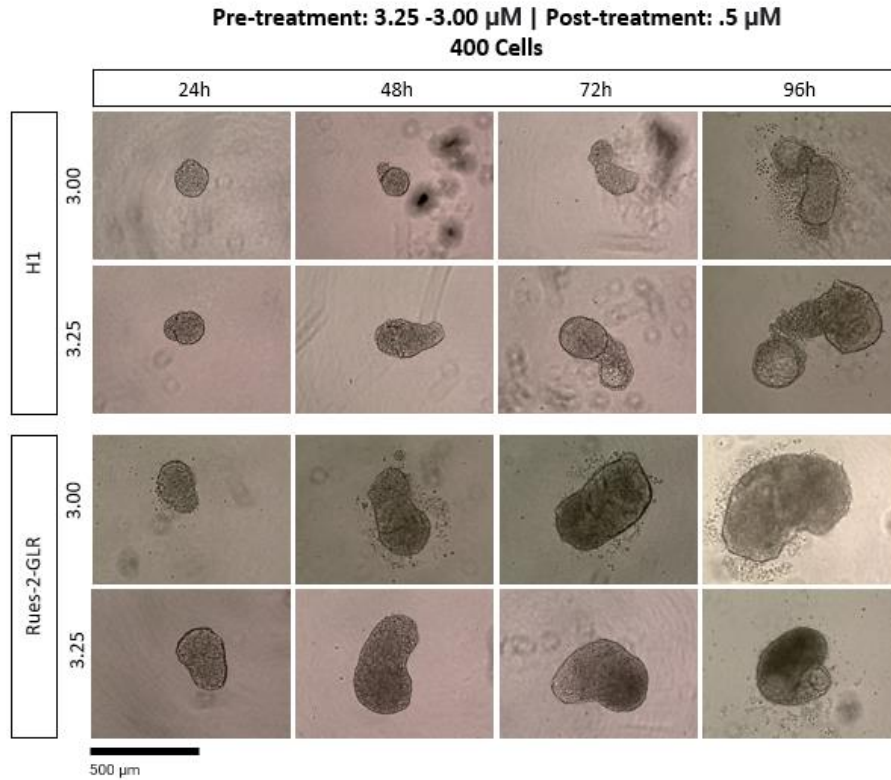


Figure 3.8: Comparison of H1 and RUES2-GLR gastruloid differentiation with 3.25 μ M / 3.00 μ M pre-treatment and 0.5 μ M post-treatment of Chiron from 24 h to 96 h.

In H1 gastruloids, elongation became evident already at 48 h with a Chiron pre-treatment of 3.25 μ M, while elongation occurred at 72 h for a lower Chiron concentration (3 μ M) . However, by 96 h in the H1 3.25 μ M group, excessive elongation was observed, likely resulting in the partial disaggregation at the gastruloid tips. Additionally, gastruloid elongation at 3 μ M Chiron for both RUES-2GLR and H1 gastruloids were not as stable when compared to their respective 3.25 μ M groups. When compared to all previous pre and post-treatment conditions of H1 3D gastruloids (Figure 3.4, 3.5 & 3.6), all H1 3D gastruloids showed less regular morphology compared to those generated from the RUES2-GLR cells (smoother, bean like shape), suggesting that RUES2-GLR gastruloids may be more robust.

In RUES2-GLR cells, elongation was slightly more pronounced at 48h in the 3.25 μM compared to the 3 μM condition. And like H1 gastruloids, both the 3.00 and 3.25 μM RUES2-GLR gastruloid groups over-elongated at 96 h, but curled instead of breaking off, again, supporting the notion that RUES2-GLR cells may show more robust morphogenesis.

Because the protocol for RUES2-GLR gastruloids, developed by Moris et al, seemed well optimized I decided to re-investigate the number of cells seeded per well to observe whether it had any effect on gastruloid formation. For this, I used 400 and 800 RUES2-GLR cells with a 3.25 μM /0.5 μM Chiron combination. As it was observed for H1 cells (**Figure 3.3**), the number of cells seeded did not significantly influence the elongation process in RUES2-GLR (**Figure 3.9**). After 24 h, the elongation became evident and continued increasing until 96 h for both conditions of the initial cell number. Over 72 h, the gastruloids' body began to curl, with no apparent difference from 96 h to 144 h. Based on these results, for subsequent experiments, I decided to use the following condition: Chiron 3.25 μM pre-treatment, 0.5 μM post-treatment, and 400 cells for both RUES2-GLR and H1 cells, unless specified otherwise.

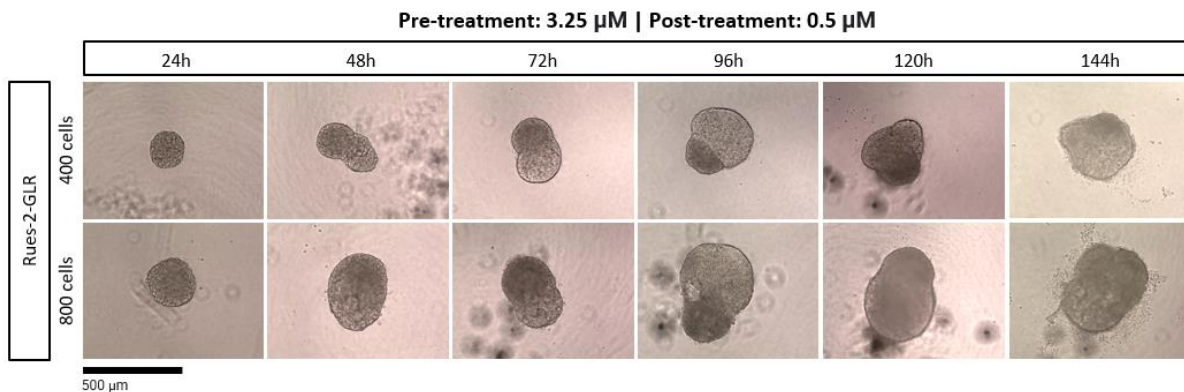


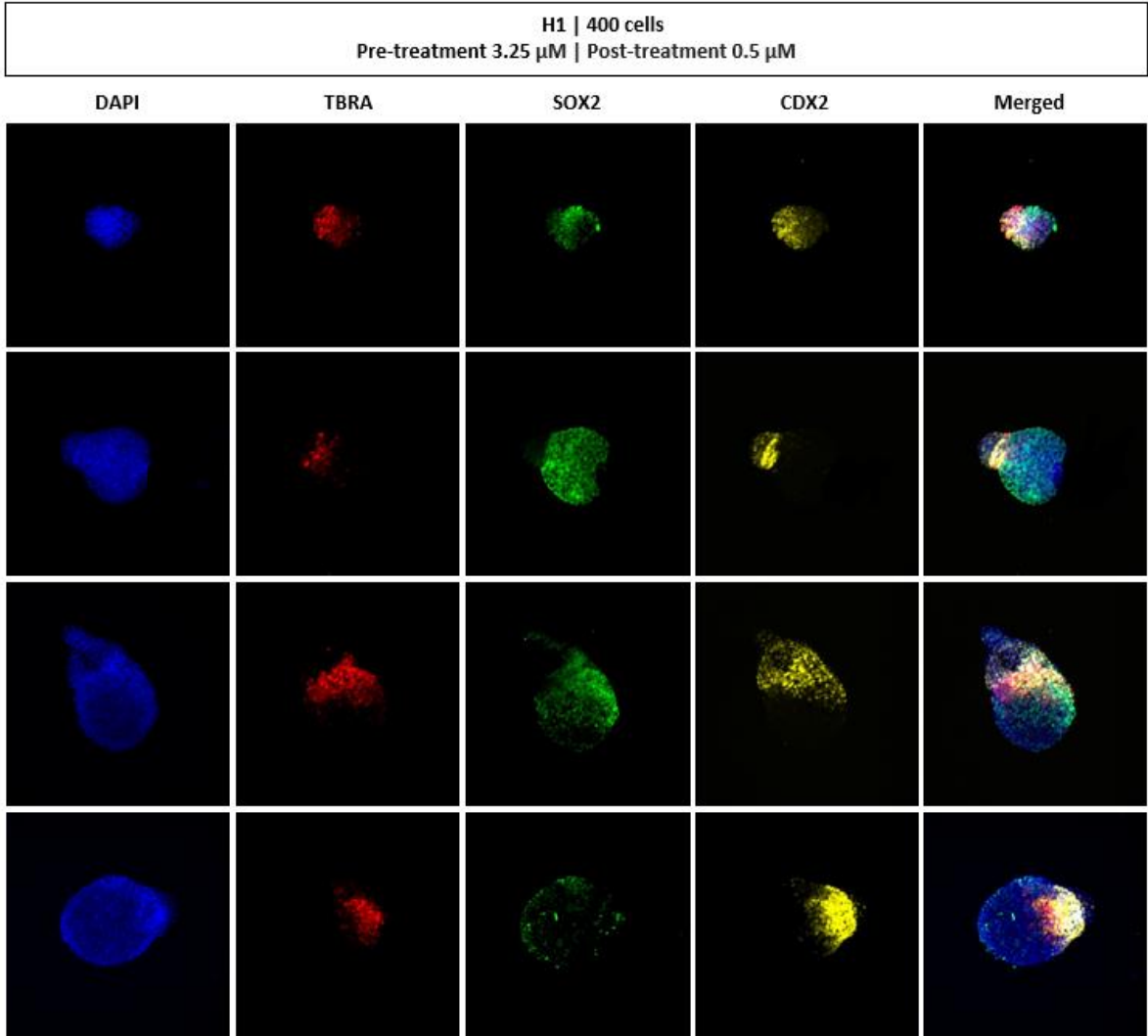
Figure 3.9: RUES-2-GLR 3D gastruloids derived from 400 and 800 cells with 3.25 μM and 0.5 μM pre/post-treatment, from 24h to 144h.

3.2 Monitoring mesoderm, endoderm and ectoderm formation in H1 and RUES2-GLR 3D gastruloid model

To affirm whether human 3D gastruloids could express markers for the three germ layers, I performed IF to identify cells expressing markers of mesoderm (T/BRA), endoderm (SOX17), neuroectoderm (SOX2), and EXE-like cells (CDX2) in both H1 and RUES2-GLR 3D 3D gastruloids. Since both Abs recognizing T/BRA and SOX17 are produced in goats, I am showing the results in separate panels, one for markers of endoderm (SOX17), and the other for mesoderm (T/BRA), each paired with the same set of markers (SOX2, CDX2). For both H1 and RUES2-GLR cells, gastruloids were made with 400 cells and a 3.25/0.5 μ M Chiron pre/post-treatment .

In H1 3D gastruloids at 24 h, T/BRA and CDX2 showed broad but overlapping expression, which eventually localized to a distinct region, typically at the tip of the gastruloid. Meanwhile, SOX2 expression was polarized away from T/BRA and CDX2, but expression decreased at 72 h to 96 h (**Figure 3.10A**). For SOX17, only a few cells expressed SOX17 at 24 h with no apparent localization, but expression increased by 48 h to 72 h and co-localized with CDX2⁺ cells. This temporal dynamics of germ layer markers in 3D gastruloids is consistent with the that reported in the 2D gastruloid model where mesoderm specification precedes endoderm formation (Minn et al., 2020). Moreover, spatially, endoderm and EXE-like cells colocalized with each other, but being separated from SOX2-expressing cells (**Figure 3.10B**). Overall, these germ layer markers were expressed in a polarized fashion, with SOX2 initially separated from CDX2, T/BRA, and SOX17, but eventually diminishing after 48 h. Meanwhile, CDX2, T/BRA, and SOX17 became more colocalized with time.

A



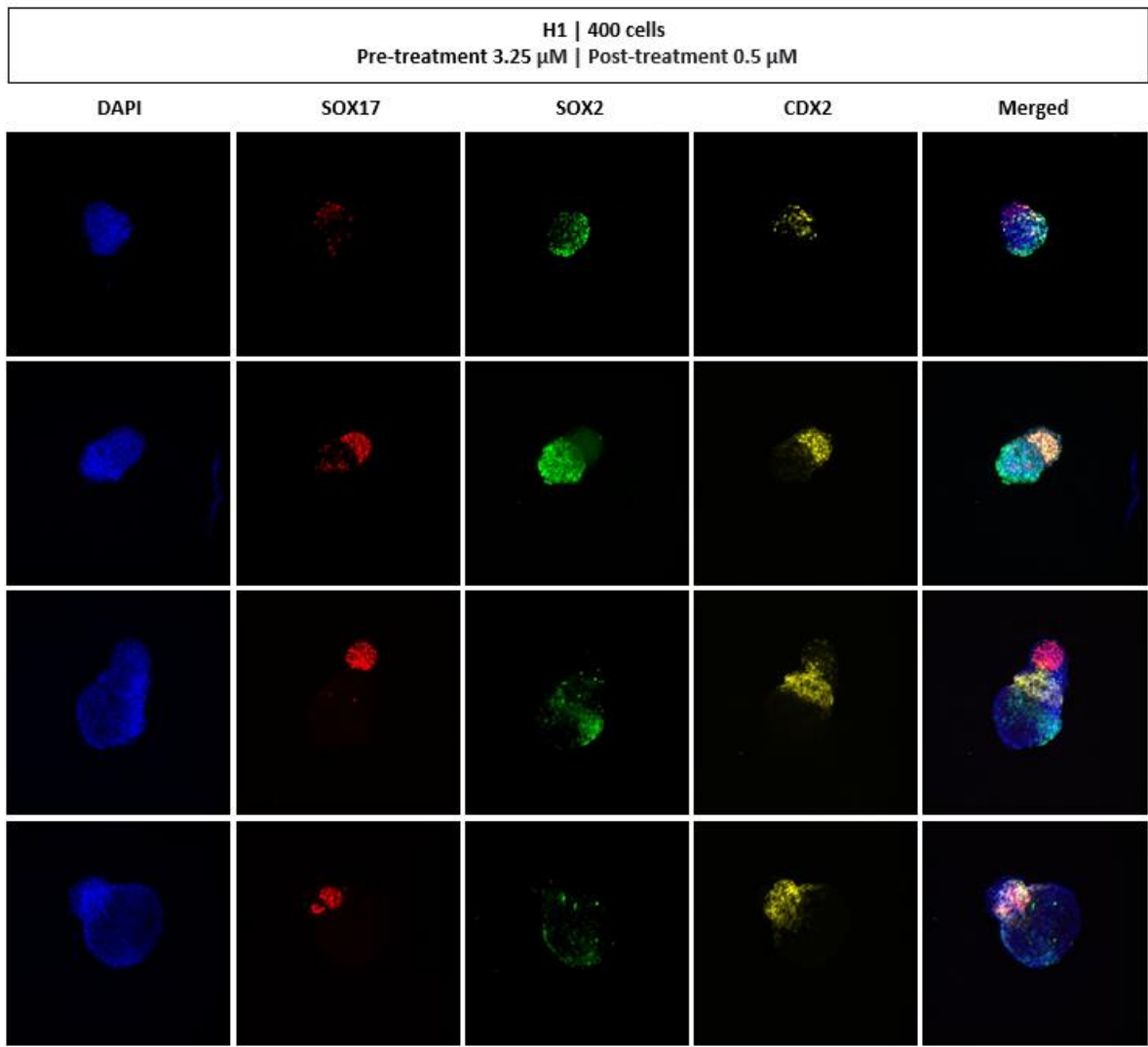
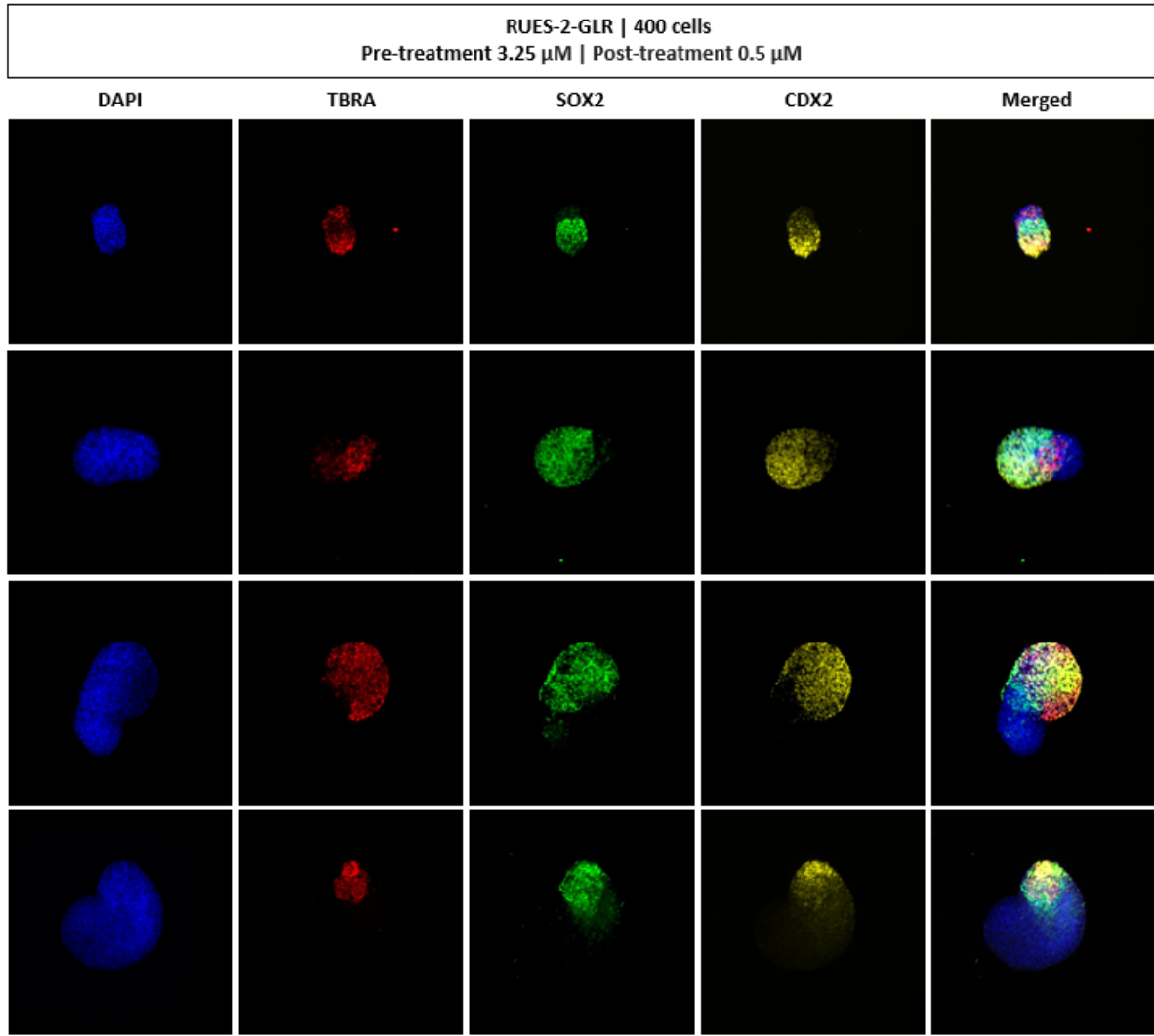
B

Figure 3.10: H1 3D gastruloids derived from 400 cells with 3.25 μ M and 0.5 μ M pre/post-treatment, Images are taken from 24 h to 96 h for the expression of TBRA (A) and SOX17 in red (B), SOX2 in green, and CDX2 in yellow

I next performed the same IF procedure from my H1 gastruloid experiment with RUES2-GLR gastruloids. At 24 h, T/BRA was already expressed and overlapping with SOX2, slightly different from what I observed in H1 3D gastruloids. Additionally, the expression of all markers seemed more localized at one pole of the gastruloids, which increased in expression over time. Differences that I've noticed compared to H1 gastruloids was that CDX2 expression was distributed more broadly in the gastruloid. Moreover, SOX2 expression remained strong from 24 h to 96 h, while in H1 gastruloids, SOX2 expression began to diminish after 48 h, indicating that the difference may be a cell line specific feature instead of a biological implication (**Figure 3.11.A**). For SOX17, similar to H1 gastruloids, SOX17 expression became more evident by 48 h. However, in RUES2-GLR 3D gastruloids, its expression diminished by 96 h, and SOX17 expression was weaker throughout all time points compared to H1 gastruloids (**Figure 3.11B**). Despite slight differences in the amount of expression, the pattern remained similar, where T/BRA, SOX17, and CDX2 are shown to co-localize away from SOX2, but slowly localizes at the point of elongation over time.

A



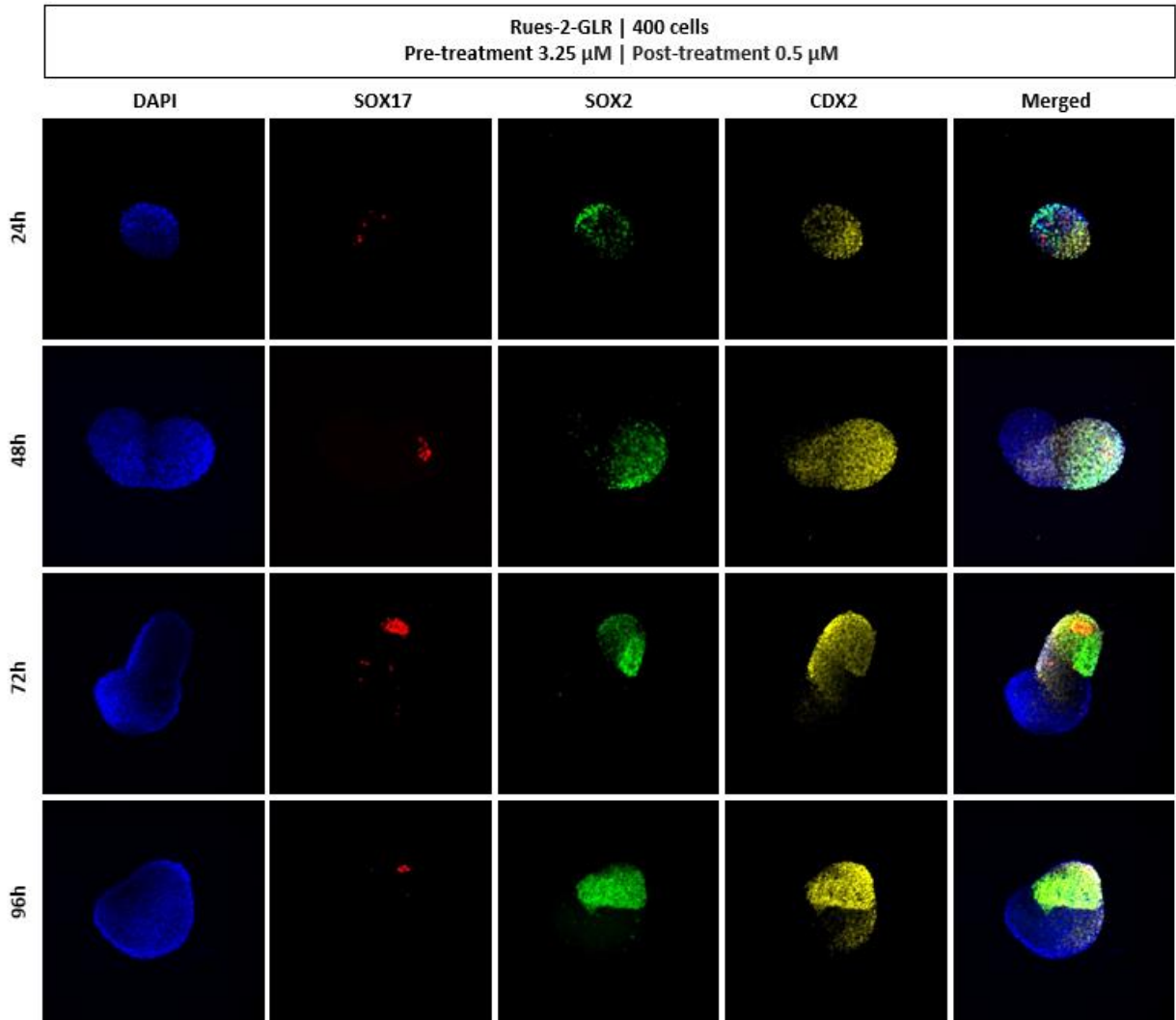
B

Figure 3.11: RUES2-GLR 3D gastruloids derived from 800 cells with 3.25 μ M and 0.5 μ M Chiron pre/post-treatment. Images were taken from 24 h to 96 h for the expression of TBRA (A) and SOX17 in red (B), SOX2 in green, and CDX2 in yellow.

3.3 3D human gastruloid germ layer cells exhibit sorting behaviors as reported for 2D gastruloids.

Cell migration is an important feature of gastrulation where cells migrate and rearrange to form and shape the germ layers and rudimentary organs. As such, cell sorting is thought to be a key driver of these early morphogenetic behaviors. To test if this feature is maintained in the human 3D gastruloids, I performed an experiment similar to that reported by Minn et al in 2020.

Briefly, 3D gastruloids were made using previously established conditions (400 cells, 3.25/0.5 μ M pre and post Chiron treatment) and cultured for 72 h. The resulting 3D gastruloids were transferred into a 15 mL tube and dissociated into a single cell suspension by centrifuging with 1:1 Accutase to mTESR. Subsequently, the dissociated cell suspension was seeded onto a 12 well micropatterned plate with 1 mL of mTESR supplemented with ROCKi and without BMP4. On average, a 96-well plate of 3D gastruloids yielded around ~100,000 to ~500,000 cells depending on the gastruloids' size and how well they were dissociated.

To begin, I decided to test 2 different cell numbers, ~100,000 and ~200,000 cells, to seed onto the micropatterned wells. Differences in density, as evident at 24 h and in the following days, suggested that ~200,000 was a better condition since there were enough cells to attach and grow onto the micropattern, similar to what's seen in the 2D gastruloid model (**Figure 3.12**).

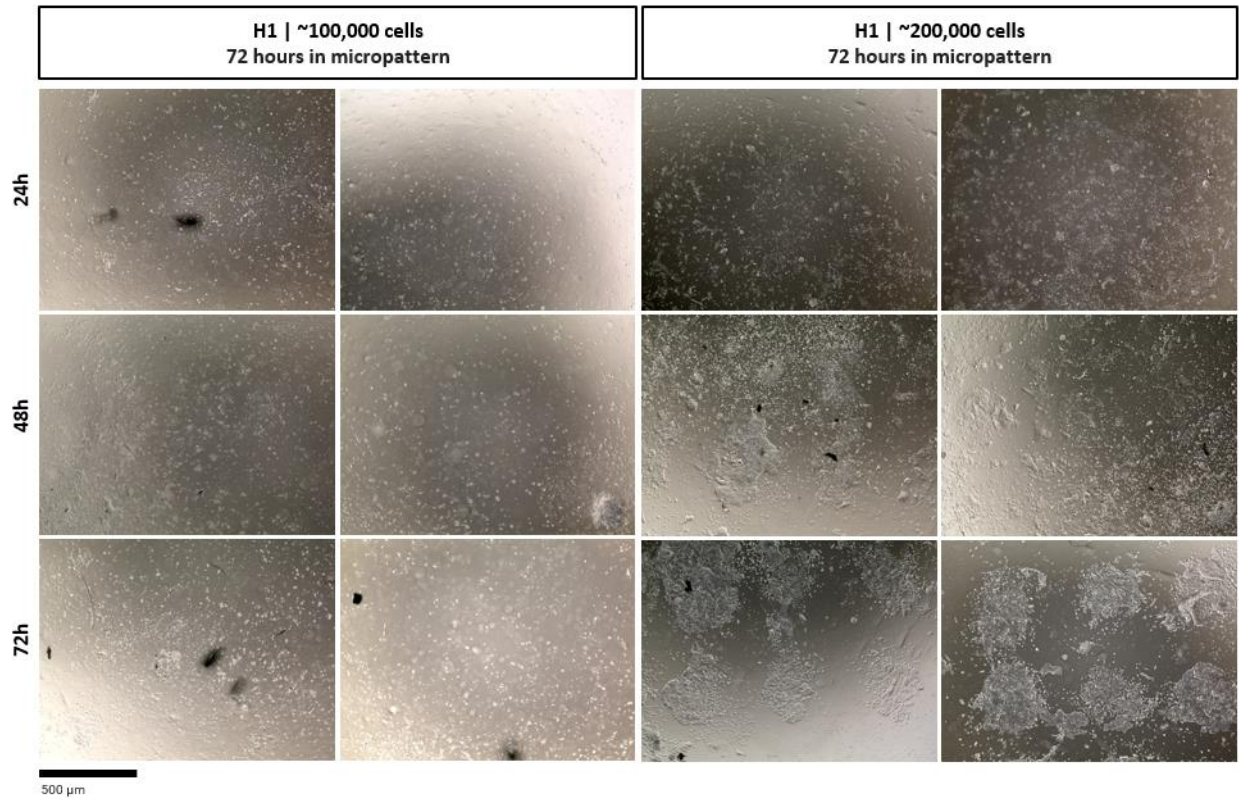
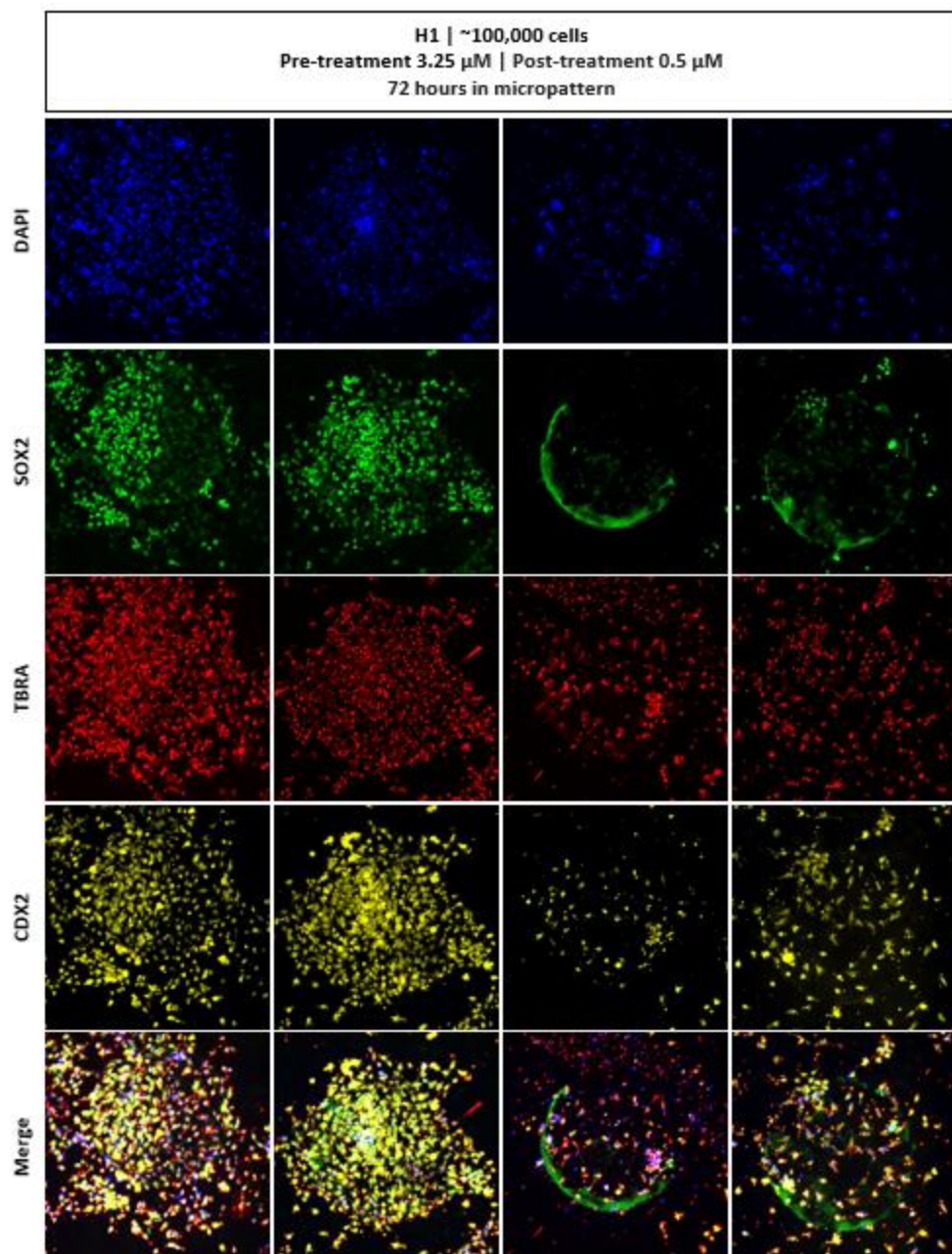


Figure 12: Cells from H1 3D gastruloids generated with 3.25/0.5 μ M Chiron pre/post-treatment, dissociated at 72h and reseeded on 2D micropattern at ~100,000 and ~200,000 cells for up to 72h.

Cell number is crucial because a lower number of cells would not be sufficient in demonstrating self-organization due to the failure of cells to form groups. On the other hand, a higher number of cells could overgrow/overlap each other, producing a false positive for self-organization in the micropattern. I performed IF on two micropattern conditions, starting with either ~100,000 and ~200,000 cell per well, and staining for markers of mesoderm (T/BRA), neuroectoderm (SOX2), and EXE cells (CDX2) to test if cells differentiated into a 3D gastruloid can self-organize upon dissociation and reseeded. IF can also help determine the optimal number of cells for subsequent experiments. **(Figure 3.13A and 3.13B)**

A



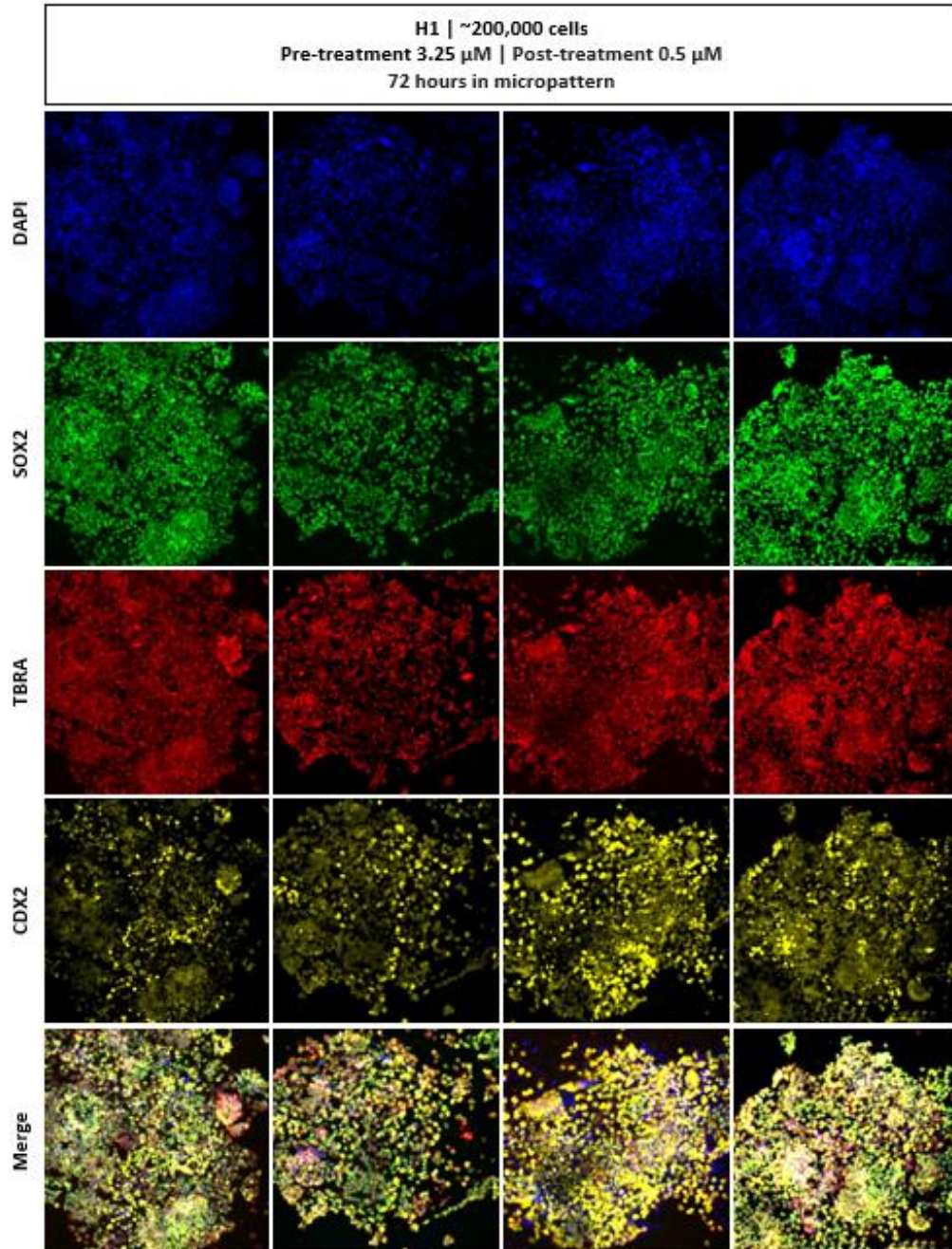
B

Figure 3.13: IF of cells from dissociated 3D gastruloids that were re-seeded onto the 2D micropattern and cultured for 72 hours. H1 3D gastruloids derived from 400 cells and 3.25/0.5 μ M Chiron grown for 72 h. Gastruloids were dissociated and reseeded in micropatterns at ~100,000 cells/well (A) and (B) ~200,000 cells/well. IF for TBRA (red), SOX2 (green), and CDX2 (yellow).

At ~100,000 cells/well, I observed that: i) number of cells were not enough to attach and grow in the matrigel stamp, ii) high heterogeneity of markers was detected in all micropatterns, showing no obvious indication of organization, iii) possible non-specific staining of T/BRA and SOX2 when compared to DAPI staining . At ~200,000 cells/well , cells were slightly over abundant, but still yielded decent micropatterned cultures. From the micropattern, SOX2 cells were seen intermixed with T/BRA- expressing cells, a pattern similar to what was observed in both RUES2-GLR and H1 3D gastruloids. Also some clustering of T/BRA cells with low SOX2 could be discerned, but this conclusion was confounded by high background for T/BRA and SOX2. Surprisingly, CDX2 expression was reduced in the cell population re-seeded onto 2D micropattern, and CDX2⁺ cells were randomly spread out, showing no signs of organization. Lastly, SOX2 was highly expressed in the micropattern, in contrast to the H1 3D gastruloids which showed diminishing expression of SOX2 after 48 h, suggesting either a differentiation toward ectoderm, or cells reverting to a form of pluripotency when reseeded into the micropattern system.

In order to verify if the ability to self-sort is present in 3D RUES2-GLR cells, I repeated the experiment with RUES2-GLR gastruloids. Like with H1 gastruloids, I collected RUES2-GLR 3D gastruloids, dissociated them, and seeded them onto the 2D micropattern with a density of ~170,000/well, and fixed at 48 h rather than 72 h. Additionally, to prepare a cell suspension from dissociated 3D gastruloids?? I used a 1 mL Eppendorf tube and centrifuged with only Accutase. Slight changes in the conditions were made based on the previous H1 experiment to help avoid overgrowth and heterogeneity in the micropattern through adjustment of the cell density and a more aggressive dissociation of gastruloids. **(Figure 3.14)**

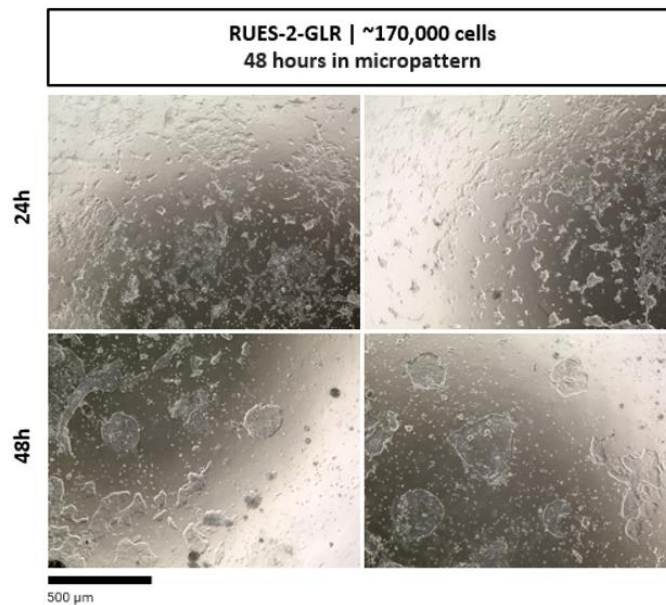
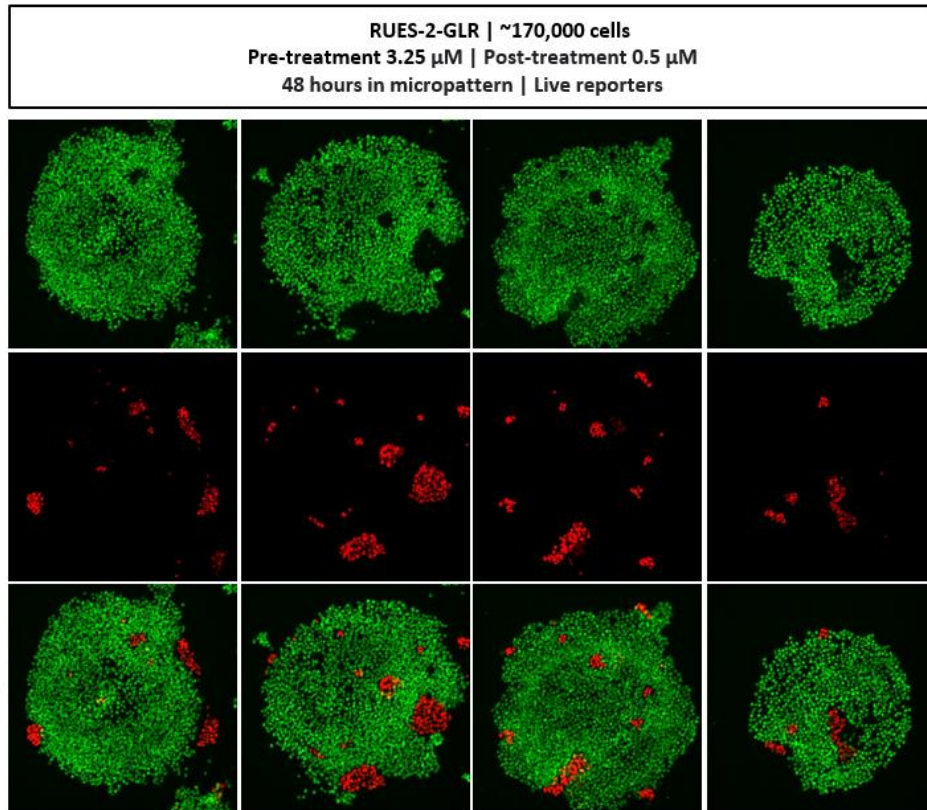


Figure 3.14: Bright field microscopic images of cells from dissociated 3D RUES2-GLR gastruloid re-seeded onto 2D Micropattern and cultured for 24 h and 48 h. Cells derived from 3D gastruloids (3.25/0.5 μM Chiron), dissociated at 72h, and micropatterned at \sim 170,000 cells for up to 48h.

RUES2-GLR harbor 3 reporters that can help detect the expression of SOX2, T/BRA and SOX17. In the 3D gastruloids, I was not able to detect the fluorescent signal of these reporters. However, I was interested if the expression would be visible once cells were seeded onto 2D micropatterns. At 48 h, only SOX2 and SOX17 live reporters were visible in the micropattern, which showed that endodermal cells aggregated together and separated from SOX2-expressing ectodermal cells (**Figure 3.15A**). Unfortunately, the filter for T/BRA reporter was not available in our confocal microscope. Therefore, I performed IF at 48 h, staining for the following combination of markers; SOX2, SOX17, and GATA3 or CDX2 (pluripotency/ectoderm, endoderm, and TE or EXE respectively); and SOX2, TBRA, and FOXA2 or CDX2 (markers of pluripotency/ectoderm, mesoderm, and endoderm or EXE) (**Figure 15B**).

A



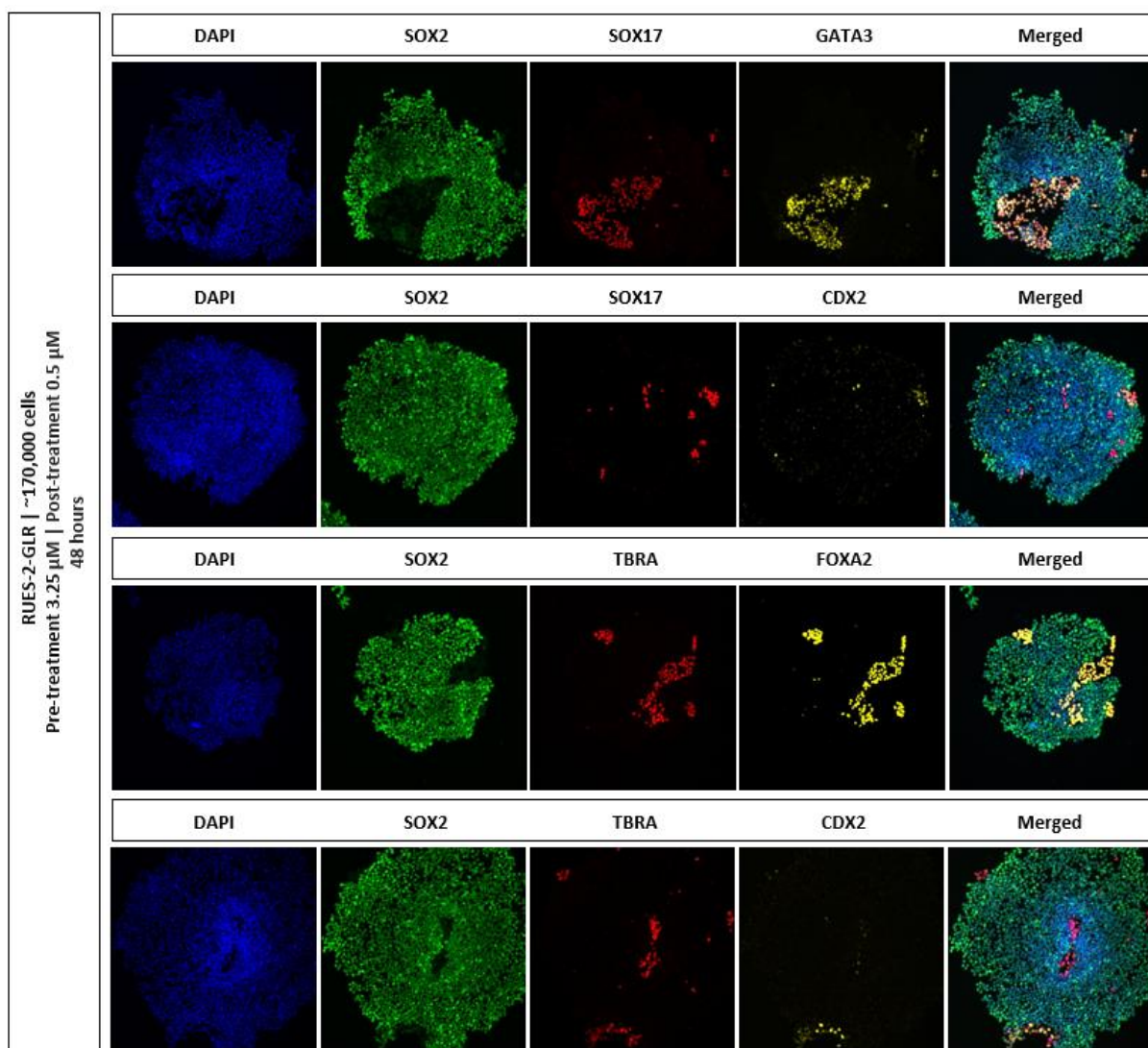
B

Figure 3.15: IF confocal microscope images of RUES2-GLR from 3D gastruloids re-seeded onto 2D Micropattern for 48h . RUES2-GLR 3D gastruloids (400 cells, 3.25/0.5 μ M Chiron, 72h) were dissociated and micropatterned at ~170,000 cells/well density for 48 h. A) Live reporters for SOX17 (red) and SOX2 (green) were taken at 24h and 48h. B) Confocal images of DAPI (blue), SOX2 (green), SOX17 (red), GATA3 (yellow), CDX2 (yellow), FOXA2 (yellow), were taken after fixing and immunostaining.

Unlike with my previous H1 reseeded micropatterns, cells from dissociated 3D RUES2-GLR gastruloids reseeded onto micropatterns showed clear indication of aggregation and separation. of TBRA⁺ and CDX2⁺ from SOX2⁺ cells. As well, other markers I tested, such as SOX17, GATA3, and FOXA2 have shown the same pattern where all markers colocalize with each other separate from SOX2. SOX17/TBRA, and FOXA2/GATA3 were also shown to have similar level of expression, with the exception of CDX2, showing lower levels of expression compared to the other markers. And similar to the H1 micropatterns, SOX2 was highly expressed in the RUES2-GLR micropatterns (**Figure 3.13**). Additionally, CDX2 expression seemed less expressed compared to all other markers similar to the H1 reseeded micropatterns, suggesting that the population of EXE cells is not growing, or they are differentiating into a different cell type.

From these results, I can speculate that cells dissociated from RUES2-GLR 3D gastruloids seeded on 2D micropatterns exhibit an ability to aggregate together in clusters of mesoderm, endoderm, TE, and EXE away from potential ectodermal or pluripotent cells. However, additional biological replicates for both H1 and RUES2-GLR gastruloids are necessary to confirm the decrease in CDX2 expression and increase in SOX2 expression. As well, a successful H1 experiment has not been conducted yet. My experiments also show the ability of dissociated cells to self-organize, yet this alone is not enough to confirm cell motility. Instead, live imaging will be required to prove this.

Chapter 4: Discussion

The goals of my experiments were, first to validate the published protocols for generation 3D hESC gastruloids with three germ layers from hESCs, optimize a protocol for a different cell line than that used previously. My second goal was to assess the morphogenetic properties seen in other models, such as self-aggregation of germ layer cells generated in 2D gastruloids in 3D gastruloids. In my work, I first performed a detailed morphologic characterization of 3D gastruloid formation in response to changes in conditions such as cell number, post-treatment of Chiron, and pre-treatment of Chiron. I then confirmed the expression of three germ layer markers in my 3D gastruloids, showing similar expression pattern seen by Moris et al's gastruloids, but also elucidating potential cell line differences between H1 and RUES2-GLR gastruloids. Finally, I demonstrate here the ability of cells from dissociated 3D gastruloids to exhibit self-organizing behavior when seeded onto 2D micropatterns, similar to what Minn et al has shown with 2D gastruloids.

4.1 H1 and RUES2-GLR protocol optimization

To find the optimal conditions for growing 3D gastruloids with H1 cells, I tested different concentrations of pre-treatment and post-treatment of Chiron, as well as the number of cells seeded per well. From these experiments, I determined that the condition: 400 cell/well, with 3.25 and 0.5 μ M Chiron pre/post treatment was sufficient for generating 3D gastruloids capable of elongation. In the process of optimizing the protocol, I was able to observe the effect each variable had on gastruloid formation. For example, the elongation of gastruloids can be inhibited by both the lack and abundance of Chiron, with a more significant impact with the pre-treatment

condition, suggesting that the pre-treatment of Chiron is important in priming cells for differentiation and morphogenesis.

The chemical used, Chiron, is a WNT agonist that inhibits GSK3, preventing phosphorylation and subsequent ubiquitylation of β -catenin, and thus causing accumulation of β -Catenin (the transcriptional effector of the WNT pathway in the cytoplasm and translocation to the nucleus to stimulate gene expression (Cohen & Goedert, 2004). Through Chiron treatment, and thus WNT pathway activation, it is thought that cells undergo something similar to mesendoderm and EMT induction, as evident by Moris et al's experiment which found lowered levels of expression in E-cadherin and higher levels of N-cadherin in colonies, a hallmark of EMT induction, after pre-treatment with Chiron (A & G, 2013). Additionally, it has been shown in mice that down-regulation of E-cadherin promoted by TF inhibiting TCF/LEF, increases WNT signaling through release of β -catenin from its interaction with E-cadherin complexes at the membrane. Wnt signaling has many key roles in early vertebrate embryogenesis. The current view is that in frog and zebrafish, maternal WNT/ β -catenin and Nodal signaling induce TFs and secreted proteins that are crucial during the cleavage and blastula stage to establish the dorsal organizer and low levels of BMP signaling mediated by Phosphorylated SMAD1/5 (P-SMAD)(Kozmikova & Kozmik, 2020). In mammalian embryos Wnt signaling from the posterior visceral/extraembryonic endoderm and subsequently in the posterior epiblast is known to induce primitive streak and mesendodermal fates (Gadue et al., 2006). WNT signaling is also known to induce mesodermal differentiation in hESC, though Moris et al has shown that a pre-treatment of Chiron does not induce mesodermal differentiation in colonies before dissociation (Davidson et al., 2012; Loh et al., 2016). From this, I reason that with insufficient Chiron, gastruloid formation

does not occur due to a lack of Wnt signaling, and consequently a lack of cells undergoing an EMT like process. On the other hand, β -catenin is also known to aid in cadherin-mediated cell-to-cell adhesion, with E-cadherin as one example (Buechel et al., 2021). Thus, administering too much Chiron can also impair gastruloid elongation possibly due to the overabundance of β -Catenin, promoting too much cell-to-cell adhesion to prevent cell behaviors driving elongation.

Another observation I made was the difference in gastruloid robustness between H1 and RUES2-GLR cells. The RUES cell line was originally obtained through donated human blastocysts from IVF clinics and was first termed RUES1 in 2006 by James et al in Brivanlou's lab. In 2009, a second iteration, termed RUES2, was created using lentiviral transduction to express EGPF under the EF1alpha promoter (James et al., 2006). Finally, the RUES2-GLR line was created in 2018 using CRISPR-Cas9 to insert three independent gene expression reporters: T/BRA (mCherry), SOX17 (td Tomato), and SOX2 (mCitrine), attached to their respective coding sequence. Specifically, mCherry and td Tomato are not directly fused to T/BRA and SOX17 respectively due to being attached to a self-cleaving peptide (P2A), unlike SOX2 which is directly fused with the mCitrine reporter (Martyn et al., 2018).

H1 on the other hand, is one of the earliest hESC lines federally approved for experimentation with NIH funding and developed by WiCell. H1 cells were originally extracted from human blastocysts in an IVF clinic by Thomson et al in 1998. However, unlike RUES2-GLR cells, H1 cells do not contain any fluorescent gene expression reporters (J. A. Thomson et al., 1998).

As both H1 and RUES-2-GLR cells are derived from human blastocysts, and both were validated through karyotyping, I expected both H1 and RUES2-GLR 3D gastruloids to be similar.

However, I found that 3D gastruloids made with RUES2-GLR cells were much more stable morphologically than H1 gastruloids. One hypothesis is the difference in the method of the lines generation. H1 cells were extracted in 1998 compared to RUES in 2006, potentially indicating a difference in extraction methods. And since H1 cells were generated in 1998, H1 cells may have been passaged more than RUES cells, potentially accumulating genetic mutations through countless iterations of mitosis, splitting, freezing, and thawing. The donor of H1 cells could also have an effect on the stability of the cell line, though not much is known about either donor of H1 and RUES-2-GLR. It should be noted, however, that the H1 line is capable of generating robust 2D gastruloids and was used to demonstrate the sorting potential of germ layer cells in re-seeding experiments by Minn et al., (2020), hinting that optimization of the protocol I established for these 3D gastruloids may still be needed.

My work on optimizing the 3D gastruloid protocol has narrowed down the condition for H1 gastruloids, such as Chiron concentration and cell number. However, H1 gastruloids did not look as robust as RUES2-GLR gastruloid, having irregular morphology and often fragmenting during elongation. Therefore, in future studies, further optimization of H1 gastruloids is needed.

Specifically, Chiron titration at the pre-treatment stages I have shown that Chiron concentration at the post-treatment stage and cell number had no significant effect on gastruloid formation.

Also, future experiments investigating the difference between the H1, RUES2-GLR, and other cell lines with similar embryonic origins should be investigated. As I have shown, potential cell line specific traits may be evident, but additional experiments are needed to validate this. Gene expression analyses, such scRNA-seq should be performed as it's been shown that differences in gene expression is present across different hiPCs (Chin et al., 2009; Wilson et al., 2009).

Allegrucci and Young have also reviewed difference in gene expression in different hESC lines even with identical laboratory conditions (Allegrucci & Young, 2007). Such gene expression differences could contribute to different differentiation and morphogenetic potential.

4.2 Confirming formation of the three germ layers in H1 and RUES2-GLR gastruloids.

One of the hallmarks of 3D gastruloid differentiation is formation of the three germ layers and gastruloid elongation (Brink et al., 2021). For this reason, I validated my H1 and RUES2-GLR gastruloids using IF.

In Moris et al's work, fluorescent imaging was done using the live reporters of numerous cell lines such as the RUES2-GLR line. Similarly, I attempted live imaging but faced some limitations related to the absence of adequate laser channels to observe the T/BRA reporter (mCherry) (**Figure 3.16**). This issue has been also experienced by other WashU researchers who have used RUES2-GLR cells, stating that the mCherry reporter is weaker compared to tdTomato and mCitrine. For this reason, I utilized immunostaining on all my gastruloids by adapting a protocol from Minn et al's protocol for staining 2D gastruloids, and observed comparable results with Moris et al's live imaging (**Figures 3.10 to 3.13**)

In my IF experiments, I was able to show, in both H1 and RUES2-GLR 3D gastruloids, expression for markers of mesoderm (T/BRA), endoderm (SOX17), ectoderm (SOX2), and EXE cells (CDX2). However, differences were observed between H1 and RUES2-GLR 3D gastruloids; after 48 h, SOX2 expression was diminished in H1 gastruloids, but not in RUES2-

GLR gastruloids; SOX17 was less expressed in RUES2-GLR gastruloid than in H1 gastruloids; and SOX2 /CDX2 expression was higher overall in RUES2-GLR than in H1 3D gastruloids. One possibility to explain these differences in expression between H1 and RUES2-GLR gastruloids may be due to incomplete optimization of the H1 gastruloid protocol. My H1 3D gastruloids have been shown to be more unstable based on the previous optimization experiments (**Figure 3.8**). Additionally, an experiment on H1 gastruloids with differing pre-treatments of Chiron (3.00 and 3.25 μM) showed SOX2 expression in the 3.00 μM group to be higher than in the 3.25 μM group (**Supplementary 2A & 2B**). However, IF data for RUES2-GLR with different Chiron pre-treatment was not conducted, therefore, further experimentation is needed.

With that said, future experiments for these 3D gastruloids should focus on confirming whether the differences I found between H1 and RUES2-GLR gastruloids are a matter of cell line specific traits, or incomplete optimization of the H1 3D gastruloid protocol. As such, IF of RUES2-GLR gastruloids should be conducted to find whether changes in expression, most notably SOX2, would be similar to what my H1 gastruloids show (diminishing expression past 48 h). If expression is similar after a change in condition, this may suggest that my H1 gastruloid protocol needs further optimization. However, if expression of RUES2-GLR does not match H1 gastruloids, this may suggest a difference in cell line. One way to confirm this would be through gene expression analyses, such as tomography-sequencing employed by Moris et al, or scRNA-seq reported by Minn et al., 2020, providing specific details on the regulation of patterned gene expression.

4.3 Reseeded 3D gastruloids onto micropatterns exhibit self-organization.

The ability for cells to self-organize and have motility is crucial during the process of gastrulation, in particular, morphogenetic events. Therefore, I provided experimental evidence that cells from dissociated 3D RUES2-GLR gastruloids display this self-organizing behavior.

Gastrulation starts with the formation of the PS on the posterior side of the epiblast disk. In mice, ExE cells surrounding the epiblast secrete Bmp4, which in turn, induces the Wnt3 and Nodal signaling cascade in the epiblast (Ciruna & Rossant, 2001; Mishina et al., 1995; Rivera-Pérez & Magnuson, 2005). At the posterior epiblast, high Nodal and Wnt3 signaling induces the expression of T/BRA, marking mesoderm precursors, which undergo EMT for PS formation and migration to form mesodermal and endodermal layers. As the EMT wave extends the PS anteriorly, mesendoderm precursors ingress beneath the epiblast via the PS, and migrate to form mesoderm and endoderm, while the remaining epiblast becomes ectoderm (Williams et al., 2012). In hESC 2D micropatterned gastruloids, it's been shown that BMP, WNT, and NODAL pathways interact to form the three germ layers and ExE cell types upon BMP4 treatment (Minn et al., 2020, Warmflash et al., 2014). As such, the ability of a cell to migrate and self-sort are important features in gastrulation, leading to major morphogenetic events related to organization and major events in gastrulation like ingression as well as convergence and extension (R. Keller, 2005).

The first instance of testing disaggregation and reaggregation of embryos were done in a classical experiment by Townes and Holtfreter in 1955, where cells from dissociated *Xenopus* embryos at the gastrula or neurula stages were able to aggregate and sort into the three germ

layers (Steinberg & Gilbert, 2004). And more recently, Minn et al shows that cells dissociated from 2D gastruloids, when reseeded onto the micropattern without BMP4, are able to sort and aggregate together. To address this question in 3D gastruloids, I followed a similar approach as Minn et al.

When conducting these experiments, I considered that both models present different geometry and different treatment for stimulation. Therefore, I hypothesized that the result of this experiment would be different. In the case of 2D gastruloids, they are derived from BMP4 stimulation, which activate WNT and NODAL downstream, while the 2D micropatterns provide the geometric cue (Ben-Haim et al., 2006; Martyn et al., 2018). In the 3D model, cells are treated with Chiron, and the geometric cues are provided through the suspension and aggregation of cells. And as discussed, Chiron activates WNT through the Inhibition of GSK to increase β -Catenin (Cohen & Goedert, 2004). Interestingly, Moris et al investigated the use of BMP4 to replace Chiron which led to spherical aggregates with no indication of elongation or differentiation (only SOX2 expression). Because of this, I expected my dissociated gastruloids to aggregate differently upon reseeded on 2D micropattern due to the variation in how we differentiate our cells. On the other hand, in both gastruloid models, cells expressing bona fide endodermal, mesodermal and ectodermal markers form and thus could display germ layer-specific behaviors.

Instead, my results show similar findings to Minn et al in terms of cell sorting and self-organization, at least with cells from RUES2-GLR 3D gastruloids (**Figure 3.15**). Since different treatment and differentiation methods will result in the same pattern of aggregation, I suspect that any kind of differentiation that activate EMT induction in hESC will give it the ability to self-organize.

Overall, I was able to demonstrate that cells from 3D gastruloids show the same ability to aggregate as the 2D gastruloids in Minn et al's work, such as the clear separation of SOX17, T/BRA, GATA3, FOXA2, and CDX2 from SOX2. However, these studies need to be repeated. Moreover, I have only demonstrated this with cells from REUS2-GLR gastruloids. As such, future experiments should focus on creating replicates for both H1 and RUES2-GLR cells. Replicates with H1 cells are particularly important because it can serve as a better comparison to what Minn et al has shown. However, as stated in discussion 4.1 and 4.2, H1 gastruloid protocol may not be optimized, potentially affecting the results. For RUES2-GLR cells, replicates are needed to confirm my findings from **figure 3.15**. And most importantly, a time-lapse video analyses should be performed after the reseeding process in either cell lines to demonstrate that cells from 3D gastruloids do in fact, show motility. Such studies could provide further insight into how different cell types interact during sorting and self-aggregation process. Additionally, testing different 3D gastruloid protocols would be interesting. For example, protocols established by Libby or Orsted show 3D gastruloids capable of demonstrating neural tube extension, axial elongation, and distinct hindbrain region from the brachial and thoracic regions. Both protocols also use Chiron and hESC, but pair it with other treatments and different cell types. As such, it would be interesting to see how cells from the gastruloids will aggregate

(Libby et al., 2021b; Olmsted & Paluh, 2021). And lastly, Minn et al has performed scRNA sequencing on his reseeded micropatterns, revealing more differentiated cells types, which should also be implemented in my micropatterns made with 3D gastruloids for comparison.

4.4 Limitations of my 3D gastruloid models.

Comparing my 3D gastruloids to more recent publications such as the EMLO gastruloids by Olmsted and Paluh, which demonstrate more advanced structures like a neuronal trunk, highlights the limitation of my current 3D gastruloid model. Additionally, all 3D gastruloids protocols require disaggregation of cells grown in colonies, and resuspension in media, where cells begin to aggregate and form embryos. This not only strays away from how most embryos develop in vivo, as germ layers arise from an epithelial epiblast, but also, many steps of gastrulation that are skipped when creating these gastruloids, such as (formation of ICM, gastruloids are not hollow, lack of primitive streak formation, etc).

Despite the advent of new protocols for more advanced 3D gastruloids, an advantage of my 3D gastruloids over other protocols is the speed at which they fully develop. Compared to EMLO embryos which takes at least 22 days to mature, with the presence of meandering gut tube, my gastruloids mature at around 48 h to 72 h as shown by the distinct patterns of expression and robust morphology (Olmsted & Paluh, 2021). This makes my 3D gastruloids perfect for studying the processes of gastrulation, rather than organogenesis, and experiments that require a high number of differentiated cells such as the micropattern reseeded experiment. These 3D gastruloids are also excellent for studying gastruloid elongation under different treatments as

demonstrated by Marikawa et al in the teratogenicity assessments on similar hESC gastruloids.
(Marikawa et al., 2020)

References

- A, G., & G, B. (2013). Cadherins and epithelial-to-mesenchymal transition. *Progress in Molecular Biology and Translational Science*, 116. <https://doi.org/10.1016/B978-0-12-394311-8.00014-5>
- Acharya, U. V., Pendharkar, H., Varma, D. R., Pruthi, N., & Varadarajan, S. (2017). Spinal dysraphism illustrated; Embryology revisited. *The Indian Journal of Radiology & Imaging*, 27(4), 417–426. https://doi.org/10.4103/ijri.IJRI_451_16
- Aguilera-Castrejon, A., Oldak, B., Shani, T., Ghanem, N., Itzkovich, C., Slomovich, S., Tarazi, S., Bayerl, J., Chugaeva, V., Ayyash, M., Ashouokhi, S., Sheban, D., Livnat, N., Lasman, L., Viukov, S., Zerbib, M., Addadi, Y., Rais, Y., Cheng, S., ... Hanna, J. H. (2021). Ex utero mouse embryogenesis from pre-gastrulation to late organogenesis. *Nature*, 593(7857), 119–124. <https://doi.org/10.1038/s41586-021-03416-3>
- Allegrucci, C., & Young, L. E. (2007). Differences between human embryonic stem cell lines. *Human Reproduction Update*, 13(2), Article 2. <https://doi.org/10.1093/humupd/dml041>
- Alom Ruiz, S., & Chen, C. S. (2007). Microcontact printing: A tool to pattern. *Soft Matter*, 3(2), 168–177. <https://doi.org/10.1039/b613349e>
- Amadei, G., Handford, C. E., Qiu, C., De Jonghe, J., Greenfeld, H., Tran, M., Martin, B. K., Chen, D.-Y., Aguilera-Castrejon, A., Hanna, J. H., Elowitz, M. B., Hollfelder, F., Shendure, J., Glover, D. M., & Zernicka-Goetz, M. (2022). Embryo model completes gastrulation to neurulation and organogenesis. *Nature*, 610(7930), 143–153. <https://doi.org/10.1038/s41586-022-05246-3>
- Amadei, G., Lau, K. Y. C., De Jonghe, J., Gantner, C. W., Sozen, B., Chan, C., Zhu, M., Kyprianou, C., Hollfelder, F., & Zernicka-Goetz, M. (2021). Inducible Stem-Cell-Derived Embryos Capture Mouse Morphogenetic Events In Vitro. *Developmental Cell*, 56(3), 366–382.e9. <https://doi.org/10.1016/j.devcel.2020.12.004>
- Baillie-Johnson, P., van den Brink, S. C., Balayo, T., Turner, D. A., & Martinez Arias, A. (2015). Generation of Aggregates of Mouse Embryonic Stem Cells that Show Symmetry Breaking, Polarization and Emergent Collective Behaviour In Vitro. *Journal of Visualized Experiments: JoVE*, 105, 53252. <https://doi.org/10.3791/53252>
- Baum, B., Settleman, J., & Quinlan, M. P. (2008). Transitions between epithelial and mesenchymal states in development and disease. *Seminars in Cell & Developmental Biology*, 19(3), 294–308. <https://doi.org/10.1016/j.semcdb.2008.02.001>
- Bedzhov, I., & Zernicka-Goetz, M. (2014). Self-organizing properties of mouse pluripotent cells initiate morphogenesis upon implantation. *Cell*, 156(5), 1032–1044. <https://doi.org/10.1016/j.cell.2014.01.023>

- Bellairs, R. (1986). The primitive streak. *Anatomy and Embryology*, 174(1), 1–14. <https://doi.org/10.1007/BF00318331>
- Bellairs, R., Breathnach, A. S., & Gross, M. (1975). Freeze-fracture replication of junctional complexes in unincubated and incubated chick embryos. *Cell and Tissue Research*, 162(2), 235–252. <https://doi.org/10.1007/BF00209209>
- Belo, J. A., Bouwmeester, T., Leyns, L., Kertesz, N., Gallo, M., Follettie, M., & De Robertis, E. M. (1997). Cerberus-like is a secreted factor with neutralizing activity expressed in the anterior primitive endoderm of the mouse gastrula. *Mechanisms of Development*, 68(1–2), 45–57. [https://doi.org/10.1016/s0925-4773\(97\)00125-1](https://doi.org/10.1016/s0925-4773(97)00125-1)
- Ben-Haim, N., Lu, C., Guzman-Ayala, M., Pescatore, L., Mesnard, D., Bischofberger, M., Naef, F., Robertson, E. J., & Constam, D. B. (2006). The Nodal Precursor Acting via Activin Receptors Induces Mesoderm by Maintaining a Source of Its Convertases and BMP4. *Developmental Cell*, 11(3), Article 3. <https://doi.org/10.1016/j.devcel.2006.07.005>
- Bertocchini, F., & Stern, C. D. (2002). The hypoblast of the chick embryo positions the primitive streak by antagonizing nodal signaling. *Developmental Cell*, 3(5), 735–744. [https://doi.org/10.1016/s1534-5807\(02\)00318-0](https://doi.org/10.1016/s1534-5807(02)00318-0)
- Blauwkamp, T. A., Nigam, S., Ardehali, R., Weissman, I. L., & Nusse, R. (2012). Endogenous Wnt signalling in human embryonic stem cells generates an equilibrium of distinct lineage-specified progenitors. *Nature Communications*, 3, 1070. <https://doi.org/10.1038/ncomms2064>
- Bonnevie, K. (1950). New facts on mesoderm formation and proamnion derivatives in the normal mouse embryo. *Journal of Morphology*, 86(3), 495–546. <https://doi.org/10.1002/jmor.1050860303>
- Bridgman, J. (1948). A morphological study of the development of the placenta of the rat; an histological and cytological study of the development of the chorioallantoic placenta of the white rat. *Journal of Morphology*, 83(2), 195–223. <https://doi.org/10.1002/jmor.1050830204>
- Brink, S. C. van den, & Oudenaarden, A. van. (2021). 3D gastruloids: A novel frontier in stem cell-based in vitro modeling of mammalian gastrulation. *Trends in Cell Biology*, 31(9), 747–759. <https://doi.org/10.1016/j.tcb.2021.06.007>
- Buechel, D., Sugiyama, N., Rubinstein, N., Saxena, M., Kalathur, R. K. R., Lüönd, F., Vafaizadeh, V., Valenta, T., Hausmann, G., Cantù, C., Basler, K., & Christofori, G. (2021). Parsing β -catenin's cell adhesion and Wnt signaling functions in malignant mammary tumor progression. *Proceedings of the National Academy of Sciences of the United States of America*, 118(34), Article 34. <https://doi.org/10.1073/pnas.2020227118>

- Camus, A., Davidson, B. P., Billiards, S., Khoo, P., Rivera-Pérez, J. A., Wakamiya, M., Behringer, R. R., & Tam, P. P. (2000). The morphogenetic role of midline mesendoderm and ectoderm in the development of the forebrain and the midbrain of the mouse embryo. *Development (Cambridge, England)*, *127*(9), 1799–1813. <https://doi.org/10.1242/dev.127.9.1799>
- Chambers, S. M., Fasano, C. A., Papapetrou, E. P., Tomishima, M., Sadelain, M., & Studer, L. (2009). Highly efficient neural conversion of human ES and iPS cells by dual inhibition of SMAD signaling. *Nature Biotechnology*, *27*(3), 275–280. <https://doi.org/10.1038/nbt.1529>
- Chawengsaksophak, K., de Graaff, W., Rossant, J., Deschamps, J., & Beck, F. (2004). Cdx2 is essential for axial elongation in mouse development. *Proceedings of the National Academy of Sciences of the United States of America*, *101*(20), 7641–7645. <https://doi.org/10.1073/pnas.0401654101>
- Chen, D., Sun, N., Hou, L., Kim, R., Faith, J., Aslanyan, M., Tao, Y., Zheng, Y., Fu, J., Liu, W., Kellis, M., & Clark, A. (2019). Human Primordial Germ Cells Are Specified from Lineage-Primed Progenitors. *Cell Reports*, *29*(13), 4568-4582.e5. <https://doi.org/10.1016/j.celrep.2019.11.083>
- Chin, M. H., Mason, M. J., Xie, W., Volinia, S., Singer, M., Peterson, C., Ambartsumyan, G., Aimiwu, O., Richter, L., Zhang, J., Khvorostov, I., Ott, V., Grunstein, M., Lavon, N., Benvenisty, N., Croce, C. M., Clark, A. T., Baxter, T., Pyle, A. D., ... Lowry, W. E. (2009). Induced pluripotent stem cells and embryonic stem cells are distinguished by gene expression signatures. *Cell Stem Cell*, *5*(1), Article 1. <https://doi.org/10.1016/j.stem.2009.06.008>
- Ciruna, B., & Rossant, J. (2001a). FGF signaling regulates mesoderm cell fate specification and morphogenetic movement at the primitive streak. *Developmental Cell*, *1*(1), 37–49. [https://doi.org/10.1016/s1534-5807\(01\)00017-x](https://doi.org/10.1016/s1534-5807(01)00017-x)
- Ciruna, B., & Rossant, J. (2001b). FGF signaling regulates mesoderm cell fate specification and morphogenetic movement at the primitive streak. *Developmental Cell*, *1*(1), Article 1. [https://doi.org/10.1016/s1534-5807\(01\)00017-x](https://doi.org/10.1016/s1534-5807(01)00017-x)
- Cohen, P., & Goedert, M. (2004). GSK3 inhibitors: Development and therapeutic potential. *Nature Reviews. Drug Discovery*, *3*(6), Article 6. <https://doi.org/10.1038/nrd1415>
- Condic, M. L. (2014). Totipotency: What it is and what it is not. *Stem Cells and Development*, *23*(8), 796–812. <https://doi.org/10.1089/scd.2013.0364>
- D'Amour, K. A., Agulnick, A. D., Eliazar, S., Kelly, O. G., Kroon, E., & Baetge, E. E. (2005). Efficient differentiation of human embryonic stem cells to definitive endoderm. *Nature Biotechnology*, *23*(12), 1534–1541. <https://doi.org/10.1038/nbt1163>

- Darnell, D. K., Stark, M. R., & Schoenwolf, G. C. (1999). Timing and cell interactions underlying neural induction in the chick embryo. *Development (Cambridge, England)*, *126*(11), 2505–2514. <https://doi.org/10.1242/dev.126.11.2505>
- Das, S. K., Wang, X. N., Paria, B. C., Damm, D., Abraham, J. A., Klagsbrun, M., Andrews, G. K., & Dey, S. K. (1994). Heparin-binding EGF-like growth factor gene is induced in the mouse uterus temporally by the blastocyst solely at the site of its apposition: A possible ligand for interaction with blastocyst EGF-receptor in implantation. *Development (Cambridge, England)*, *120*(5), 1071–1083. <https://doi.org/10.1242/dev.120.5.1071>
- Davidson, K. C., Adams, A. M., Goodson, J. M., McDonald, C. E., Potter, J. C., Berndt, J. D., Biechele, T. L., Taylor, R. J., & Moon, R. T. (2012). Wnt/ β -catenin signaling promotes differentiation, not self-renewal, of human embryonic stem cells and is repressed by Oct4. *Proceedings of the National Academy of Sciences of the United States of America*, *109*(12), Article 12. <https://doi.org/10.1073/pnas.1118777109>
- de Bree, K., de Bakker, B. S., & Oostra, R.-J. (2018). The development of the human notochord. *PloS One*, *13*(10), e0205752. <https://doi.org/10.1371/journal.pone.0205752>
- Desbaillets, I., Ziegler, U., Groscurth, P., & Gassmann, M. (2000). Embryoid bodies: An in vitro model of mouse embryogenesis. *Experimental Physiology*, *85*(6), 645–651.
- Diaz-Cuadros, M., Wagner, D. E., Budjan, C., Hubaud, A., Tarazona, O. A., Donnelly, S., Michaut, A., Al Tanoury, Z., Yoshioka-Kobayashi, K., Niino, Y., Kageyama, R., Miyawaki, A., Touboul, J., & Pourquié, O. (2020). In vitro characterization of the human segmentation clock. *Nature*, *580*(7801), 113–118. <https://doi.org/10.1038/s41586-019-1885-9>
- Doetschman, T. C., Eistetter, H., Katz, M., Schmidt, W., & Kemler, R. (1985). The in vitro development of blastocyst-derived embryonic stem cell lines: Formation of visceral yolk sac, blood islands and myocardium. *Journal of Embryology and Experimental Morphology*, *87*, 27–45.
- Durston, A. J. (2019). What are the roles of retinoids, other morphogens, and Hox genes in setting up the vertebrate body axis? *Genesis (New York, N.Y.: 2000)*, *57*(7–8), e23296. <https://doi.org/10.1002/dvg.23296>
- Eiraku, M., Takata, N., Ishibashi, H., Kawada, M., Sakakura, E., Okuda, S., Sekiguchi, K., Adachi, T., & Sasai, Y. (2011). Self-organizing optic-cup morphogenesis in three-dimensional culture. *Nature*, *472*(7341), 51–56. <https://doi.org/10.1038/nature09941>
- Eiraku, M., Watanabe, K., Matsuo-Takasaki, M., Kawada, M., Yonemura, S., Matsumura, M., Wataya, T., Nishiyama, A., Muguruma, K., & Sasai, Y. (2008). Self-organized formation of polarized cortical tissues from ESCs and its active manipulation by extrinsic signals. *Cell Stem Cell*, *3*(5), 519–532. <https://doi.org/10.1016/j.stem.2008.09.002>

- Enders, A. C., Schlafke, S., & Hendrickx, A. G. (1986). Differentiation of the embryonic disc, amnion, and yolk sac in the rhesus monkey. *The American Journal of Anatomy*, *177*(2), 161–185. <https://doi.org/10.1002/aja.1001770205>
- Eyal-Giladi, H., Debby, A., & Harel, N. (1992). The posterior section of the chick's area pellucida and its involvement in hypoblast and primitive streak formation. *Development*, *116*(3), 819–830. <https://doi.org/10.1242/dev.116.3.819>
- Ferretti, E., & Hadjantonakis, A.-K. (2019). Mesoderm specification and diversification: From single cells to emergent tissues. *Current Opinion in Cell Biology*, *61*, 110–116. <https://doi.org/10.1016/j.ceb.2019.07.012>
- Gadue, P., Huber, T. L., Paddison, P. J., & Keller, G. M. (2006). Wnt and TGF-beta signaling are required for the induction of an in vitro model of primitive streak formation using embryonic stem cells. *Proceedings of the National Academy of Sciences of the United States of America*, *103*(45), 16806–16811. <https://doi.org/10.1073/pnas.0603916103>
- Gilbert, S., & Barresi, M. (2016). *Developmental Biology* (11th ed.). Sinauer Associates is an imprint of Oxford University Press.
- Girgin, M. U., Broguiere, N., Mattolini, L., & Lutolf, M. P. (2021). Gastruloids generated without exogenous Wnt activation develop anterior neural tissues. *Stem Cell Reports*, *16*(5), 1143–1155. <https://doi.org/10.1016/j.stemcr.2021.03.017>
- Gray, S. D., & Dale, J. K. (2010). Notch signalling regulates the contribution of progenitor cells from the chick Hensen's node to the floor plate and notochord. *Development (Cambridge, England)*, *137*(4), 561–568. <https://doi.org/10.1242/dev.041608>
- Hafez, S. (2017). Comparative Placental Anatomy: Divergent Structures Serving a Common Purpose. *Progress in Molecular Biology and Translational Science*, *145*, 1–28. <https://doi.org/10.1016/bs.pmbts.2016.12.001>
- Harrison, S. E., Sozen, B., Christodoulou, N., Kyprianou, C., & Zernicka-Goetz, M. (2017). Assembly of embryonic and extraembryonic stem cells to mimic embryogenesis in vitro. *Science (New York, N.Y.)*, *356*(6334), eaal1810. <https://doi.org/10.1126/science.aal1810>
- Hill, M. A. (2018). Developing the Digital Kyoto Collection in Education and Research. *Anatomical Record (Hoboken, N.J.: 2007)*, *301*(6), 998–1003. <https://doi.org/10.1002/ar.23783>
- Höpfl, G., Gassmann, M., & Desbaillets, I. (2004). Differentiating embryonic stem cells into embryoid bodies. *Methods in Molecular Biology (Clifton, N.J.)*, *254*, 79–98. <https://doi.org/10.1385/1-59259-741-6:079>

- James, D., Noggle, S. A., Swigut, T., & Brivanlou, A. H. (2006). Contribution of human embryonic stem cells to mouse blastocysts. *Developmental Biology*, 295(1), Article 1. <https://doi.org/10.1016/j.ydbio.2006.03.026>
- Kanda, S., Akiyama, T., Chikuda, H., Yamaguchi, T., & Saita, K. (2015). An Unusual Presentation of Adult Tethered Cord Syndrome Associated with Severe Chest and Upper Back Pain. *Case Reports in Orthopedics*, 2015, 926185. <https://doi.org/10.1155/2015/926185>
- Kane, D., & Adams, R. (2002). Life at the edge: Epiboly and involution in the zebrafish. *Results and Problems in Cell Differentiation*, 40, 117–135. https://doi.org/10.1007/978-3-540-46041-1_7
- Kattman, S. J., Witty, A. D., Gagliardi, M., Dubois, N. C., Niapour, M., Hotta, A., Ellis, J., & Keller, G. (2011). Stage-specific optimization of activin/nodal and BMP signaling promotes cardiac differentiation of mouse and human pluripotent stem cell lines. *Cell Stem Cell*, 8(2), 228–240. <https://doi.org/10.1016/j.stem.2010.12.008>
- Kawano, Y., & Kypta, R. (2003). Secreted antagonists of the Wnt signalling pathway. *Journal of Cell Science*, 116(Pt 13), 2627–2634. <https://doi.org/10.1242/jcs.00623>
- Keller, R. (1996). Holtfreter revisited: Unsolved problems in amphibian morphogenesis. *Developmental Dynamics: An Official Publication of the American Association of Anatomists*, 205(3), 257–264. [https://doi.org/10.1002/\(SICI\)1097-0177\(199603\)205:3<257::AID-AJA6>3.0.CO;2-H](https://doi.org/10.1002/(SICI)1097-0177(199603)205:3<257::AID-AJA6>3.0.CO;2-H)
- Keller, R. (2005). Cell migration during gastrulation. *Current Opinion in Cell Biology*, 17(5), Article 5. <https://doi.org/10.1016/j.ceb.2005.08.006>
- Keller, R. E. (1980). The cellular basis of epiboly: An SEM study of deep-cell rearrangement during gastrulation in *Xenopus laevis*. *Journal of Embryology and Experimental Morphology*, 60, 201–234.
- Kimmel, C. B., Ballard, W. W., Kimmel, S. R., Ullmann, B., & Schilling, T. F. (1995). Stages of embryonic development of the zebrafish. *Developmental Dynamics: An Official Publication of the American Association of Anatomists*, 203(3), 253–310. <https://doi.org/10.1002/aja.1002030302>
- Koch, F., Scholze, M., Wittler, L., Schifferl, D., Sudheer, S., Grote, P., Timmermann, B., Macura, K., & Herrmann, B. G. (2017). Antagonistic Activities of Sox2 and Brachyury Control the Fate Choice of Neuro-Mesodermal Progenitors. *Developmental Cell*, 42(5), 514–526.e7. <https://doi.org/10.1016/j.devcel.2017.07.021>
- Kozmikova, I., & Kozmik, Z. (2020). Wnt/ β -catenin signaling is an evolutionarily conserved determinant of chordate dorsal organizer. *ELife*, 9, e56817. <https://doi.org/10.7554/eLife.56817>

- Kremer, M. E. B., Althof, J. F., Derikx, J. P. M., van Baren, R., Heij, H. A., Wijnen, M. H. W. A., Wijnen, R. M. H., van der Zee, D. C., & van Heurn, L. W. E. (2018). The incidence of associated abnormalities in patients with sacrococcygeal teratoma. *Journal of Pediatric Surgery*, *53*(10), 1918–1922. <https://doi.org/10.1016/j.jpedsurg.2018.01.013>
- Kwon, G. S., Viotti, M., & Hadjantonakis, A.-K. (2008). The endoderm of the mouse embryo arises by dynamic widespread intercalation of embryonic and extraembryonic lineages. *Developmental Cell*, *15*(4), 509–520. <https://doi.org/10.1016/j.devcel.2008.07.017>
- Lancaster, M. A., Renner, M., Martin, C.-A., Wenzel, D., Bicknell, L. S., Hurles, M. E., Homfray, T., Penninger, J. M., Jackson, A. P., & Knoblich, J. A. (2013). Cerebral organoids model human brain development and microcephaly. *Nature*, *501*(7467), 373–379. <https://doi.org/10.1038/nature12517>
- Le Douarin, N. (1996). Patterning of the early neural primordium in the avian embryo. *The International Journal of Developmental Biology*, *Suppl 1*, 51S.
- Lee, H. C., Choi, H. J., Park, T. S., Lee, S. I., Kim, Y. M., Rengaraj, D., Nagai, H., Sheng, G., Lim, J. M., & Han, J. Y. (2013). Cleavage events and sperm dynamics in chick intrauterine embryos. *PLoS One*, *8*(11), e80631. <https://doi.org/10.1371/journal.pone.0080631>
- Libby, A. R. G., Joy, D. A., Elder, N. H., Bulger, E. A., Krakora, M. Z., Gaylord, E. A., Mendoza-Camacho, F., Butts, J. C., & McDevitt, T. C. (2021a). Axial elongation of caudalized human organoids mimics aspects of neural tube development. *Development (Cambridge, England)*, *148*(12), dev198275. <https://doi.org/10.1242/dev.198275>
- Libby, A. R. G., Joy, D. A., Elder, N. H., Bulger, E. A., Krakora, M. Z., Gaylord, E. A., Mendoza-Camacho, F., Butts, J. C., & McDevitt, T. C. (2021b). Axial elongation of caudalized human organoids mimics aspects of neural tube development. *Development (Cambridge, England)*, *148*(12), Article 12. <https://doi.org/10.1242/dev.198275>
- Loh, K. M., Ang, L. T., Zhang, J., Kumar, V., Ang, J., Auyeong, J. Q., Lee, K. L., Choo, S. H., Lim, C. Y. Y., Nichane, M., Tan, J., Noghabi, M. S., Azzola, L., Ng, E. S., Durruthy-Durruthy, J., Sebastiano, V., Poellinger, L., Elefanty, A. G., Stanley, E. G., ... Lim, B. (2014). Efficient endoderm induction from human pluripotent stem cells by logically directing signals controlling lineage bifurcations. *Cell Stem Cell*, *14*(2), 237–252. <https://doi.org/10.1016/j.stem.2013.12.007>
- Loh, K. M., Chen, A., Koh, P. W., Deng, T. Z., Sinha, R., Tsai, J. M., Barkal, A. A., Shen, K. Y., Jain, R., Morganti, R. M., Shyh-Chang, N., Fernhoff, N. B., George, B. M., Wernig, G., Salomon, R. E. A., Chen, Z., Vogel, H., Epstein, J. A., Kundaje, A., ... Weissman, I. L. (2016). Mapping the Pairwise Choices Leading from Pluripotency to Human Bone, Heart, and Other Mesoderm Cell Types. *Cell*, *166*(2), Article 2. <https://doi.org/10.1016/j.cell.2016.06.011>

- Lovell-Badge, R., Anthony, E., Barker, R. A., Bubela, T., Brivanlou, A. H., Carpenter, M., Charo, R. A., Clark, A., Clayton, E., Cong, Y., Daley, G. Q., Fu, J., Fujita, M., Greenfield, A., Goldman, S. A., Hill, L., Hyun, I., Isasi, R., Kahn, J., ... Zhai, X. (2021). ISSCR Guidelines for Stem Cell Research and Clinical Translation: The 2021 update. *Stem Cell Reports*, 16(6), Article 6. <https://doi.org/10.1016/j.stemcr.2021.05.012>
- Ma, H., Zhai, J., Wan, H., Jiang, X., Wang, X., Wang, L., Xiang, Y., He, X., Zhao, Z.-A., Zhao, B., Zheng, P., Li, L., & Wang, H. (2019). In vitro culture of cynomolgus monkey embryos beyond early gastrulation. *Science (New York, N.Y.)*, 366(6467), eaax7890. <https://doi.org/10.1126/science.aax7890>
- Ma, S., & Cd, S. (1991). Fate mapping and cell lineage analysis of Hensen's node in the chick embryo. *Development (Cambridge, England)*, 112(2). <https://doi.org/10.1242/dev.112.2.615>
- Marikawa, Y., Chen, H.-R., Menor, M., Deng, Y., & Alarcon, V. B. (2020). Exposure-based assessment of chemical teratogenicity using morphogenetic aggregates of human embryonic stem cells. *Reproductive Toxicology (Elmsford, N.Y.)*, 91, 74–91. <https://doi.org/10.1016/j.reprotox.2019.10.004>
- Martyn, I., Kanno, T. Y., Ruzo, A., Siggia, E. D., & Brivanlou, A. H. (2018). Self-organization of a human organizer by combined Wnt and Nodal signalling. *Nature*, 558(7708), Article 7708. <https://doi.org/10.1038/s41586-018-0150-y>
- McGowen, M. R., Erez, O., Romero, R., & Wildman, D. E. (2014). The evolution of embryo implantation. *The International Journal of Developmental Biology*, 58(2–4), 155–161. <https://doi.org/10.1387/ijdb.140020dw>
- Minn, K. T., Fu, Y. C., He, S., Dietmann, S., George, S. C., Anastasio, M. A., Morris, S. A., & Solnica-Krezel, L. (2020). High-resolution transcriptional and morphogenetic profiling of cells from micropatterned human ESC gastruloid cultures. *ELife*, 9, e59445. <https://doi.org/10.7554/eLife.59445>
- Mishina, Y., Suzuki, A., Ueno, N., & Behringer, R. R. (1995a). Bmpr encodes a type I bone morphogenetic protein receptor that is essential for gastrulation during mouse embryogenesis. *Genes & Development*, 9(24), 3027–3037. <https://doi.org/10.1101/gad.9.24.3027>
- Mishina, Y., Suzuki, A., Ueno, N., & Behringer, R. R. (1995b). Bmpr encodes a type I bone morphogenetic protein receptor that is essential for gastrulation during mouse embryogenesis. *Genes & Development*, 9(24), Article 24. <https://doi.org/10.1101/gad.9.24.3027>
- Molè, M. A., Coorens, T. H. H., Shahbazi, M. N., Weberling, A., Weatherbee, B. A. T., Gantner, C. W., Sancho-Serra, C., Richardson, L., Drinkwater, A., Syed, N., Engley, S., Snell, P.,

- Christie, L., Elder, K., Campbell, A., Fishel, S., Behjati, S., Vento-Tormo, R., & Zernicka-Goetz, M. (2021). A single cell characterisation of human embryogenesis identifies pluripotency transitions and putative anterior hypoblast centre. *Nature Communications*, *12*(1), 3679. <https://doi.org/10.1038/s41467-021-23758-w>
- Molè, M. A., Weberling, A., & Zernicka-Goetz, M. (2020). Comparative analysis of human and mouse development: From zygote to pre-gastrulation. *Current Topics in Developmental Biology*, *136*, 113–138. <https://doi.org/10.1016/bs.ctdb.2019.10.002>
- Montero, J.-A., Carvalho, L., Wilsch-Bräuninger, M., Kilian, B., Mustafa, C., & Heisenberg, C.-P. (2005). Shield formation at the onset of zebrafish gastrulation. *Development (Cambridge, England)*, *132*(6), 1187–1198. <https://doi.org/10.1242/dev.01667>
- Morgani, S. M., & Hadjantonakis, A.-K. (2020a). Signaling regulation during gastrulation: Insights from mouse embryos and in vitro systems. *Current Topics in Developmental Biology*, *137*, 391–431. <https://doi.org/10.1016/bs.ctdb.2019.11.011>
- Morgani, S. M., & Hadjantonakis, A.-K. (2020b). Signaling regulation during gastrulation: Insights from mouse embryos and in vitro systems. *Current Topics in Developmental Biology*, *137*, 391–431. <https://doi.org/10.1016/bs.ctdb.2019.11.011>
- Morgani, S. M., Metzger, J. J., Nichols, J., Siggia, E. D., & Hadjantonakis, A.-K. (2018). Micropattern differentiation of mouse pluripotent stem cells recapitulates embryo regionalized cell fate patterning. *eLife*, *7*, e32839. <https://doi.org/10.7554/eLife.32839>
- Moris, N., Alev, C., Pera, M., & Martinez Arias, A. (2021). Biomedical and societal impacts of in vitro embryo models of mammalian development. *Stem Cell Reports*, *16*(5), 1021–1030. <https://doi.org/10.1016/j.stemcr.2021.03.023>
- Moris, N., Anlas, K., van den Brink, S. C., Alemany, A., Schröder, J., Ghimire, S., Balayo, T., van Oudenaarden, A., & Martinez Arias, A. (2020). An in vitro model of early anteroposterior organization during human development. *Nature*, *582*(7812), 410–415. <https://doi.org/10.1038/s41586-020-2383-9>
- Müller, F., & O’Rahilly, R. (2004). The primitive streak, the caudal eminence and related structures in staged human embryos. *Cells, Tissues, Organs*, *177*(1), 2–20. <https://doi.org/10.1159/000078423>
- Nakano, T., Ando, S., Takata, N., Kawada, M., Muguruma, K., Sekiguchi, K., Saito, K., Yonemura, S., Eiraku, M., & Sasai, Y. (2012). Self-formation of optic cups and storable stratified neural retina from human ESCs. *Cell Stem Cell*, *10*(6), 771–785. <https://doi.org/10.1016/j.stem.2012.05.009>
- New, D. A. T. (1956). The Formation of Sub-blastodermic Fluid in Hens’ Eggs. *Development*, *4*(3), 221–227. <https://doi.org/10.1242/dev.4.3.221>

- Nie, S., & Chang, C. (2007). PI3K and Erk MAPK mediate ErbB signaling in *Xenopus* gastrulation. *Mechanisms of Development*, *124*(9–10), 657–667. <https://doi.org/10.1016/j.mod.2007.07.005>
- Niu, Y., Sun, N., Li, C., Lei, Y., Huang, Z., Wu, J., Si, C., Dai, X., Liu, C., Wei, J., Liu, L., Feng, S., Kang, Y., Si, W., Wang, H., Zhang, E., Zhao, L., Li, Z., Luo, X., ... Tan, T. (2019). Dissecting primate early post-implantation development using long-term in vitro embryo culture. *Science (New York, N.Y.)*, *366*(6467), eaaw5754. <https://doi.org/10.1126/science.aaw5754>
- Olmsted, Z. T., & Paluh, J. L. (2021). Co-development of central and peripheral neurons with trunk mesendoderm in human elongating multi-lineage organized gastruloids. *Nature Communications*, *12*(1), Article 1. <https://doi.org/10.1038/s41467-021-23294-7>
- O’Rahilly, R., & Müller, F. (2010). Developmental stages in human embryos: Revised and new measurements. *Cells, Tissues, Organs*, *192*(2), 73–84. <https://doi.org/10.1159/000289817>
- Ozair, M. Z., Noggle, S., Warmflash, A., Krzyspiak, J. E., & Brivanlou, A. H. (2013). SMAD7 directly converts human embryonic stem cells to telencephalic fate by a default mechanism. *Stem Cells (Dayton, Ohio)*, *31*(1), 35–47. <https://doi.org/10.1002/stem.1246>
- Pijuan-Sala, B., Griffiths, J. A., Guibentif, C., Hiscock, T. W., Jawaid, W., Calero-Nieto, F. J., Mulas, C., Ibarra-Soria, X., Tyser, R. C. V., Ho, D. L. L., Reik, W., Srinivas, S., Simons, B. D., Nichols, J., Marioni, J. C., & Göttgens, B. (2019). A single-cell molecular map of mouse gastrulation and early organogenesis. *Nature*, *566*(7745), 490–495. <https://doi.org/10.1038/s41586-019-0933-9>
- Piliszek, A., Grabarek, J. B., Frankenberg, S. R., & Plusa, B. (2016). Cell fate in animal and human blastocysts and the determination of viability. *Molecular Human Reproduction*, *22*(10), Article 10. <https://doi.org/10.1093/molehr/gaw002>
- Pratt, H. P., Chakraborty, J., & Surani, M. A. (1981). Molecular and morphological differentiation of the mouse blastocyst after manipulations of compaction with cytochalasin D. *Cell*, *26*(2 Pt 2), 279–292. [https://doi.org/10.1016/0092-8674\(81\)90310-x](https://doi.org/10.1016/0092-8674(81)90310-x)
- Pratt, H. P., Ziomek, C. A., Reeve, W. J., & Johnson, M. H. (1982). Compaction of the mouse embryo: An analysis of its components. *Journal of Embryology and Experimental Morphology*, *70*, 113–132.
- Rivera-Pérez, J. A., & Hadjantonakis, A.-K. (2014). The Dynamics of Morphogenesis in the Early Mouse Embryo. *Cold Spring Harbor Perspectives in Biology*, *7*(11), a015867. <https://doi.org/10.1101/cshperspect.a015867>
- Rivera-Pérez, J. A., & Magnuson, T. (2005a). Primitive streak formation in mice is preceded by localized activation of Brachyury and Wnt3. *Developmental Biology*, *288*(2), 363–371. <https://doi.org/10.1016/j.ydbio.2005.09.012>

- Rivera-Pérez, J. A., & Magnuson, T. (2005b). Primitive streak formation in mice is preceded by localized activation of Brachyury and Wnt3. *Developmental Biology*, 288(2), Article 2. <https://doi.org/10.1016/j.ydbio.2005.09.012>
- Sadler, T. W., & Langman, J. (2015). *Langman's Medical Embryology* (15th ed.). Lippincott Williams & Wilkins.
- Sakai, Y., & Nakazawa, K. (2007). Technique for the control of spheroid diameter using microfabricated chips. *Acta Biomaterialia*, 3(6), 1033–1040. <https://doi.org/10.1016/j.actbio.2007.06.004>
- Sakai, Y., Yoshiura, Y., & Nakazawa, K. (2011). Embryoid body culture of mouse embryonic stem cells using microwell and micropatterned chips. *Journal of Bioscience and Bioengineering*, 111(1), 85–91. <https://doi.org/10.1016/j.jbiosc.2010.08.014>
- Samal, S. K., & Rathod, S. (2015). Sirenomelia: The mermaid syndrome: Report of two cases. *Journal of Natural Science, Biology, and Medicine*, 6(1), 264–266. <https://doi.org/10.4103/0976-9668.149227>
- Sasai, Y., Eiraku, M., & Suga, H. (2012). In vitro organogenesis in three dimensions: Self-organising stem cells. *Development (Cambridge, England)*, 139(22), 4111–4121. <https://doi.org/10.1242/dev.079590>
- Schindelin, J., Arganda-Carreras, I., Frise, E., Kaynig, V., Longair, M., Pietzsch, T., Preibisch, S., Rueden, C., Saalfeld, S., Schmid, B., Tinevez, J.-Y., White, D. J., Hartenstein, V., Eliceiri, K., Tomancak, P., & Cardona, A. (2012). Fiji: An open-source platform for biological-image analysis. *Nature Methods*, 9(7), 676–682. <https://doi.org/10.1038/nmeth.2019>
- Schoenwolf, G. C., Garcia-Martinez, V., & Dias, M. S. (1992). Mesoderm movement and fate during avian gastrulation and neurulation. *Developmental Dynamics: An Official Publication of the American Association of Anatomists*, 193(3), 235–248. <https://doi.org/10.1002/aja.1001930304>
- Sepich, D. S., Calmelet, C., Kiskowski, M., & Solnica-Krezel, L. (2005). Initiation of convergence and extension movements of lateral mesoderm during zebrafish gastrulation. *Developmental Dynamics: An Official Publication of the American Association of Anatomists*, 234(2), 279–292. <https://doi.org/10.1002/dvdy.20507>
- Shao, Y., Taniguchi, K., Gurdziel, K., Townshend, R. F., Xue, X., Yong, K. M. A., Sang, J., Spence, J. R., Gumucio, D. L., & Fu, J. (2017). Self-organized amniogenesis by human pluripotent stem cells in a biomimetic implantation-like niche. *Nature Materials*, 16(4), 419–425. <https://doi.org/10.1038/nmat4829>

- Shao, Y., Taniguchi, K., Townshend, R. F., Miki, T., Gumucio, D. L., & Fu, J. (2017). A pluripotent stem cell-based model for post-implantation human amniotic sac development. *Nature Communications*, 8(1), 208. <https://doi.org/10.1038/s41467-017-00236-w>
- Shen, H., Yang, M., Li, S., Zhang, J., Peng, B., Wang, C., Chang, Z., Ong, J., & Du, P. (2021). Mouse totipotent stem cells captured and maintained through spliceosomal repression. *Cell*, 184(11), 2843-2859.e20. <https://doi.org/10.1016/j.cell.2021.04.020>
- Shih, J., & Fraser, S. E. (1995). Distribution of tissue progenitors within the shield region of the zebrafish gastrula. *Development (Cambridge, England)*, 121(9), 2755–2765. <https://doi.org/10.1242/dev.121.9.2755>
- Shih, J., & Fraser, S. E. (1996). Characterizing the zebrafish organizer: Microsurgical analysis at the early-shield stage. *Development (Cambridge, England)*, 122(4), 1313–1322. <https://doi.org/10.1242/dev.122.4.1313>
- Siemens, H., Jackstadt, R., Hüntten, S., Kaller, M., Menssen, A., Götz, U., & Hermeking, H. (2011). MiR-34 and SNAIL form a double-negative feedback loop to regulate epithelial-mesenchymal transitions. *Cell Cycle (Georgetown, Tex.)*, 10(24), 4256–4271. <https://doi.org/10.4161/cc.10.24.18552>
- Solnica-Krezel, L. (2005). Conserved patterns of cell movements during vertebrate gastrulation. *Current Biology: CB*, 15(6), R213-228. <https://doi.org/10.1016/j.cub.2005.03.016>
- Solnica-Krezel, L., & Sepich, D. S. (2012). Gastrulation: Making and shaping germ layers. *Annual Review of Cell and Developmental Biology*, 28, 687–717. <https://doi.org/10.1146/annurev-cellbio-092910-154043>
- Solnica-Krezel, L., Stemple, D. L., Mountcastle-Shah, E., Rangini, Z., Neuhauss, S. C., Malicki, J., Schier, A. F., Stainier, D. Y., Zwartkruis, F., Abdelilah, S., & Driever, W. (1996). Mutations affecting cell fates and cellular rearrangements during gastrulation in zebrafish. *Development (Cambridge, England)*, 123, 67–80. <https://doi.org/10.1242/dev.123.1.67>
- Sozen, B., Amadei, G., Cox, A., Wang, R., Na, E., Czukiewska, S., Chappell, L., Voet, T., Michel, G., Jing, N., Glover, D. M., & Zernicka-Goetz, M. (2018). Self-assembly of embryonic and two extra-embryonic stem cell types into gastrulating embryo-like structures. *Nature Cell Biology*, 20(8), 979–989. <https://doi.org/10.1038/s41556-018-0147-7>
- Steinberg, M. S., & Gilbert, S. F. (2004). Townes and Holtfreter (1955): Directed movements and selective adhesion of embryonic amphibian cells. *Journal of Experimental Zoology. Part A, Comparative Experimental Biology*, 301(9), Article 9. <https://doi.org/10.1002/jez.a.114>

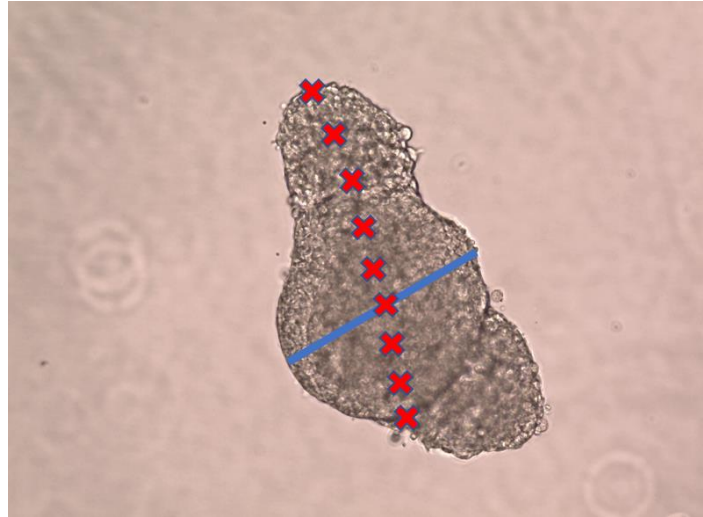
- Sun, X., Meyers, E. N., Lewandoski, M., & Martin, G. R. (1999). Targeted disruption of *Fgf8* causes failure of cell migration in the gastrulating mouse embryo. *Genes & Development*, *13*(14), 1834–1846. <https://doi.org/10.1101/gad.13.14.1834>
- Teo, A. K. K., Arnold, S. J., Trotter, M. W. B., Brown, S., Ang, L. T., Chng, Z., Robertson, E. J., Dunn, N. R., & Vallier, L. (2011). Pluripotency factors regulate definitive endoderm specification through eomesodermin. *Genes & Development*, *25*(3), 238–250. <https://doi.org/10.1101/gad.607311>
- Thiery, J. P., Acloque, H., Huang, R. Y. J., & Nieto, M. A. (2009). Epithelial-mesenchymal transitions in development and disease. *Cell*, *139*(5), 871–890. <https://doi.org/10.1016/j.cell.2009.11.007>
- Thomson, J. A., Itskovitz-Eldor, J., Shapiro, S. S., Waknitz, M. A., Swiergiel, J. J., Marshall, V. S., & Jones, J. M. (1998). Embryonic Stem Cell Lines Derived from Human Blastocysts. *Science*, *282*(5391), Article 5391. <https://doi.org/10.1126/science.282.5391.1145>
- Thomson, M., Liu, S. J., Zou, L.-N., Smith, Z., Meissner, A., & Ramanathan, S. (2011). Pluripotency factors in embryonic stem cells regulate differentiation into germ layers. *Cell*, *145*(6), 875–889. <https://doi.org/10.1016/j.cell.2011.05.017>
- Turner, D. A., Rué, P., Mackenzie, J. P., Davies, E., & Arias, A. M. (2014). *Brachyury cooperates with Wnt/ β -Catenin signalling to elicit Primitive Streak like behaviour in differentiating mouse ES cells* (p. 003871). bioRxiv. <https://doi.org/10.1101/003871>
- Tyser, R. C. V., Mahammadov, E., Nakanoh, S., Vallier, L., Scialdone, A., & Srinivas, S. (2021). Single-cell transcriptomic characterization of a gastrulating human embryo. *Nature*, *600*(7888), Article 7888. <https://doi.org/10.1038/s41586-021-04158-y>
- V, W., & Rs, B. (1996). Cell fate and morphogenetic movement in the late mouse primitive streak. *Mechanisms of Development*, *55*(1). [https://doi.org/10.1016/0925-4773\(95\)00493-9](https://doi.org/10.1016/0925-4773(95)00493-9)
- VAKAET, L. (1984). The Initiation of Gastrular Ingression in the Chick Blastoderm1. *American Zoologist*, *24*(3), 555–562. <https://doi.org/10.1093/icb/24.3.555>
- Valenzano, M., Paoletti, R., Rossi, A., Farinini, D., Garlaschi, G., & Fulcheri, E. (1999). Sirenomelia. Pathological features, antenatal ultrasonographic clues, and a review of current embryogenic theories. *Human Reproduction Update*, *5*(1), 82–86. <https://doi.org/10.1093/humupd/5.1.82>
- van den Brink, S. C., Baillie-Johnson, P., Balayo, T., Hadjantonakis, A.-K., Nowotschin, S., Turner, D. A., & Martinez Arias, A. (2014). Symmetry breaking, germ layer specification and axial organisation in aggregates of mouse embryonic stem cells. *Development (Cambridge, England)*, *141*(22), 4231–4242. <https://doi.org/10.1242/dev.113001>

- Varshney, G. K., & Burgess, S. M. (2014). Mutagenesis and phenotyping resources in zebrafish for studying development and human disease. *Briefings in Functional Genomics*, *13*(2), 82–94. <https://doi.org/10.1093/bfpg/elt042>
- Veenvliet, J. V., Bolondi, A., Kretzmer, H., Haut, L., Scholze-Wittler, M., Schifferl, D., Koch, F., Guignard, L., Kumar, A. S., Pustet, M., Heimann, S., Buschow, R., Wittler, L., Timmermann, B., Meissner, A., & Herrmann, B. G. (2020). Mouse embryonic stem cells self-organize into trunk-like structures with neural tube and somites. *Science (New York, N.Y.)*, *370*(6522), eaba4937. <https://doi.org/10.1126/science.aba4937>
- Vincent, S. D., Dunn, N. R., Hayashi, S., Norris, D. P., & Robertson, E. J. (2003). Cell fate decisions within the mouse organizer are governed by graded Nodal signals. *Genes & Development*, *17*(13), 1646–1662. <https://doi.org/10.1101/gad.1100503>
- Wang, X., Chen, C., Wang, L., Chen, D., Guang, W., & French, J. (2003). Conception, early pregnancy loss, and time to clinical pregnancy: A population-based prospective study. *Fertility and Sterility*, *79*(3), 577–584. [https://doi.org/10.1016/s0015-0282\(02\)04694-0](https://doi.org/10.1016/s0015-0282(02)04694-0)
- Wang, Z., Oron, E., Nelson, B., Razis, S., & Ivanova, N. (2012). Distinct lineage specification roles for NANOG, OCT4, and SOX2 in human embryonic stem cells. *Cell Stem Cell*, *10*(4), 440–454. <https://doi.org/10.1016/j.stem.2012.02.016>
- Warga, R. M., & Kimmel, C. B. (1990). Cell movements during epiboly and gastrulation in zebrafish. *Development (Cambridge, England)*, *108*(4), 569–580. <https://doi.org/10.1242/dev.108.4.569>
- Warmflash, A., Sorre, B., Etoc, F., Siggia, E. D., & Brivanlou, A. H. (2014). A method to recapitulate early embryonic spatial patterning in human embryonic stem cells. *Nature Methods*, *11*(8), 847–854. <https://doi.org/10.1038/nmeth.3016>
- Williams, M., Burdsal, C., Periasamy, A., Lewandoski, M., & Sutherland, A. (2012a). Mouse primitive streak forms in situ by initiation of epithelial to mesenchymal transition without migration of a cell population. *Developmental Dynamics: An Official Publication of the American Association of Anatomists*, *241*(2), 270–283. <https://doi.org/10.1002/dvdy.23711>
- Williams, M., Burdsal, C., Periasamy, A., Lewandoski, M., & Sutherland, A. (2012b). Mouse primitive streak forms in situ by initiation of epithelial to mesenchymal transition without migration of a cell population. *Developmental Dynamics: An Official Publication of the American Association of Anatomists*, *241*(2), Article 2. <https://doi.org/10.1002/dvdy.23711>
- Wilson, K. D., Venkatasubrahmanyam, S., Jia, F., Sun, N., Butte, A. J., & Wu, J. C. (2009). MicroRNA profiling of human-induced pluripotent stem cells. *Stem Cells and Development*, *18*(5), Article 5. <https://doi.org/10.1089/scd.2008.0247>

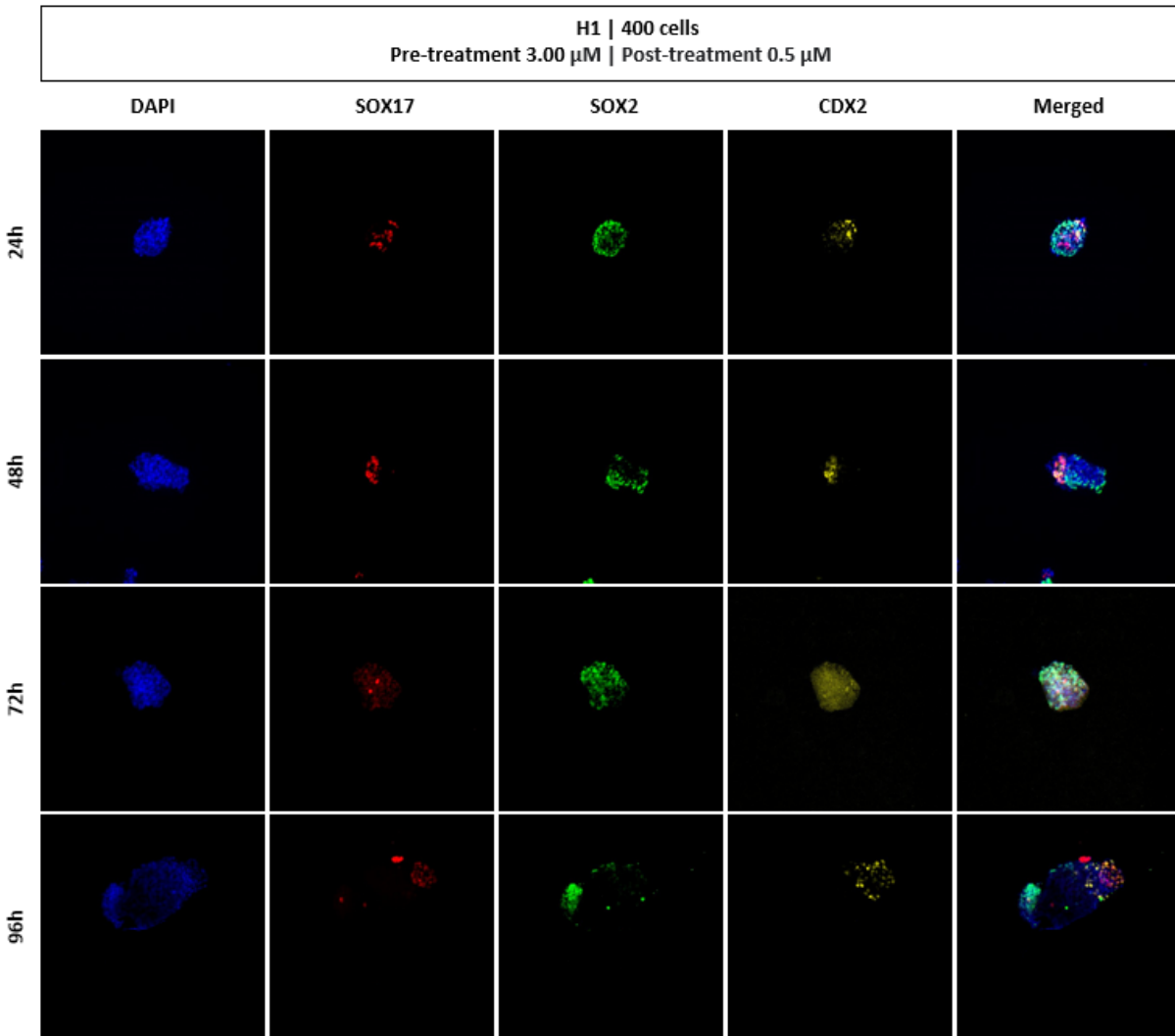
- Winnier, G., Blessing, M., Labosky, P. A., & Hogan, B. L. (1995). Bone morphogenetic protein-4 is required for mesoderm formation and patterning in the mouse. *Genes & Development*, 9(17), 2105–2116. <https://doi.org/10.1101/gad.9.17.2105>
- Wt, W. (1984). Warnock report on human fertilisation and embryology. *Lancet (London, England)*, 2(8401). <https://pubmed.ncbi.nlm.nih.gov/6147600/>
- Wu, S.-Y., Ferkowicz, M., & McClay, D. R. (2007). Ingression of primary mesenchyme cells of the sea urchin embryo: A precisely timed epithelial mesenchymal transition. *Birth Defects Research. Part C, Embryo Today: Reviews*, 81(4), 241–252. <https://doi.org/10.1002/bdrc.20113>
- Wymeersch, F. J., Wilson, V., & Tsakiridis, A. (2021). Understanding axial progenitor biology in vivo and in vitro. *Development (Cambridge, England)*, 148(4), dev180612. <https://doi.org/10.1242/dev.180612>
- Y, M., Hr, C., M, M., Y, D., & Vb, A. (2020). Exposure-based assessment of chemical teratogenicity using morphogenetic aggregates of human embryonic stem cells. *Reproductive Toxicology (Elmsford, N.Y.)*, 91. <https://doi.org/10.1016/j.reprotox.2019.10.004>
- Yamaguchi, T. P., Harpal, K., Henkemeyer, M., & Rossant, J. (1994). Fgfr-1 is required for embryonic growth and mesodermal patterning during mouse gastrulation. *Genes & Development*, 8(24), 3032–3044. <https://doi.org/10.1101/gad.8.24.3032>
- Yen, W. W., Williams, M., Periasamy, A., Conaway, M., Burdsal, C., Keller, R., Lu, X., & Sutherland, A. (2009). PTK7 is essential for polarized cell motility and convergent extension during mouse gastrulation. *Development (Cambridge, England)*, 136(12), 2039–2048. <https://doi.org/10.1242/dev.030601>
- Zhang, H. T., & Hiiragi, T. (2018). Symmetry Breaking in the Mammalian Embryo. *Annual Review of Cell and Developmental Biology*, 34, 405–426. <https://doi.org/10.1146/annurev-cellbio-100617-062616>
- Zheng, Y., Xue, X., Shao, Y., Wang, S., Esfahani, S. N., Li, Z., Muncie, J. M., Lakins, J. N., Weaver, V. M., Gumucio, D. L., & Fu, J. (2019). Controlled modelling of human epiblast and amnion development using stem cells. *Nature*, 573(7774), 421–425. <https://doi.org/10.1038/s41586-019-1535-2>
- Zinaman, M. J., Clegg, E. D., Brown, C. C., O'Connor, J., & Selevan, S. G. (1996). Estimates of human fertility and pregnancy loss. *Fertility and Sterility*, 65(3), 503–509.
- Zinski, J., Tajer, B., & Mullins, M. C. (2018). TGF- β Family Signaling in Early Vertebrate Development. *Cold Spring Harbor Perspectives in Biology*, 10(6), a033274. <https://doi.org/10.1101/cshperspect.a033274>

Appendix

Supplementary figures



Supplementary 1: Example of how length-to-width ratio is obtained from gastruloids. Blue represents width, red X represents how the length was measured (for this gastruloid, the length axis could be drawn differently (into the “lobe”).



Supplementary 2 : H1 gastruloids derived from 400 cells with 3.00 μ M and 0.5 μ M pre/post-treatment, Images are taken from 24 h to 96 h for the expression of SOX17 (red), SOX2 (green), and CDX2 (yellow).